AD-A078 264 HEWLETT-PACKARD CO PALO ALTO CALIF SOLID STATE LAB F/G 20/12
VPE GROWTH OF (AL, GA)AS.(U)
OCT 79 G B STRINGFELLOW
UNCLASSIFIED RADC-TR-79-207 F19628-77-C-0199 NL

1 OF 2
AD A078264

LEVEL II (12)

RADC-TR-79-207
Final Technical Report
October 1979

AD A078264

VPE GROWTH OF (A1, Ga)As

Hewlett-Packard Company,

G. B. Stringfellow

DDC
RECEIVED
DEC 14 1979
E

APPROVED FOR PUBLIC RELEASE; DISTRIBUTION UNLIMITED

DDC FILE COPY

ROME AIR DEVELOPMENT CENTER
Air Force Systems Command
Griffiss Air Force Base, New York 13441

79 12 12 016

This report has been reviewed by the RADC Public Affairs Office (PA) and is releasable to the National Technical Information Service (NTIS). At NTIS it will be releasable to the general public, including foreign nations.

RADC-TR-79-207 has been reviewed and is approved for publication.

APPROVED: John K. Kennedy

JOHN K. KENNEDY
Project Engineer

APPROVED: Robert M. Barrett

ROBERT M. BARRETT, Director
Solid State Sciences Division

FOR THE COMMANDER: John P. Huss

JOHN P. HUSS
Acting Chief, Plans Office

If your address has changed or if you wish to be removed from the RADC mailing list, or if the addressee is no longer employed by your organization, please notify RADC (ESM), Hanscom AFB MA 01731. This will assist us in maintaining a current mailing list.

Do not return this copy. Retain or destroy.

UNCLASSIFIED

SECURITY CLASSIFICATION OF THIS PAGE (When Data Entered)

REPORT DOCUMENTATION PAGE

READ INSTRUCTIONS BEFORE COMPLETING FORM

1. REPORT NUMBER: RADC-TR-79-207	2. GOVT ACCESSION NO.
3. RECIPIENT'S CATALOG NUMBER	
4. TITLE (and Subtitle): VPE GROWTH OF (Al, Ga)As	5. TYPE OF REPORT & PERIOD COVERED: Final Technical Report. 15 Aug 1977 — 15 Feb 1979
6. PERFORMING ORG. REPORT NUMBER: N/A	
7. AUTHOR(s): G. B. Stringfellow	8. CONTRACT OR GRANT NUMBER(s): F19628-77-C-0199
9. PERFORMING ORGANIZATION NAME AND ADDRESS: Hewlett-Packard Laboratories, 1501 Page Mill Road, Palo Alto CA 94304	10. PROGRAM ELEMENT, PROJECT, TASK AREA & WORK UNIT NUMBERS: 62702F, 23061125, JL
11. CONTROLLING OFFICE NAME AND ADDRESS: Deputy for Electronic Technology (RADC/ESM), Hanscom AFB MA 01731	12. REPORT DATE: October 1979
	13. NUMBER OF PAGES: 132
14. MONITORING AGENCY NAME & ADDRESS (if different from Controlling Office): Same	15. SECURITY CLASS. (of this report): UNCLASSIFIED
	15a. DECLASSIFICATION/DOWNGRADING SCHEDULE: N/A

16. DISTRIBUTION STATEMENT (of this Report)

Approved for public release; distribution unlimited.

17. DISTRIBUTION STATEMENT (of the abstract entered in Block 20, if different from Report)

Same

18. SUPPLEMENTARY NOTES

RADC Project Engineer: John K. Kennedy (ESM)

19. KEY WORDS (Continue on reverse side if necessary and identify by block number)

$Al_xGa_{1-x}As$
Semiconductor
Vapor Phase Epitaxy
Organometallic CVD
Crystal Growth
Lasers

20. ABSTRACT (Continue on reverse side if necessary and identify by block number)

The organometallic vapor phase epitaxial (OMVPE) growth process was utilized for the growth of $Al_xGa_{1-x}As$ alloys in both hot wall and cold wall reactor systems. Growth parameters including substrate temperature, V/III ratio, flow ratio, etc. were studied together with their influence on the electrical transport and luminescent properties of the epitaxial layers. Both p-type (Zn) and n-type (Te) dopants were used to achieve the desired doping profiles.

(Cont'd)

DD FORM 1 JAN 73 1473

UNCLASSIFIED

SECURITY CLASSIFICATION OF THIS PAGE (When Data Entered)

403302

Item 20 (Cont'd)

Carbon and oxygen were found to be significant contaminants in these layers and two approaches to minimizing their concentration were studied. In the hot wall system HCl was added to the gas stream; in the cold wall system the use of graphite baffles was found to reduce the concentration of non-radiative centers. The photoluminescence efficiency of layers grown under optimized conditions were found to be comparable to that of LPE layers. Deep level transient spectroscopy (DLTS) measurements revealed two characteristic levels at approximately 0.41 eV and 0.49 eV respectively, with a weak dependence on compositions.

Double heterostructure lasers were successfully fabricated from these layers and exhibited threshold current densities within a factor of 2 of layers of the same geometry using LPE material.

Accession For
NTIS GRA&I
DDC TAB
Unannounced
Justification
By
Distribution/
Availability Codes
Dist. | Avail and/or special
A

PREFACE

This report covers work performed under Contract No. F1978-77-C-0199 from 15 August 1977 through 15 February 1979 by the Solid State Laboratory of Hewlett-Packard Laboratories, 1501 Page Mill Road, Palo Alto, California 94304.

The purpose of this contract was to assess and demonstrate the applicability of a chemical vapor deposition process using organometallic compounds for the epitaxial and heteroeptiaxial growth of GaAs and AlGaAs device structures on single crystal GaAs substrates.

The technical contract monitor for this project was Mr. John Kennedy. The work was conducted by Mr. Gilbert Hom and Mr. Tracy Hall under the project supervision of Dr. Gerald Stringfellow in HP Laboratories Materials Research Department. Contributions by Dr. E. Wagner and Mr. D. Mars are also acknowledged.

TABLE OF CONTENTS

Section		Page
I.	Introduction	1
II.	Experimental	6
	A. Ion Implantation	6
	1. Hot Wall Reactor	6
	2. Cold Wall Reactor	12
	B. Characterization	14
	1. Growth Properties	14
	2. Photoluminescence	14
	3. Carrier Concentration and Mobility	17
	4. Deep Level Transient Spectroscopy (DLTS)	20
	5. Trace Impurity Analysis	20
III.	Results and Discussion	23
	A. Hot Wall Reactor	23
	1. Optimization of Growth Parameters	23
	a. V/III Ratio	23
	b. HCl/III Ratio	26
	c. Substrate Temperature	28
	d. Diluent Flow Rate	31
	e. Growth of Heterostructures	36
	f. Analysis of Growth Rate and Composition	40
	g. P-Type Doping	45
	h. Photoluminescence Characterization	49
	i. Room Temperature PL	49
	i. Growth of Laser Structures	65
	B. Cold Wall Reactor	70
	1. Effect of Baffles	70
	2. Effect of V/III Ratio and T	77
	3. N-Type Doping	82
	4. Laser Performance	85
	C. Characterization of Hot- and Cold-Wall OMVPE	91
	1. Electron Mobility	91
	a. Analysis	94
	2. SIMS and Auger Analysis	105
	3. Deep Level Transient Spectroscopy	106
	D. Summary and Conclusions	113

LIST OF ILLUSTRATIONS

Figure No.		Page
1	Schematic diagram of reactor used for "Hybrid" VPE growth of $Al_xGa_{1-x}As$.	8
2	Schematic diagram of the gas control system for VPE reaction.	9
3	Detailed diagram of the graphite mixing zone for the hot wall VPE reactor.	10
4	Schematic diagram of reactor used for cold wall organo-metallic VPE growth of $Al_xGa_{1-x}As$.	13
5	PL spectra for two typical specimens of VPE $Al_xGa_{1-x}As$	15
6	IR reflectance spectrum for sample of $Al_{.36}Ga_{.64}As$.	18
7	Wavelength of plasma minimum versus n determined from van der Pauw measurements.	19
8	Width at half maximum versus doping level for both n- and p-type $Al_xGa_{1-x}As$ grown by VPE and LPE.	21
9	Schematic diagram of DLTS apparatus.	22
10	Growth rate and X^s_{AlAs} versus V/III ratio in the gas stream.	24
11	Edge and 1.2 eV PL intensities versus V/III ratio in the gas stream.	25
12	Growth rate and Al distribution coefficient versus ratio of HCl alkyls entering the reactor.	27
13	Edge and 1.2 eV peak intensities versus HCL/III ratio.	29
14	Growth rate versus 1/T for four orientations.	30
15	SEM photographs of growth pits formed in $Al_{.38}Ga_{.62}As$ layer with conditions such that surface kinetics limit growth rate.	32
16	AlAs mole fraction in the solid versus substrate temperature.	33
17	PL intensity and $I_{1.2}/I_{edge}$ versus substrate temperature during growth.	34
18	Growth rate and Al distribution coefficient versus total flow rate.	35
19	Solid composition vs V/III ratio for different total flow rate.	37

LIST OF ILLUSTRATIONS (CONT'D)

Figure No.		Page
20	PL intensity and ratio of peak intensities for the 1.2 eV and edge peaks versus total flow rate.	38
21	Schematic diagram showing the range of growth parameters yield high quality $Al_xGa_{1-x}As$ layers in the hot wall OMVPE system.	39
22	Cross section of multilayer structure.	41
23	High resolution Auger profile of alternating ultra-thin layers of $Al_{.35}Ga_{.65}As$ and $Al_{.06}Ga_{.94}As$.	42
24	Hole concentration vs DEZ partial pressure.	47
25	PL halfwidth versus p-type doping level.	48
26	Edge PL intensity versus 1.2 eV peak intensity.	50
27	Edge PL intensity vs $N_D - N_A$ for hot wall OMVPE $Al_xGa_{1-x}As$.	53
28	Energy of IR peak versus energy band gap	55
29	PL spectra of hot wall OMVPE samples at 296°K and 96°K.	56
30	IR peak intensity versus reciprocal temperature.	57
31	IR peak energy versus temperature.	59
32	IR peak halfwidth versus $\sqrt{T}$.	60
33	Emission peak energy and halfwidth versus r_{GE}/r for $V_{AS}Ge_{AS}$, $V_{AS}Si_{AS}$ and the 1.2 eV center.	62
34	IR peak energy versus edge emission peak for undoped, Zn doped and Ge doped samples.	63
35	EBIC photograph of the cross section of a laser structure grown by the hot wall OMVPE technique.	68
36	PL intensity versus $N_D - N_A$ for cold wall OMVPE samples.	74
37	Growth rate versus number of baffles in the gas stream.	76
38	Carrier concentration versus V/III reactor.	79
39	Carrier concentration versus AsH_3 flow rate.	80
40	PL intensity versus growth temperature for cold wall OMVPE $Al_xGa_{1-x}As$.	81

LIST OF ILLUSTRATIONS (CONT'D)

Figure No.		Page
41	N-Type doping level versus dopant partial pressure.	84
42	EBIC photographs of cross sections for cold wall OMVPE laser structures.	86
43	Threshold current density of OMVPE lasers with $Al_xGa_{1-x}As$ active layers versus results for LPE lasers.	89
44	Mobility (300°K) versus $N_D - N_A$.	92
45	Mobility (77°K) versus $N_D - N_A$.	93
46	Mobility versus T for $Al_xGa_{1-x}As$.	95
47	Mobility versus T for $Al_xGa_{1-x}As$.	96
48	N_sQ (space charge scattering) versus X.	100
49	N_A vs N_sQ.	101
50	Mobility reduction due to alloying versus X.	104
51	DLTS spectra at various values of decay time constant for sample LS-122 in the cold wall OMVPE system.	108
52	Emission rate (1/ normalized by $1/T^2$) versus reciprocal temperature for OMVPE specimens.	109
53	Free electron concentration (296°K) versus sum of E_2 and E_3 concentrations for samples grown in the cold wall VPE system containing 3 baffles and 6 baffles plus SiC coated pedestal.	111
54	I_{PL}/n versus the sum of E_2 and E_3 trap concentrations.	112
55	Activation energies for E_2 and E_3 versus alloy composition E_a vs x is included for comparison.	114

LIST OF TABLES

Table No.		Page
I	Materials Used for VPE Growth of $Al_xGa_{1-x}As$	7
II	Summary of Data for Mg and Ge Doped VPE $Al_xGa_{1-x}As$	46
III	Properties of 1.2 eV luminescence	64
IV	Molar Flow Ratios	66
V	Characteristics of 3- and 4-Layer Strucutres for Lasers	67
VI	Summary of Laser Data	69
VII	Characteristics of $Al_xGa_{1-x}As$ Layers Grown With and Without the Presence of Cold Baffles	73
VIII	Summary of the Effects of V/III Ratio and Temperature	78
IX	Summary of N-Type Doping Runs	83
X	Summary of Laser Performance of Material From the Cold Wall Reactor	87
XI	Summary of Parameters for $Al_xGa_{1-x}As$	97
XII	Summary of Deep Level Transient Spectroscopy Results	110

EVALUATION

The $Al_x Ga_{-x} As$ III-V ternary alloy system has been the object of an intensive research effort since 1970. The nearly exact lattice match between alloys of this material and GaAs permits the growth of lattice matched heterostructural source and detector devices with direct bandgap energies from 1.43 to > 2.0 eV, an important range for opto-electronic devices. This alloy system has already been used to fabricate opto-electronic devices such as lasers, high radiance optical LEDs for optical communications systems, visible LEDs, integrated optics elements and circuits and high efficiency solar cells.

Several growth techniques have been used to try to prepare structures such as those listed above, however, by far the most successful, and the one used to prepare all of the above devices, has been liquid phase epitaxy (LPE). The LPE technique, however, is a technique primarily suited to laboratory useage and even there it suffers from several serious growth problems. From an economic point of view LPE offers little potential for scaling up for production. Vapor Phase Epitaxy (VPE) is the epitaxial technique which has been used in all large scale commerical semiconductor growth processes. Normal "Chloride" and "Hydride" VPE systems have had little success in handling the $Al_x Ga_{-x} As$ system. The objective of this contract was to investigate

the potential of a VPE system using organometallic and hydride intermediate for the growth of GaAs-Al_xGa_{1-x} as double heterojunction laser structures. If successful this work would provide a truly scalable VPE technique for the fabrication of devices based on the GaAs-$Al_xGa_{1-x}As$ system. This work is in direct consonance with RADC-TPO-5 (C^3 systems Availability) in that it would provide the technology base for the fabrication of opto-electronic devices for optical communications systems.

This was a very successful contract. The results clearly indicate that a combincation of organometallic and hydride intermediate can be successfully used to prepare lattice matched GaAs-Al_x Ga_{1-x} as heterostructures and that double heterojunction lasers with J_{th} values approximately 2 times those of equivalent LPE material can be easily prepared. This system is also scalable for production. Such a scale-up should have a dramatic effect on reducing the cost of all GaAs-Al_x Ga_{1-x} as heterostructure devices.

JOHN K. KENNEDY
Project Engineer

SECTION I

INTRODUCTION

Since 1970, interest in $Al_xGa_{1-x}As$ has grown to the point that currently the R&D efforts on this material surpass those of all other III/V compounds and alloys. This is because the nearly exact lattice parameter match between GaAs (a_o = 5.654) and AlAs (a_o = 5.661) allows the growth of lattice matched heterosturctures with nearly ideal interfaces and direct bandgap energies covering an important range for optoelectronic devices from 1.43 to > 2.0 eV. This combination of properties has allowed fabrication of such optoelectronic devices as lasers, high radiance IR LEDs for optical communication applications, visible LEDs, integrated optics elements and circuits, and high efficiency solar cells.[1]

A number of techniques used for the growth of III/V semiconductors might be applied to the growth of $Al_xGa_{1-x}As$, including liquid phase, vapor phase and molecular beam epitaxial growth (LPE, VPE and MBE, respectively).

Nearly all of the devices listed above are fabricated in $Al_xGa_{1-x}As$ grown by the LPE technique. This technique is relatively simple and is well suited for the small scale laboratory efforts where scale, yield (uniformity and reproducibility) and economics play little role in determining the optimum growth technique. However, the LPE process suffers from several important problems: thickness nonuniformity, compositional nonuniformity in lateral and vertical directions and most importantly, growth defects such as incomplete melt removal, terraces,[2] and "meniscus line" defects.[3] The latter have recently been shown to introduce actual discontinuities in the thin (0.2 μm) active layers of injection laser structures.[4,5] These defects are unique to LPE.[3] Another difficulty with LPE is that multilayer growth requires a

series of substrate insertion - growth - substrate removal steps. This compounds the problems. VPE and MBE techniques appear to be much more suitable for multilayer growth.

MBE is basically a highly controlled physical vapor deposition process. It has great advantages for the growth of laser structures because of the very slow growth rate and precise control of doping and composition profiles obtainable by this technique.[6] However, it is still a very exploratory technique the practical usefulness of which may be limited by the fact that it is performed in a relatively expensive high vacuum apparatus and because of the inherently slow growth rate ($\sim$ 0.02 μm/min) and limited deposition area.

Vapor phase epitaxy is the technique used for all large scale commercial semiconductor growth operations. For these systems, the limitations of LPE can be overcome even in large scale operations where over 1300 cm^2 of material are produced in each run with excellent control of thickness, composition (for $GaAs_xP_{1-x}$ alloys) and doping level. The vapor phase process is generally superior to LPE in the areas of morphology and defect control. Since the surface of the growing layer contacts only the vapor phase, there are naturally no problems with either wipe-off or meniscus line defects. Since the growth process is not driven by the supersaturation due to cooling, the taper of composition with layer thickness inherent in typical LPE processes is eliminated, as well as effects of convection and constitutional supercooling. An equally important advantage of VPE for $Al_xGa_{1-x}As$ structures is the ease with which composition or doping level can be changed by simply changing the flow rate of the appropriate gas or gases during the growth cycle. Effects such as an intentional taper in composition or doping level which are impossible by LPE are standard in VPE.

Since VPE has so many advantages over LPE and the $GaAs_xP_{1-x}$ VPE process was developed before the surge of activity in $Al_xGa_{1-x}As$ which began in ~ 1969, early attempts were made to apply the chloride transport process to the growth of $Al_xGa_{1-x}As$.[7-10] This work was never successful for the alloys because of inherent thermodynamic problems related to the fact that the optimum growth temperatures for GaAs and AlAs from the chlorides are so different.[11]

Another approach which has been somewhat more successful has been the growth of $Al_xGa_{1-x}As$ by using volatile organometallic Al and Ga compounds to transport the metals into the reaction zone. Very little work has been reported in this area, but early results indicate that lower temperature growth is possible with excellent control of both alloy composition and morphology.[12] Unfortunately, problems with high levels of C and/or O contamination initially resulted in highly compensated materials with photoluminescence intensities many orders of magnitude lower than in comparable LPE material.[11,13]

The problem of oxygen contamination in VPE growth of $Al_xGa_{1-x}As$ as compared to LPE growth can be simply illustrated. In LPE the stability of Al_2O_3 results in the gettering of essentially <u>all</u> oxygen from the melt to form a thin Al_2O_3 crust at the surface. At 1000°K the free energy of formation of Al_2O_3 is -325 kcal/mole.[14] Even for x_{Al} as low as 10^{-4} in the liquid the equilibrium oxygen concentration is $\sim 10^{-42}$. Even though the solid-liquid distribution coefficient would be very large, it is clear that for a reasonable growth rate, near equilibrium, essentially no oxygen could be incorporated into the solid. In real cases nonequilibrium factors, such as allowing insufficient time for the oxygen to diffuse from the inside of

the melt to the solid crust, result in some oxygen incorporation, but carefully controlled growth conditions result in very low levels of oxygen contamination. This "gettering" of oxygen is not normally effective during VPE growth. Under normal growth conditions of 2 ℓ/min total flow rate and 1 ppm of O_2 or H_2O contamination from minute leaks and desorption from walls, large amounts of oxygen are incorporated into the solid. Assuming a large O distribution coefficient and a 5% reactor efficiency, i.e., 5% of the gas passing through the reactor is able to equilibrate with the substrate, $> 10^{18}$ oxygen atoms per cm^3 could be incorporated into the solid grown by VPE.

Carbon contamination must also be considered. Because every Al atom is bonded to three carbon atoms in the vapor phase, and the Al-C bond is very strong, considerable carbon contamination of the solid might be anticipated.

Two approaches to minimizing C and O contamination have been pursued during the 18 month contract period. The first was to use a hot wall system with HCl added to replace $-CH_3$ by -Cl in the gas phase to reduce C contamination. The second approach was to use graphite baffles to catalyze the reaction between $Al(CH_3)_3$ and residual O_2 and/or H_2O to form solid Al_2O_3. This approach was also used in the cold wall system where cold graphite baffles, were used without the addition of HCl to the system, with the hope that the presence of baffles would lower the nucleation barrier and allow growth of Al_2O_3 on the baffle surfaces even at room temperature. Each of the two appraoches will be described in separate sections.

The conclusion reached after comparing results for the two techniques is that the cold wall system with baffles is superior in both simplicity of operation and control and in actual material quality. Photoluminescence

efficiencies have been obtained which are similar to those obtained in comparable LPE material, and the doping level is typically $\sim 10^{15}$ cm^{-3}. Stripe geometry double heterostructure lasers have been fabricated in early material of this type yielding $J_{th} \approx 6$ kA/cm^2 approximately 2x higher than obtained using comparable LPE material.

SECTION II
EXPERIMENTAL

A. CRYSTAL GROWTH

The transport agents used in the various phases of the project are listed in Table I. TMA, TEG, AsH_3 and HCl were used for the experiments in the hot wall system and TMA, TMG and AsH_3 were used for the cold wall system with DEZ used for p-type doping (GeH_4 and Mg were tried without success) and H_2S, SiH_4 and DETe for n-type doping. The latter were purchased diluted in H_2 and thus the entry in the last column simply represents their concentration in the cylinder.

The substrates used were n^+ (Te-doped) and semi-insulating (Cr-doped) GaAs obtained from the Optoelectronics Division of Hewlett-Packard. They were oriented on the (100) plane to within 1/2° and polished using standard bromine and methanol techniques.

1. Hot Wall Reactor

The hot wall reactor used for this study is shown schematically in Fig. 1. It is basically an rf heated, hot wall system fabricated using high purity Poco graphite. Hydrogen is bubbled through temperature controlled cylinders of triethylgallium (TEG) and trimethylaluminum (TMA) as shown in the diagram of the gas control system, Fig. 2. AsH_3 is used as the source of the As and purified H_2 as the carrier gas. HCl is added to the system to reduce C contamination in the $Al_xGa_{1-x}As$.[11] A detailed diagram of the interior mixing region of the apparatus is shown in Fig. 3. This has been varied somewhat in an attempt to attain complete mixing, but this particular configuration was finally settled upon. It contains the following desirable

TABLE I.

Materials Used For VPE Growth of $Al_xGa_{1-x}As$

Material	Source
Triethylgallium (TEG)	Alpha Ventron Sumitomo Chemical Co., Ltd. (Semiconductor Grade)
Trimethylgallium (TMG)	Alpha Ventron
Trimethylaluminum (TMA)	Alpha Ventron Sumitomo Chemical Co., Ltd. (Semiconductor Grade)
HCl	Scientific Gas Products
AsH_3	Scientific Gas Products
Diethylzinc (DEZ)	Alpha Ventron
Diethyltelluride (DETe)	Scientific Gas Products
H_2S	Scientific Gas Products
SiH_4	Scientific Gas Products
GaAs (Te-Doped)	Optoelectronic Division (Hewlett-Packard)
GaAs (Si-Doped)	Laser Diode Lab

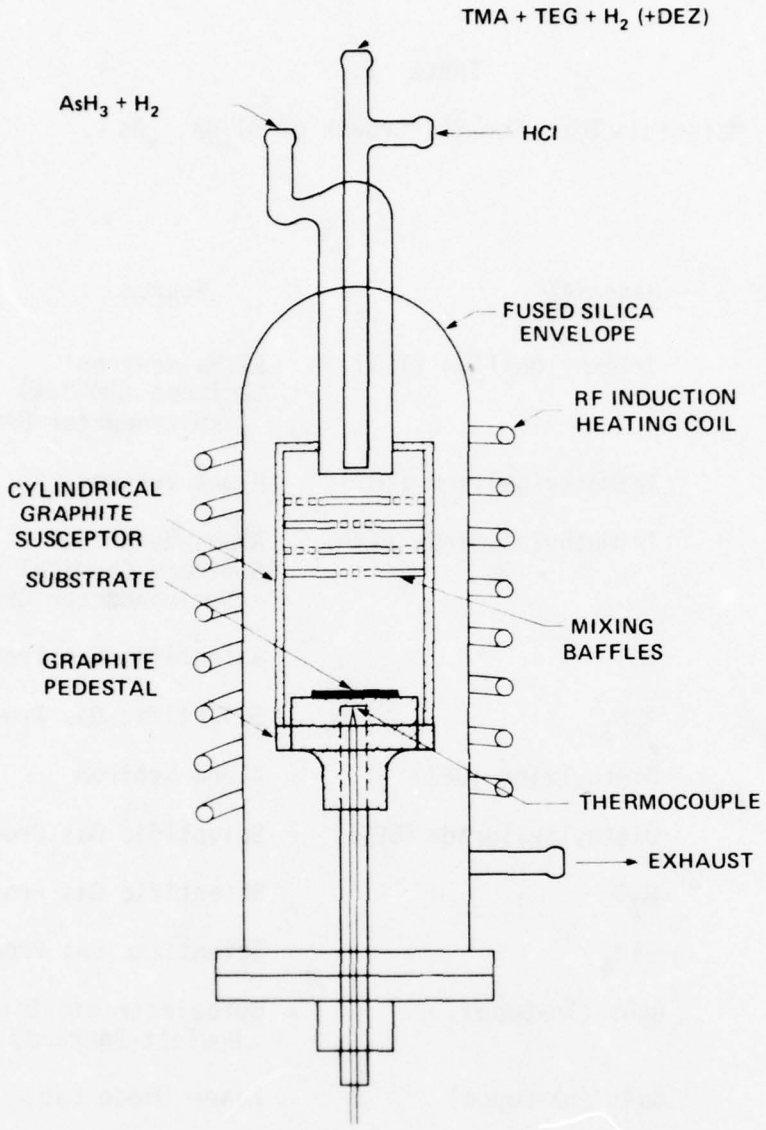

Figure 1. Schematic diagram of reactor used for "Hybrid" VPE growth of $Al_xGa_{1-x}As$.

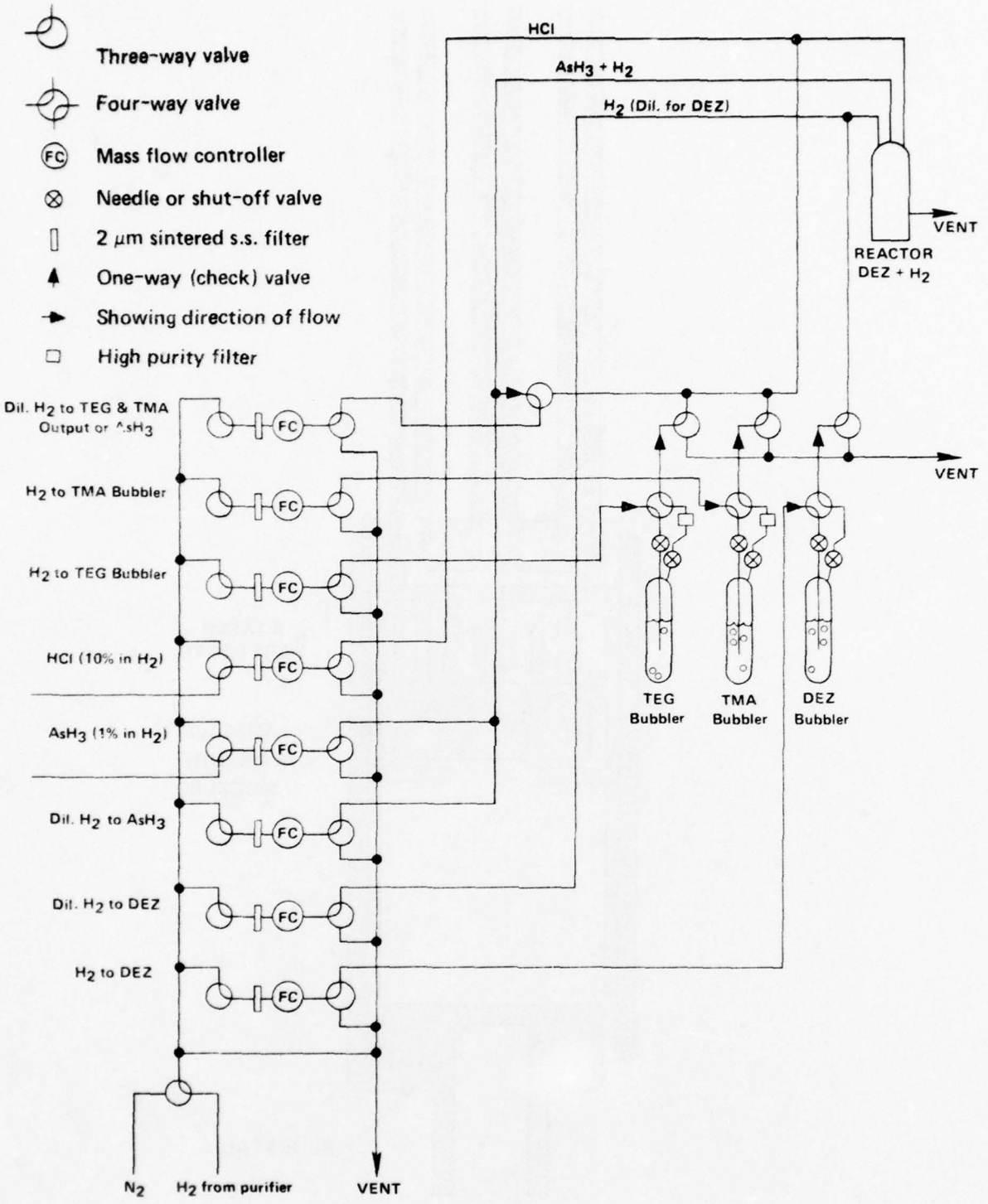

Figure 2. Schematic diagram of the gas control system for VPE reactor.

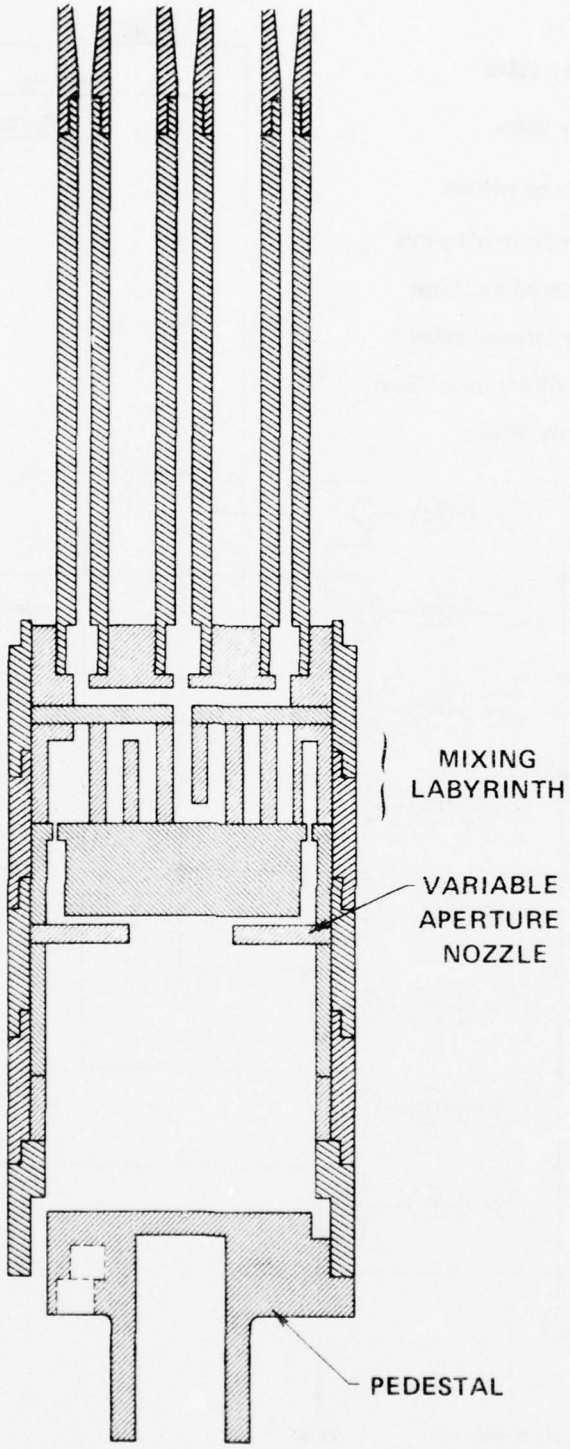

Figure 3. Detailed diagram of the graphite mixing zone for the hot wall VPE reactor.

features:

1. Confinement of the mixing region to the very hottest part of the reactor which should eliminate AlAs predeposition on lower temperature baffles
2. Elimination of a final perforated baffle used in earlier designs, to improve homogeneity of flow rate to the pedestal. For earlier designs the hole pattern of the baffle was often reproduced in the morphology of the epilayer.
3. Use of a "nozzle" as the final baffle to allow control of the gas velocity impinging upon the substrate.

The gases enter the graphite through three graphite tubes and are immediately mixed and forced through a 2 mm diameter opening into a mixing labyrinth. The mixing is very thorough because the gases must pass through a long tortuous path. The gases exit through the "nozzle", an annular disk for which the diameter of the exit hole may be selected in the range from 0.2 to 4 cm. No graphite parts are in the central portion of the gas stream in the decreasing temperature zone where predeposition might occur.

Particular effort was devoted to ensuring that the growth system was as leak-free as possible, since the formation of Al_2O_3 during growth would be expected to prevent the growth of high quality layers. An oxygen monitor (Research Inc., Minneapolis, Minnesota) used to monitor oxygen concentration in the exit gas stream before the beginning of growth typically indicated oxygen concentrations of < 0.3 ppm.

In order to detemine with the least possible uncertainty the effect of a single parameter on the growth and materials characteristics, many multilayer experiments were performed. In these experiments, the

parameter of interest was varied in steps in a single growth run. The morphology and growth rate for each layer were determined by examining a cleaved cross section of the multilayered structure. The composition and photoluminescence (PL) characteristics were measured by careful etching to reveal the layer of interest. This technique was found to avoid small run-to-run variations in any parameters which we cannot measure or control such as tiny leaks, variations in substrate quality, orientation or preparation, etc.

2. Cold Wall Reactor

The cold wall reactor used in these studies is similar to systems reported previously. However, we have inserted a number of graphite baffles (disks with $\sim$ 300 1.5 mm diameter holes) directly into the gas stream just above the substrate. They are separated from the substrate by a distance of between 3.8 and 6.5 cm, far enough to avoid extensive heating of the baffles by radiation from the pedestal or by coupling into the rf field used to heat the pedestal.

As will be discussed in a later section the baffles are added to essentially catalyze the reaction of TMA with residual O_2 and/or H_2O in the system to allow gettering similar to that obtained during LPE growth of $Al_xGa_{1-x}As$.

The growth experiments were carried out in a conventional vertical, cold wall OMVPE system using TMA, TMG and AsH_3 in a purified H_2 ambient. The O_2 partial pressure was measured at the exhaust using a Research Inc. O_2 monitor and found to be < 0.4 ppm in all cases. The typical configuration is shown schematically in Fig. 4.

The substrate temperature was varied between 700°C and 760°C and the total flow rate was $\sim$ 2 ℓ/min. The AsH_3, TMA and TMG partial pressures

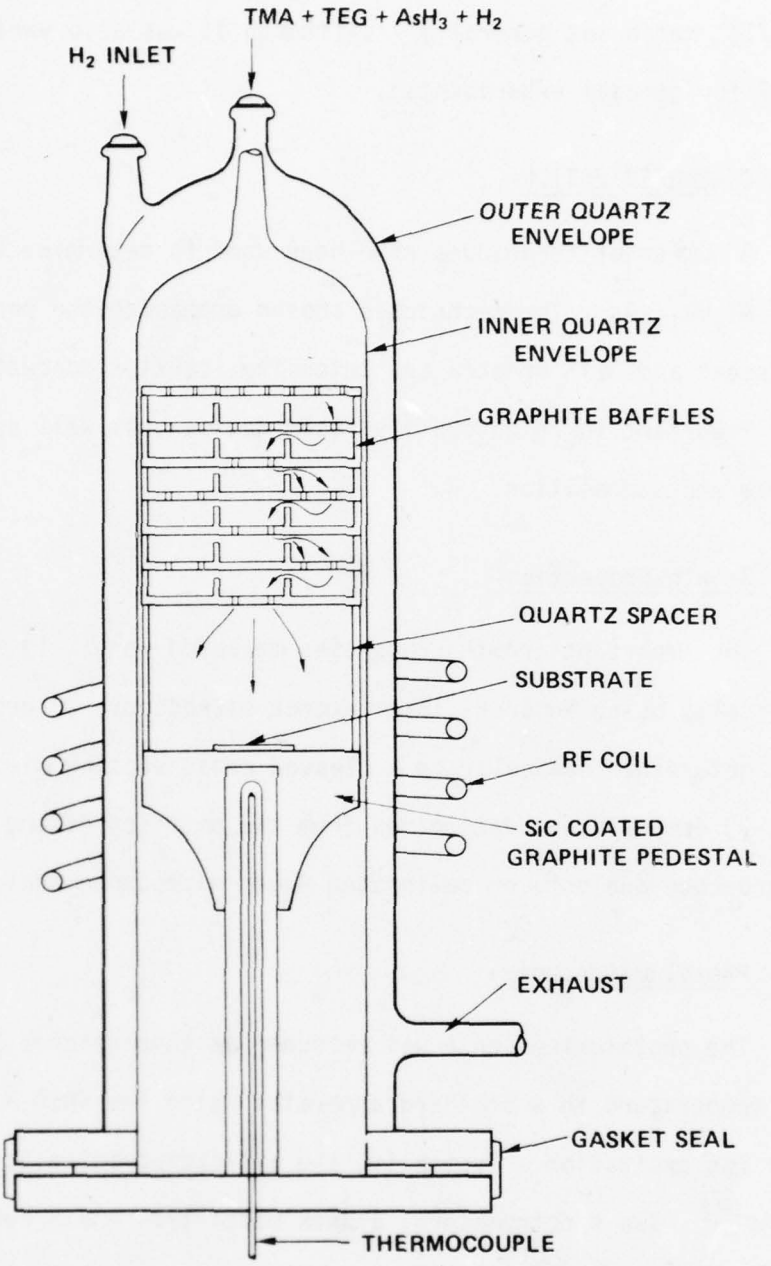

Figure 4. Schematic diagram of reactor used for cold wall organometallic VPE growth of $Al_xGa_{1-x}As$.

were varied but the AsH_3 flow rate was in the range 10^{-4} - 10^{-3} moles/min and the V/III ratio was generally 7 (although it was also varied between 2.4 and 27 for special experiments).

B. CHARACTERIZATION

A number of techniques have been used to determine the quality of the OMVPE $Al_xGa_{1-x}As$. The techniques chosen emphasize the properties, such as luminescent and DLTS spectra and intensity, carrier concentration and mobility, important for high quality laser devices, as well as morphology, growth rate and composition.

1. Growth Properties

The important growth properties measured were: 1) morphology, judged visually using Nomarski interference microscopy, 2) growth rate, thickness determined optically on a cleaved cross section divided by growth time and, 3) composition, determined from the position of the edge PL peak, x-ray microprobe analysis or calibrated Auger microprobe analysis.

2. Photoluminescence

The photoluminescence was measured at temperatures between 96°K and room temperature in a standard apparatus using the 4880 Å line from an Ar^+ laser for excitation. Typically, the excitation intensity was $\sim 2 \times 10^3$ W/cm^2. Two spectrometers, a Spex model 1704 and a Perkin Elmer model 13 were used with gratings blazed at 0.5 μm, 0.75 μm and 1.4 μm used in the appropriate wavelength ranges. Typical spectra for samples with $x = 0.05$ and $x = 0.32$ are shown in Fig. 5. The edge emission was detected using a cooled S-1 photomultiplier tube. The nonedge emission typically peaks in the

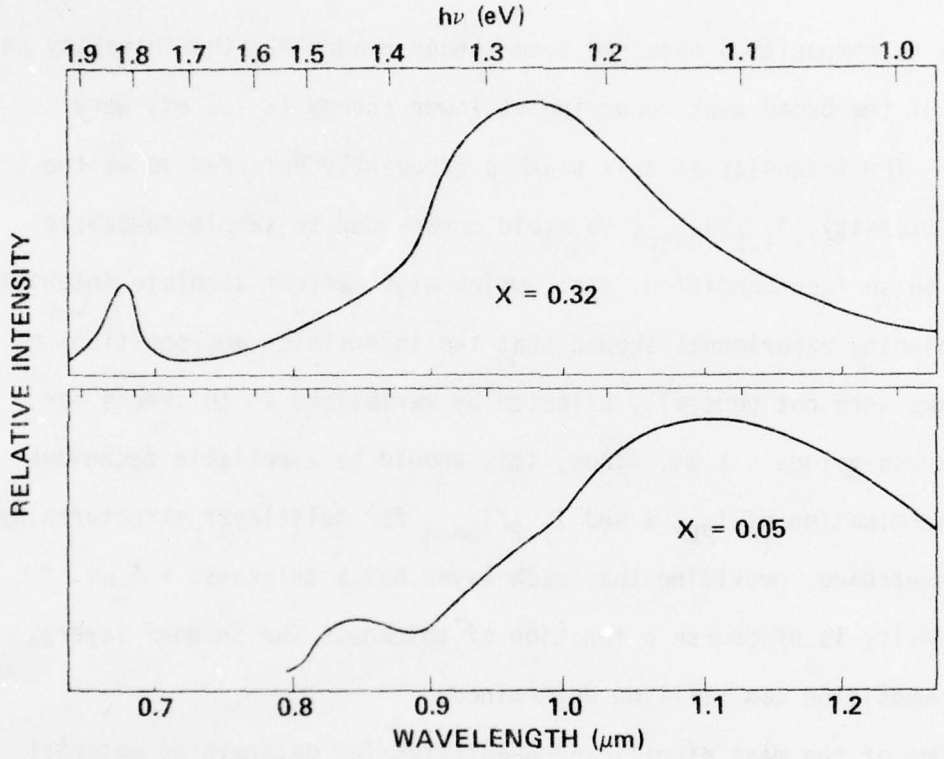

Figure 5. PL spectra for two typical specimens of VPE $Al_xGa_{1-x}As$.

$\sim$ 1.2 eV region where the S-1 response is rapidly decreasing. Hence an InAs photovoltaic detector cooled to 77°K was used. In both cases the spectra were corrected for detector response. The spectra shown in Fig. 5 are a synthesis of the S-1 and InAs spectra joined at $\sim$ 9200 Å. The composition was determined from the peak wavelength of the room temperature near edge emission using the relation.[15]

$$h\upsilon = 1.424 + 1.247\ x\ . \qquad (1)$$

In addition to composition obtained from the near edge PL, the intensity and wavelength of the broad peak occurring at lower energy ($\sim$ 1.2 eV) were determined. The intensity of this peak is frequently referred to as the edge peak intensity, $I_{1.2}/I_{edge}$, to avoid errors due to sample-to-sample variations in surface condition, etc., which might effect absolute intensity values. Thinning experiments showed that the intensities and positions of the two peaks were not generally affected by variations in thickness for total thickness values > 1 μm. Thus, this should be a reliable technique for the determination of I_{PL}, x and $I_{1.2}/I_{edge}$ for multilayer structures by progressive etching, providing that each layer has a thickness > 1 μm. The PL intensity is of course a function of thickness for thinner layers, although composition can still be determined.

One of the most significant quantities for determining material quality was found to be the intensity of the edge PL emission. This is always compared to the intensity of an LPE GaAs standard with $n = 3 \times 10^{17}$ cm^{-3}, so that minor changes in the apparatus do not affect the results and the PL efficiency of the OMVPE material can be compared directly to that of LPE material. For samples with $n < 5 \times 10^{15}$ cm^{-3} care must be taken because the ratio $I_{sample}/I_{standard}$ was found to vary with excitation intensity.

This is because of conductivity modulation of the sample and is avoided by simply measuring at lower laser intensity where the ratio is excitation intensity independent.

3. Carrier Concentration and Mobility

The carrier concentration was measured using a number of techniques: The standard van der Pauw measurement was used for single layer structures grown on semi-insulating substrates. Currents of 10^{-2} to 1 ma (depending on doping level) and magnetic field of 5 kG were typically used. On several specimens, the C-V measurement of Schottky barriers were used. This technique is most useful for fairly low doping levels. Another technique which is useful for thin, highly doped ($n > 5 \times 10^{17}$ cm^{-3}) n-type GaAs samples is the IR reflection technique. The position of the minimum due to plasma resonance has been found to be uniquely related to carrier concentration.[16] Because we need a technique for rapid evaluation of n in thin layers, not grown directly on semi-insulating substrates, we applied this technique to $Al_xGa_{1-x}As$ layers with $x < 0.3$ for which the carrier concentration was determined using the van der Pauw technique. The IR reflectance spectrum reproduced in Fig. 6 shows two minima in $Al_xGa_{1-x}As$,[17] characteristic of pure GaAs and pure AlAs phonons. Thus for the alloys, the first minimum must be a function of both x and n. The data for pure GaAs and $Al_xGa_{1-x}As$ alloys with $x \sim 0.10$ and $x \sim 0.30$ grown by both LPE and VPE are plotted in Fig. 7. At low doping levels, the positions of the two minima are clearly determined by x, but at high doping levels, the data seem to merge into a single line. Thus knowing x, the value of n can be determined using the IR reflection technique.

Another property which is a function of doping level and can be measured on thin layers in a multilayer structure is the halfwidth of the

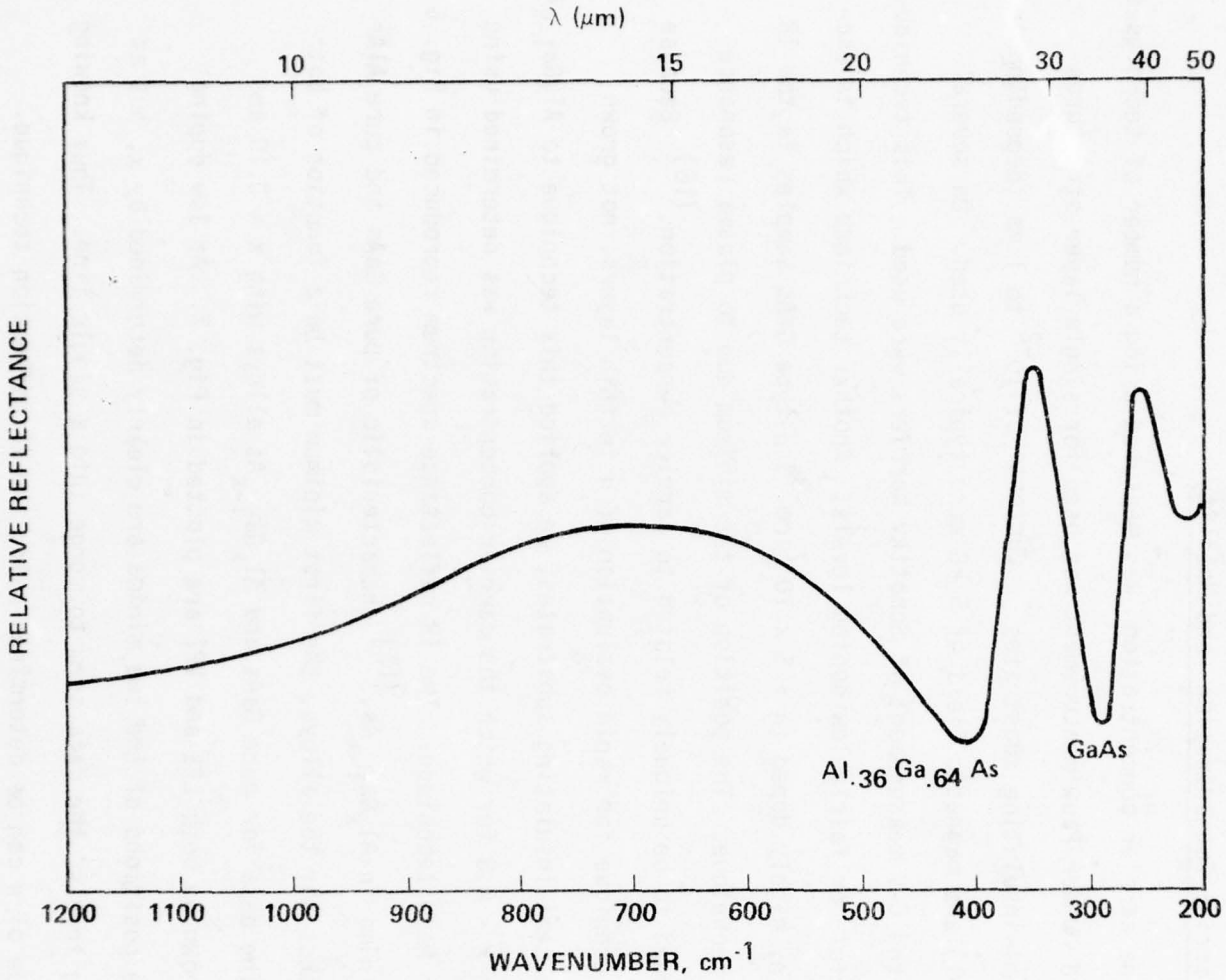

Figure 6. IR reflectance spectrum for sample of $Al_{.36}Ga_{.64}As$.

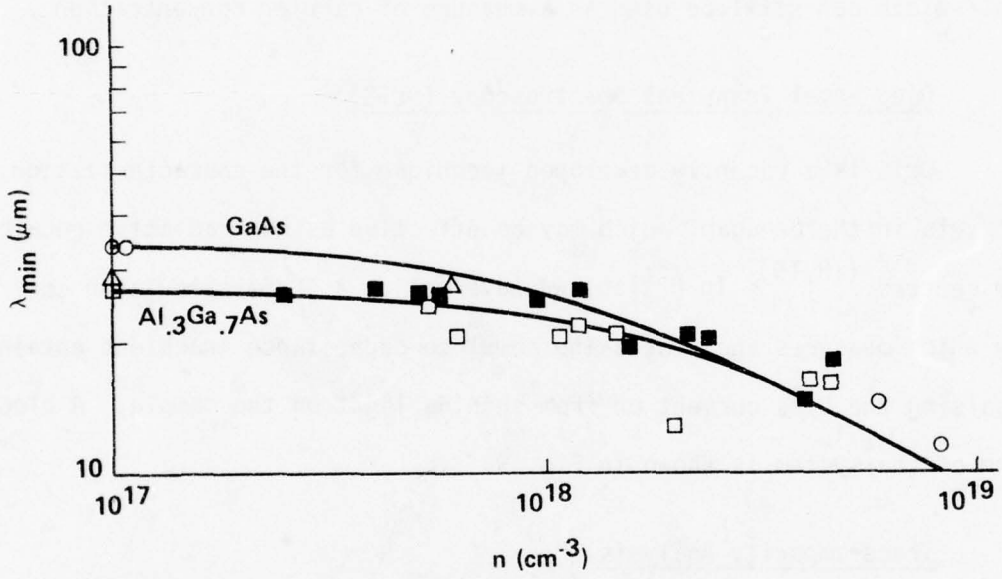

Figure 7. Wavelength of plasma minimum versus n determined from van der Pauw measurements.

edge PL emission peak. Because the effective mass changes so little with composition for $x < 0.35$ the half-width in meV is largely determined by n and is nearly composition independent. The half-width is plotted versus n for both LPE and VPE specimens with $x < 0.35$ in Fig. 8. The half-widths are observed to be somewhat broader for VPE specimens, but half-width does appear to be an indicator of maximum carrier concentration. For p-type material the effect is less pronounced due to the large hole effective mass, but half-width can still be used as a measure of carrier concentration.

4. Deep Level Transient Spectroscopy (DLTS)

DLTS is a recently developed technique for the characterization of deep levels in the bandgap, which may be effective as non-radiative recombination centers.[18,19] In HP labs we have set up a 9825A calculator controlled system which measures and stores the complete capacitance transient obtained from pulsing the bias current or from shining light on the sample. A block diagram of the system is shown in Fig. 9.

5. Trace Impurity Analysis

In-house Auger spectroscopy has been used to determine the O, C and Si content of the OMVPE layers. Through collaboration with the University of Illinois and Cameca Inc. in France we have also obtained SIMS analyses of several specimens.

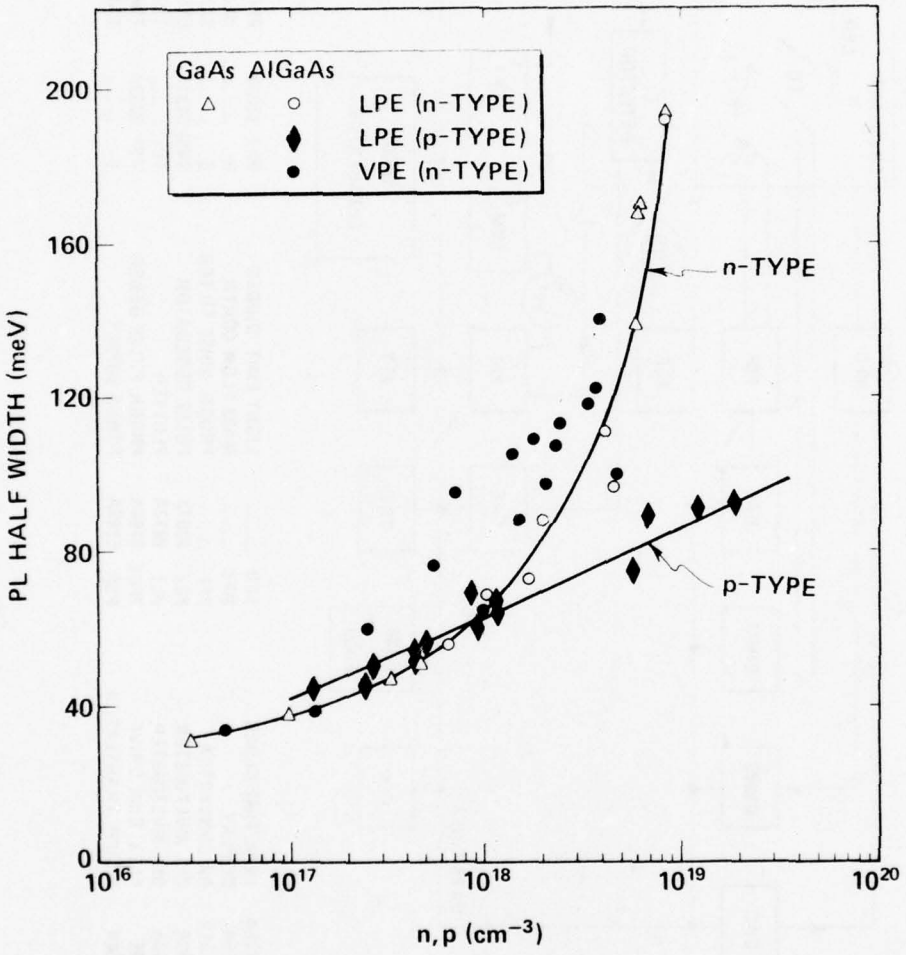

Figure 8. Width at half maximum versus doping level for both n- and p-type $Al_xGa_{1-x}As$ grown by VPE and LPE.

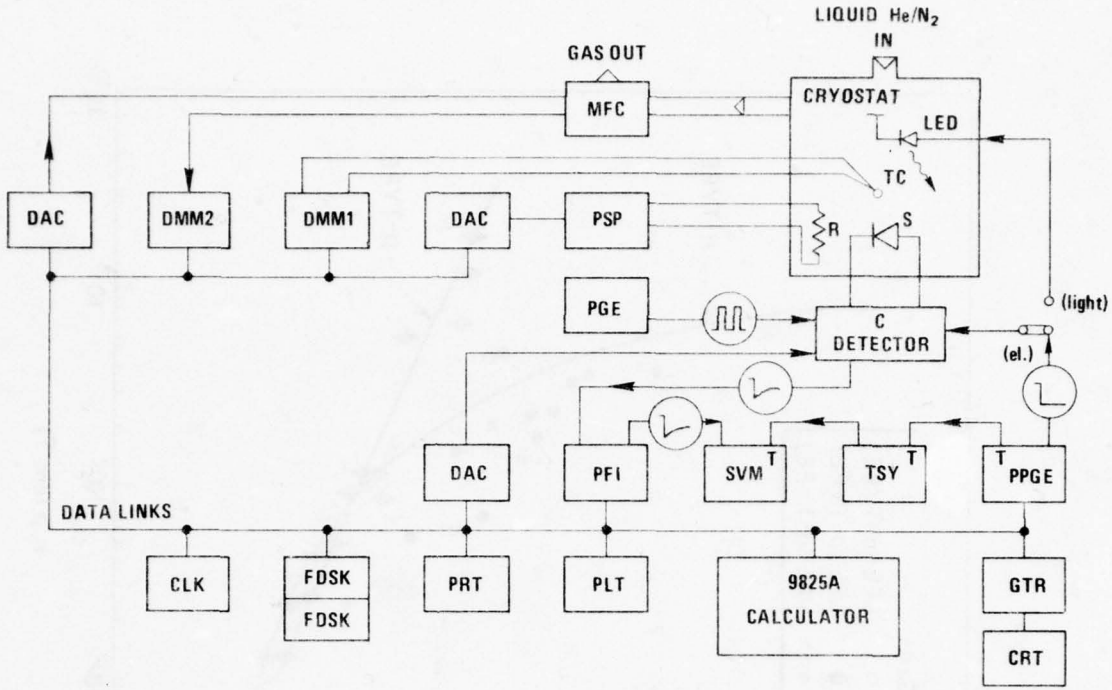

CLK	98035A	REAL TIME CLOCK	LED	.....	LIGHT EMIT. DIODES	PRT	9866A	PRINTER
CRT	1311A	DISPLAY	MFC	.....	MASS FLOW CONTR.	R	.....	HEATER
DAC	59501A	DA CONVERTER	PFI	.....	PROGR. NOISE FILTER	S	.....	SAMPLE
DMM1	3490A	DIG. MULTIMETER	PGE	8007B	PULSE GENERATOR	SVM	3437A	SYSTEM VOLTMETER
DMM2	3438A	DIG. MULTIMETER	PLT	9872A	PLOTTER	TC	.....	THERMOCOUPLE
FDSK	9885	FLEX. DISK DRIVE	PPGE	8160A	PROGR. PULSE GENER.	TSY	5359A	TIME SYNTHESIZER
GTR	1350A	GRAPH. TRANSLATOR	PSP	6289A	POWER SUPPLY	T	.....	TRIGGER IN/OUTPUT

Figure 9. Schematic diagram of DLTS apparatus.

SECTION III
RESULTS AND DISCUSSION

A. HOT WALL REACTOR

1. Optimization of Growth Parameters

a. V/III Ratio

The V/III ratio (moles of AsH_3/moles of TMA + TEG) in the input gas stream was varied by simply varying the initial AsH_3 flow rate into the reactor keeping all other parameters constant (T = 754°C, HCl/III = 1.21, Al/III = 0.43, total flow rate = 0.82 ℓ/min). The total alkyl flow rate was 2.445 sccm for all the data presented for the hot wall reactor. The results are plotted in Fig. 10. The general trend to decreasing growth rate for lower V/III ratio is understandable since for V/III ratios of less than unity the mass transport of As to the growing interface would likely be the controlling step. The Al distribution coefficient is found to be quite insensitive to the V/III ratio in this range. The dependence of PL intensity on V/III ratio is more interesting. As shown in Fig. 11 the edge emission intensity increases and the 1.2 eV emission intensity decreases as the V/III ratio increases. This is the inverse behavior of III/V compounds grown in pure chloride systems.[20,21] The background doping level changes by less than 50% with changing V/III ratio, similar to earlier results.[11]

In pure organometallic systems, good morphologies are obtained for high V/III ratios, in the range of 3-6.[12,22] In this hybrid system, V/III ratio has a relatively small effect on morphology. However, at very low values of V/III ratio, stacking faults appear in the layers, similar to those causing pyramids for chloride VPE of other III-V systems at low

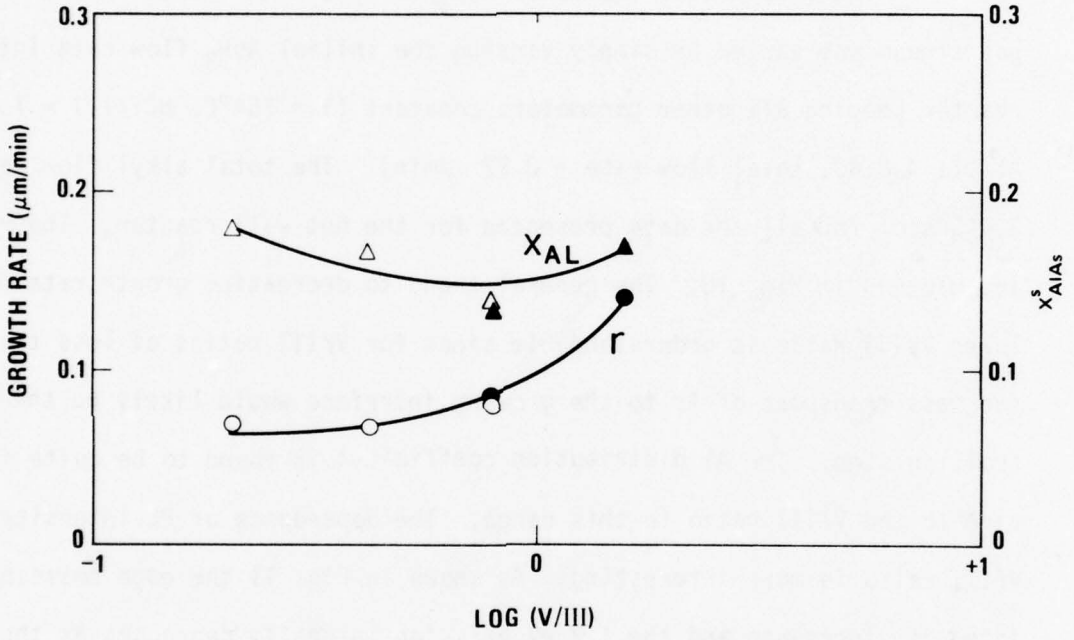

Figure 10. Growth rate and X^S_{AlAs} versus V/III ratio in the gas stream.

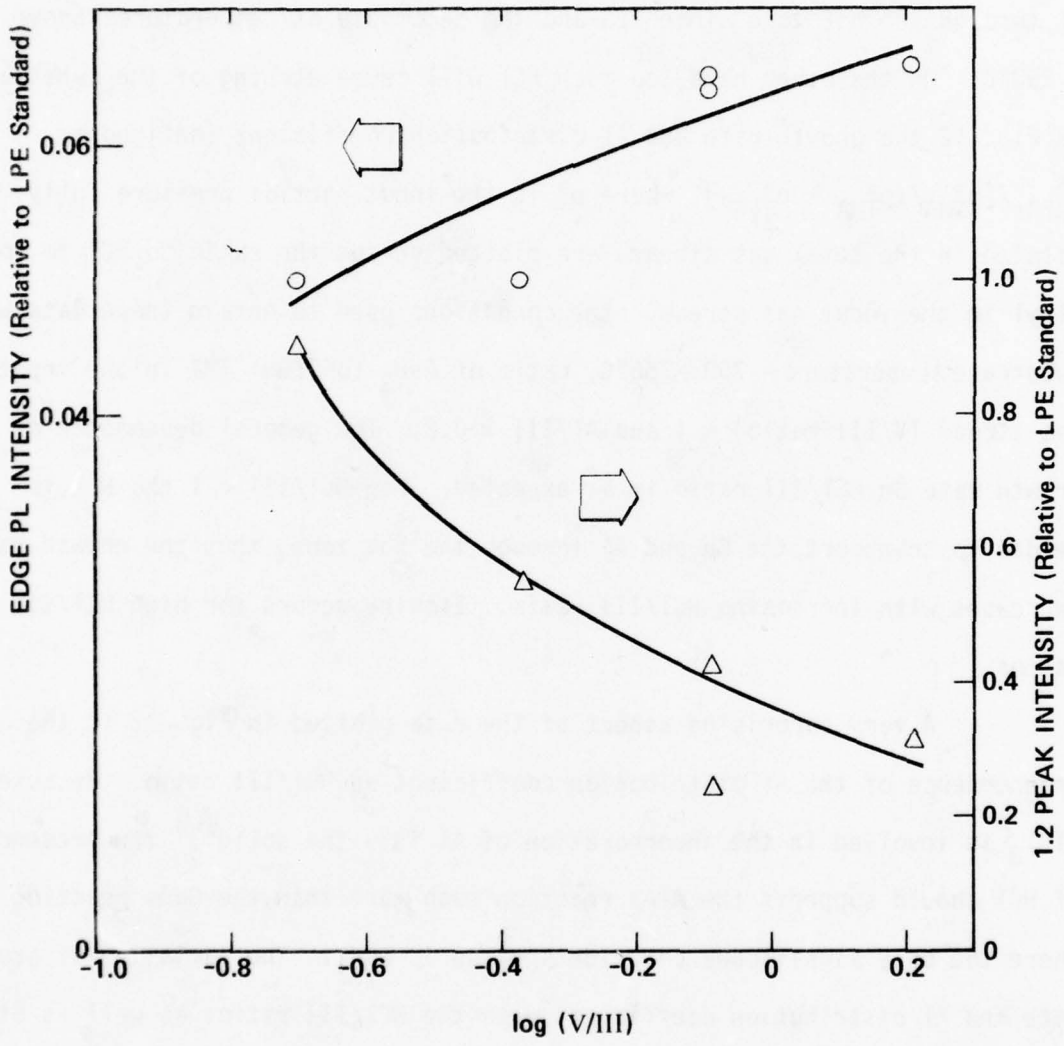

Figure 11. Edge and 1.2 eV PL intensities versus V/III ratio in the gas stream.

V/III ratios.[23]

b. HCl/III Ratio

An important parameter in the hybrid system is the amount of HCl entering the reactor. The HCl is necessary to allow transport of the Ga and Al through the hot zone since TEG and TMA decompose at temperatures above $\sim$ 250°C. On the other hand too much HCl will cause etching of the substrate. In Fig. 12 the growth rate and Al distribution coefficient (defined as $x^s_{AlAs}/[p^\circ_{TMA}/(p^\circ_{TMA} + p^\circ_{TEG})]$, where p° is the input partial pressure fully diluted in the total gas stream) are plotted versus the ratio fo HCl to total alkyl in the input gas stream. the conditions used to obtain these data were: substrate temperature = 750°-756°C, ratio of AsH_3 to TEG + TMA in the input gas stream (V/III ratio) $\approx$ 1 and Al/III $\approx$ 0.2. The general dependence of growth rate on HCl/III ratio is as expected. For HCl/III < 1 the HCl is needed to tranpsort the Ga and Al through the hot zone, thus the growth rate increases with increasing HCl/III ratio. Etching occurs for high HCl/III ratios.

A very surprising aspect of the data plotted in Fig. 12 is the independence of the Al distribution coefficient on HCl/III ratio. Because $AlCl_3$ is involved in the incorporation of Al into the solid[11] the presence of HCl should suppress the AlAs reaction much more than the GaAs reaction where the only significant chloride species is GaCl. The variation of growth rate and Al distribution coefficient with the HCl/III ratio, as well as other growth parameters will be discussed and compared with the results of a thermodynamic calculation in section f below.

The PI intensity measured relative to a standard of typical good quality LPE GaAs grown at Hewlett-Packard Labs with $n = 3 \times 10^{17}$ cm^{-3} is

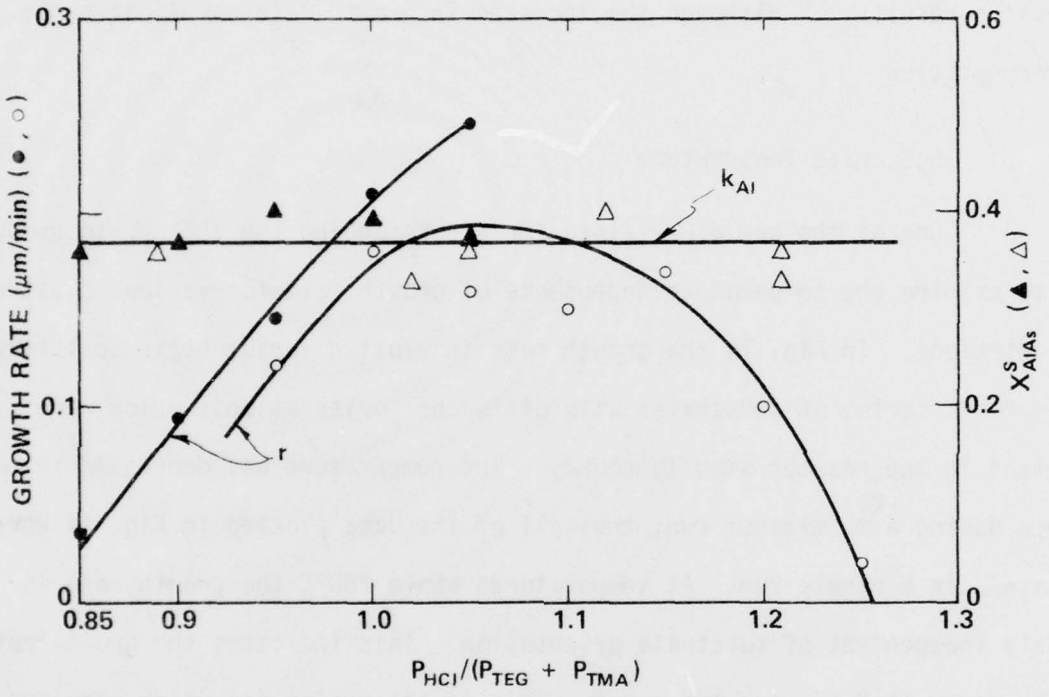

Figure 12. Growth rate and Al distribution coefficient versus ratio of HCl alkyls entering the reactor.

plotted versus HCl/III ratio in Fig. 13. It increases by nearly an order of magnitude as HCl/III is increased from 0.85 to 1.05. The intensity of the IR peak shown in Fig. 5, termed the 1.2 eV emission peak, is also plotted in Fig. 13. It gradually decreases as HCl/III increases. These data were obtained from the PL half-width varied by only $\sim$ 20%. The increase in PL intensity may be related to reduced C incorporation as suggested by previous results,[11] although the increase in growth rate complicates the interpretation.

c. Substrate Temperature

One of the key experiments for understanding the VPE growth process is to examine the temperature dependence of growth rate for various substrate orientations. In Fig. 14 the growth rate is plotted versus reciprocal temperature for a series of substrates with different orientations, which were present in the reactor simultaneously. The temperature was decreased in steps during a multilayer run; thus all of the data plotted in Fig. 14 were obtained in a single run. At temperatures above 750°C the growth rate is nearly independent of substrate orientation. This indicates the growth rate to be controlled by mass transport. This is the region for which previous experiments indicated the growth rate to be mass tranpsort limited.[11] At lower temperatures the growth rate is strongly dependent on substrate orientation. This indicates the growth rate to be controlled by surface kinetic processes. The ordering $r_{(111)A} > r_{(100)} > r_{(110)} > r_{(111)B}$ is the same as reported by Shaw[24] for the chloride VPE growth of GaAs, although this is likely to be dependent on exact growth conditions. At low temperatures the growth on (100) oriented substrates is clearly unstable in the sense that pits which might form having (111)B and/or (110) faces would be stable and

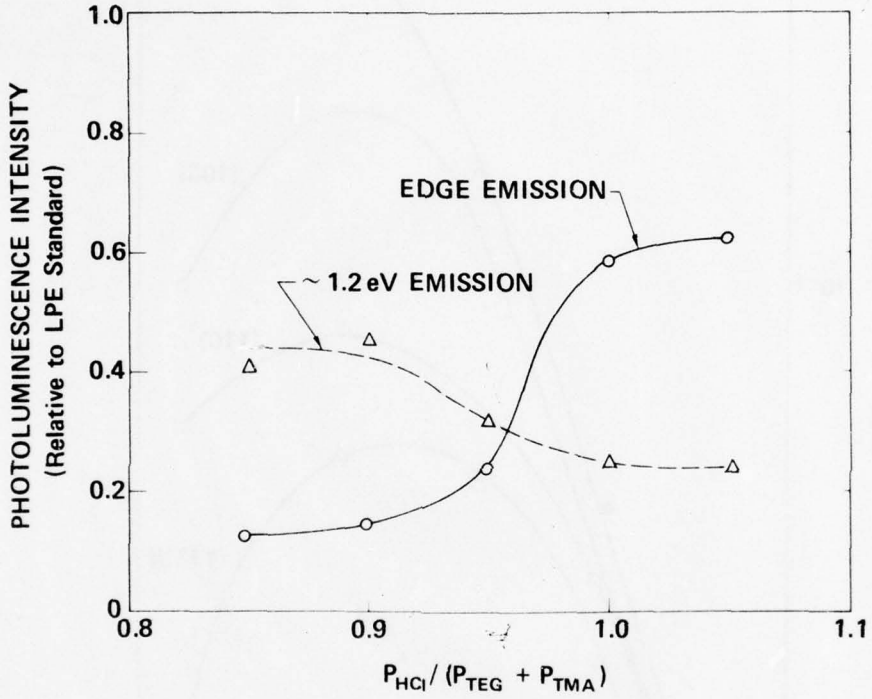

Figure 13. Edge and 1.2 eV peak intensities versus HCL/III ratio.

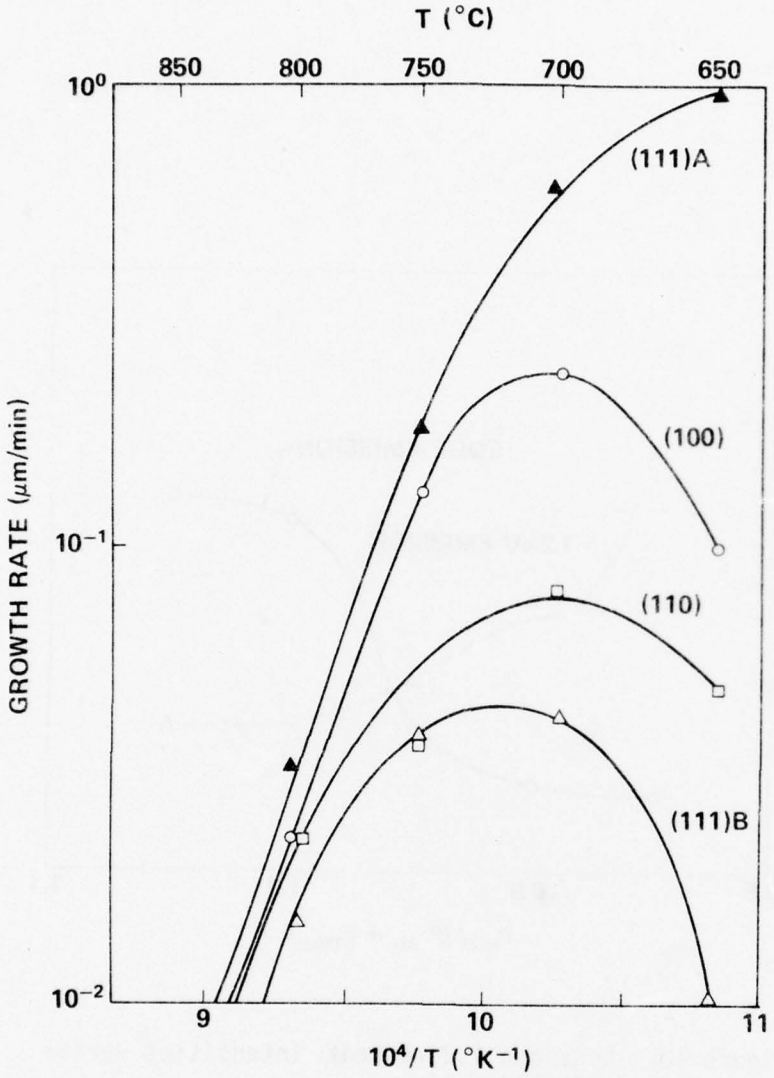

Figure 14. Growth rate versus 1/T for four orientations.

would become progressively larger during growth of the layer. Such pits are indeed observed as shown in the SEM photographs of Fig. 15. Under these growth conditions the substrate temperature must be kept above 750°C to achieve reproducibly good surface morphology.

The effect of growth temperature on Al distribution coefficient is shown in Fig. 16 for a series of runs grown under various conditions. The dependence is generally as expected from the thermodynamic calculations previously reported.[11] As temperature is increased the driving force for the formation of GaAs decreases and a more AlAs rich layer results. This interpretation is only qualitative since kinetics apparently control growth rate at the lower temeratures.

The effect of growth temperature on PL is summarized in Fig. 17. A sample of each orientation was etched a step at a time with the PL spectrum measured after each etching step. The growth temperature has a very large effect on PL efficiency with the PL being nearly as strong as for comparable LPE material for growth at very low temperatures. The intensity of the $\sim$ 1.2 eV peak decreases considerably as the growth temperature is decreased.

d. Diluent Flow Rate

The total flow rate was varied by changing the flow rate of the H_2 carrier gas, keeping all other flow rates constant. The growth rates plotted in Fig. 18 for both pure GaAs and the $Al_xGa_{1-x}As$ alloys at growth temperatures of 735°C and 750°C vary as approximately $F_T^{-1/2}$, as would be expected for mass transport limited growth as discussed in Ref. (11).

(a)

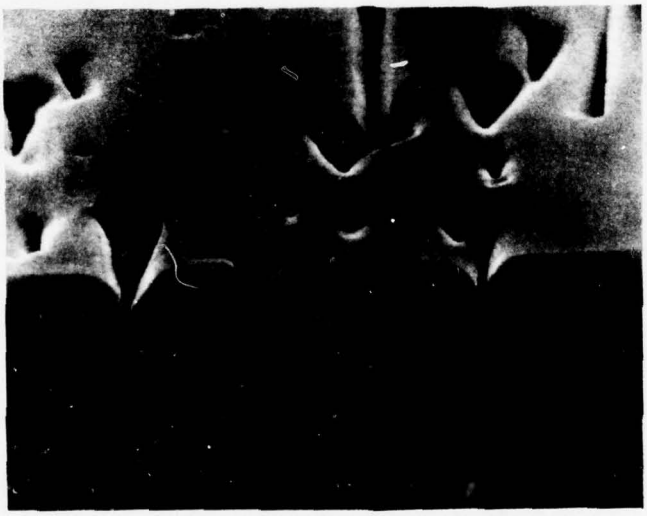

(b)

Figure 15. SEM photographs of growth pits formed in $Al_{.38}Ga_{.62}As$ layer with conditions such that surface kinetics limit growth rate.

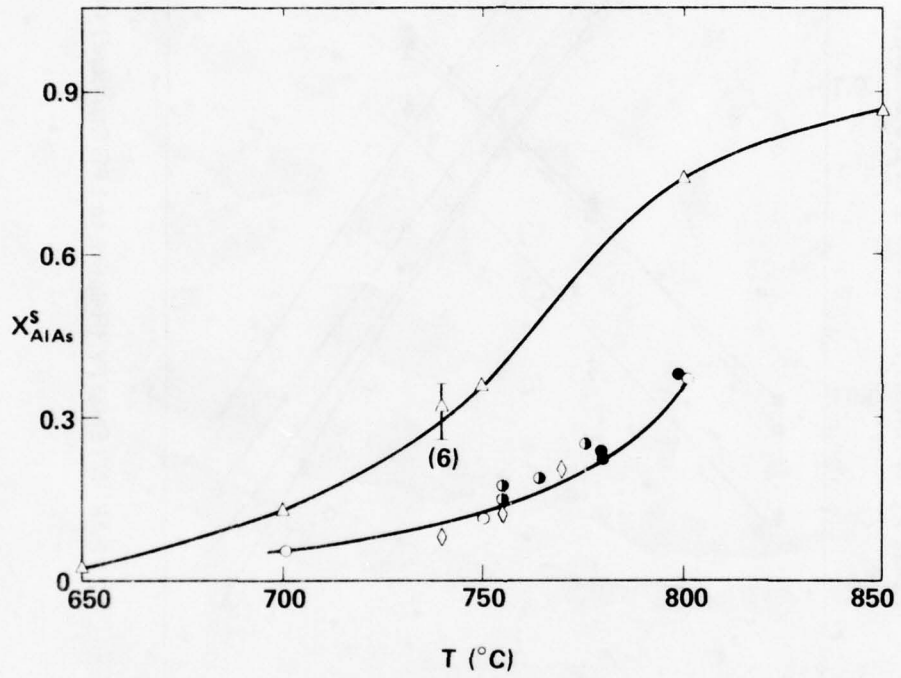

Figure 16. AlAs mole fraction in the solid versus substrate temperature.

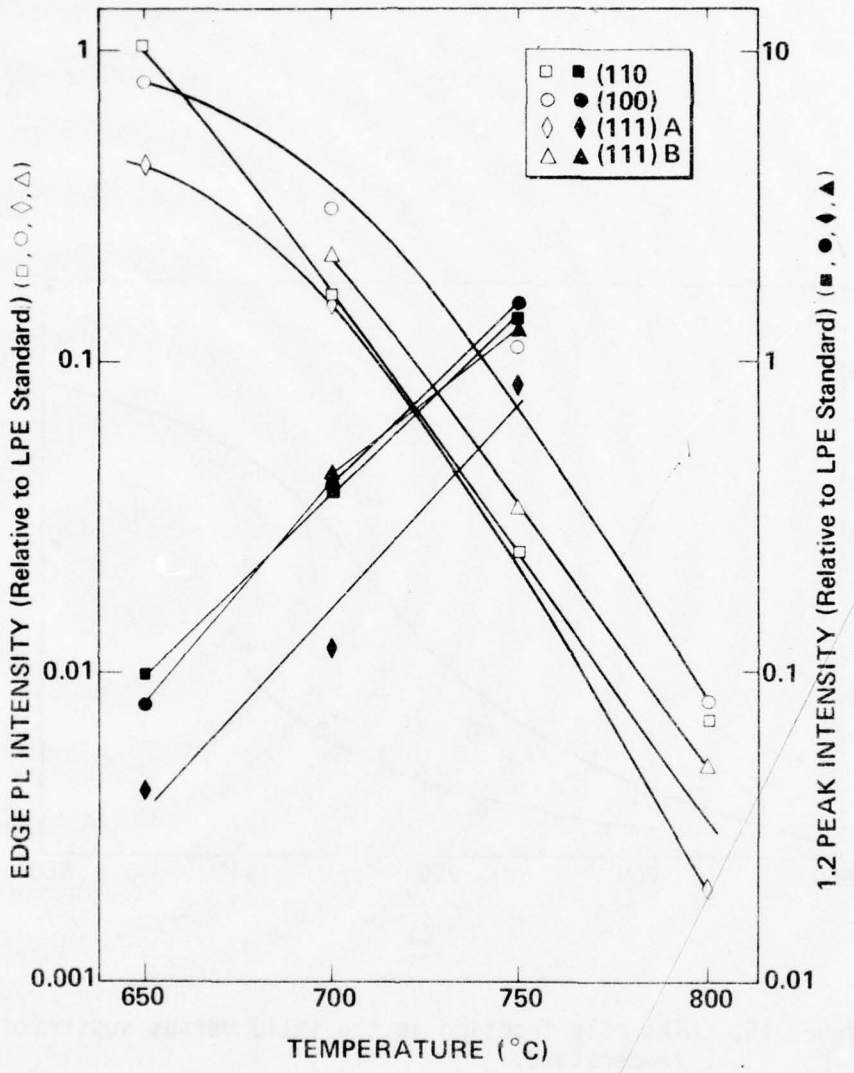

Figure 17. PL intensity and $I_{1.2}/I_{edge}$ versus substrate temperature during growth.

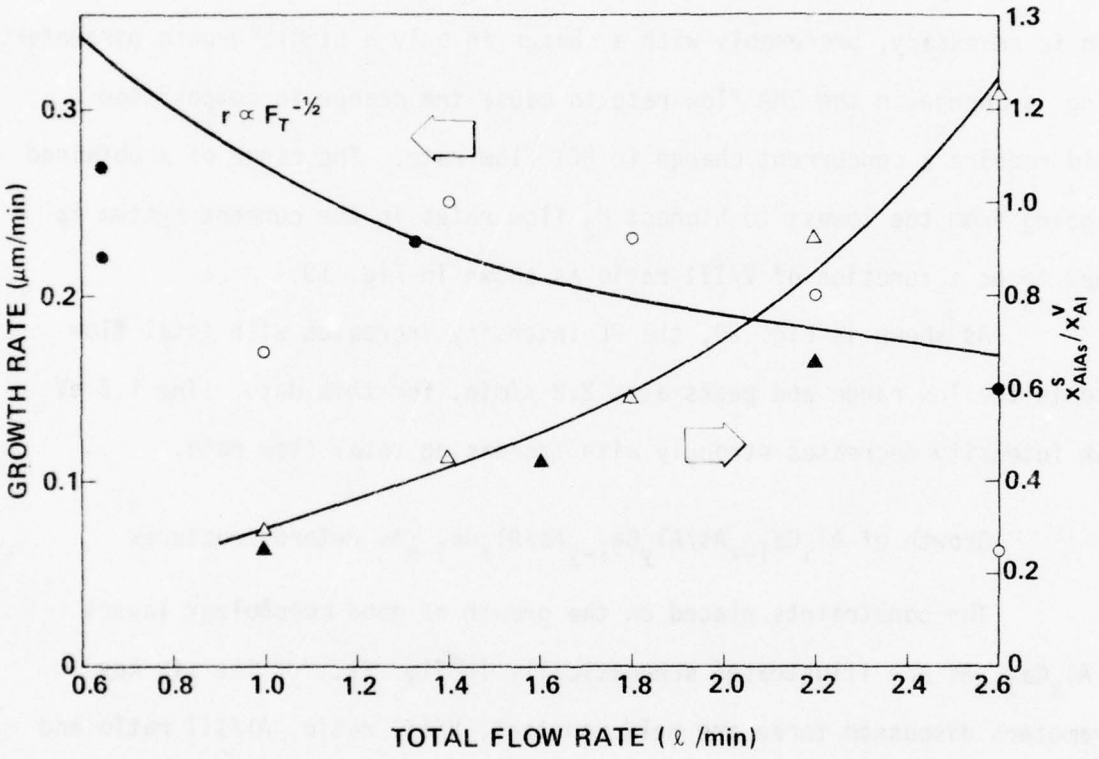

Figure 18. Growth rate and Al distribution coefficient versus total flow rate.

The Al distribution coefficient is a strong function of hydrogen flow rate, increasing by a factor of 4 for an increase of F_T from 1.0 to 2.6 ℓ/min., in close agreement with results of thermodynamic calculations to be discussed in section (f). The reason is that dilution favors the AlAs reaction from $AlCl_3$ which produces three molecules of HCl as opposed to the single molecule of HCl produced by the GaAs reaction. This feature is very attractive for the growth of multilayers where a rapid change in composition is necessary, preferably with a change in only a single growth parameter. Using a change in the TMA flow rate to cause the change in composition would require a concurrent change in HCl flow rate. The range of x obtained by going from the lowest to highest H_2 flow rates in the current system is found to be a function of V/III ratio as shown in Fig. 19.

As shown in Fig. 20, the PL intensity increases with total flow rate in the low range and peaks at $\sim$ 2.2 ℓ/min. for this data. The 1.2 eV peak intensity decreases strongly with increasing total flow rate.

e. Growth of $Al_xGa_{1-x}As/Al_yGa_{1-y}As/Al_xGa_{1-x}As$ Heterostructures

The constraints placed on the growth of good morphology layers of $Al_xGa_{1-x}As$ are illustrated schematically in Fig. 21. Of the six key parameters discussed three are held constant, V/III ratio, Al/III ratio and substrate orientation. Under these conditions the growth temperature must be above 750°C in order to avoid surface morphology problems. At temperatures above 800°C the Al distribution coefficient becomes too large, the growth rate becomes too small and the PL intensity too low for practical purposes. The range of allowable growth temperature is shown schematically in Fig. 21 as the shaded area. The constraints on HCl/III ratio are due

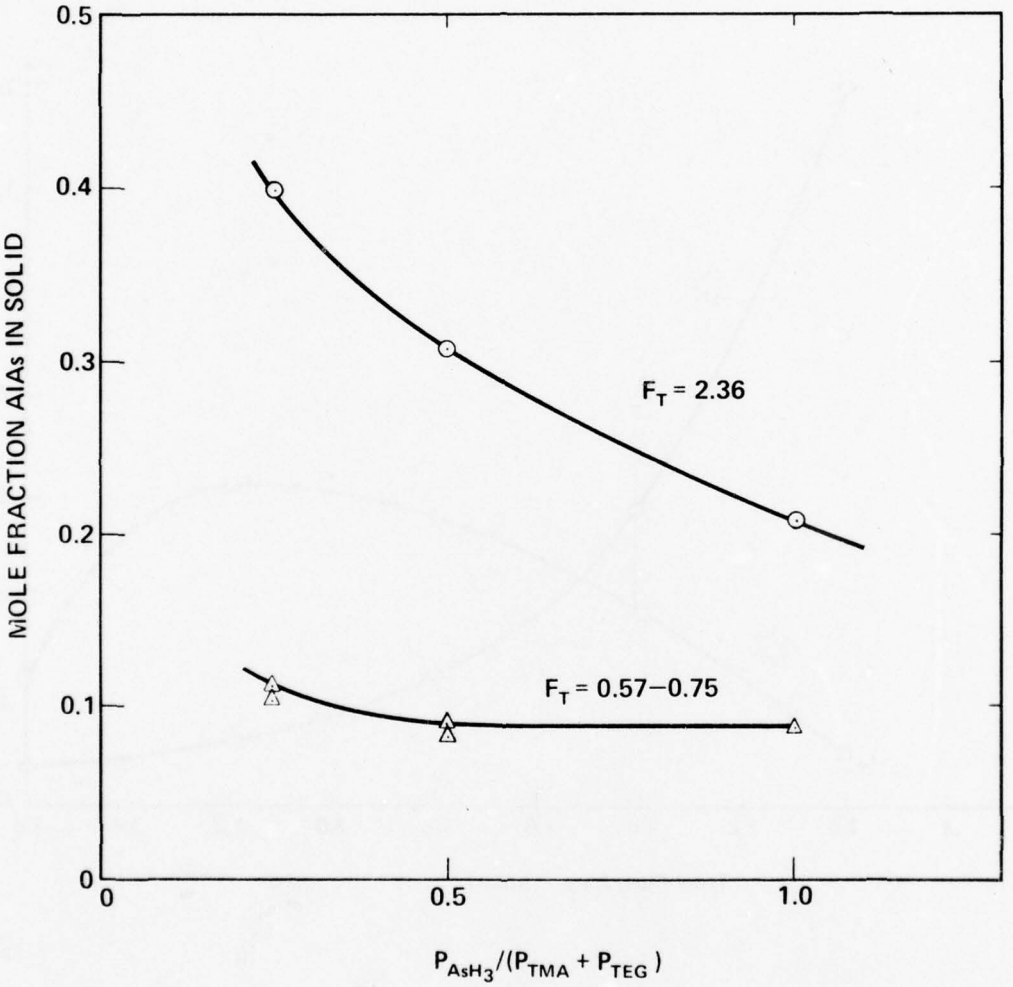

Figure 19. Solid composition vs V/III ratio for different total flow rates.

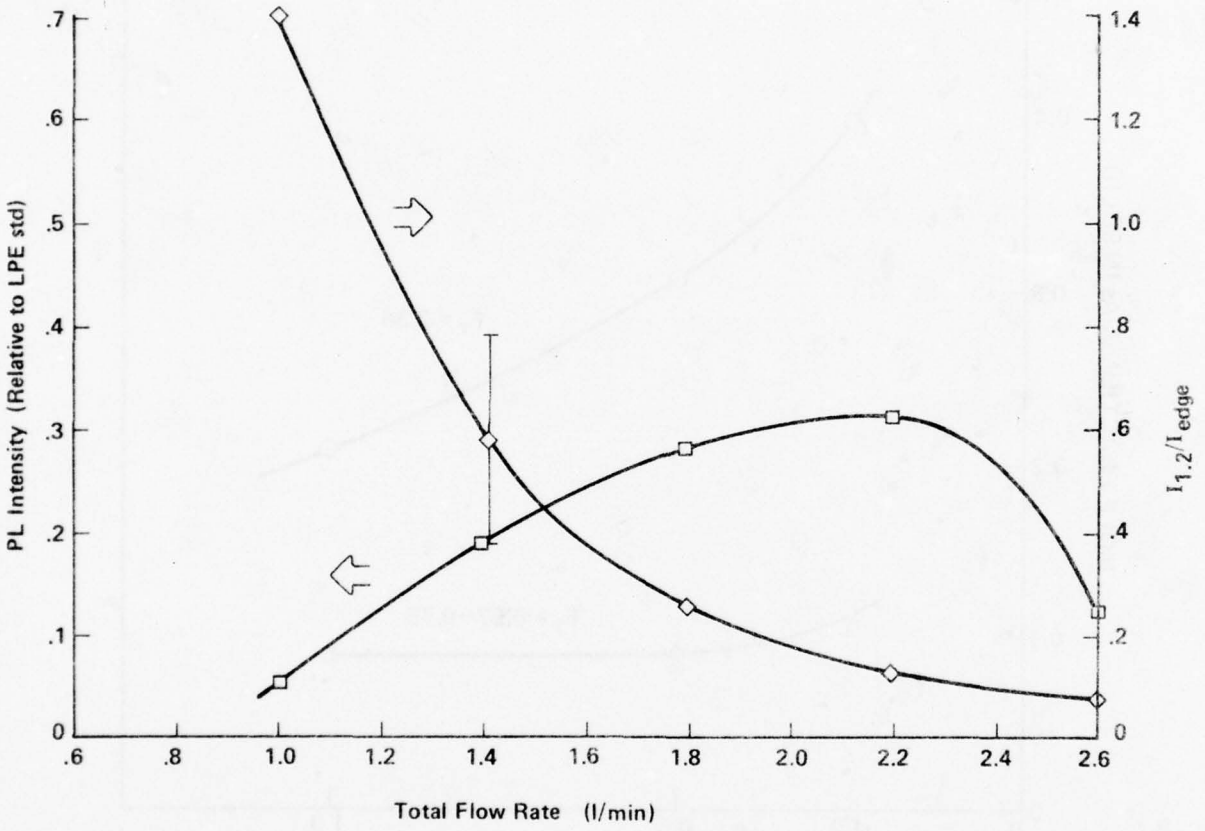

Figure 20. PL intensity and ratio of peak intensities for the 1.2 eV and edge peaks versus total flow rate.

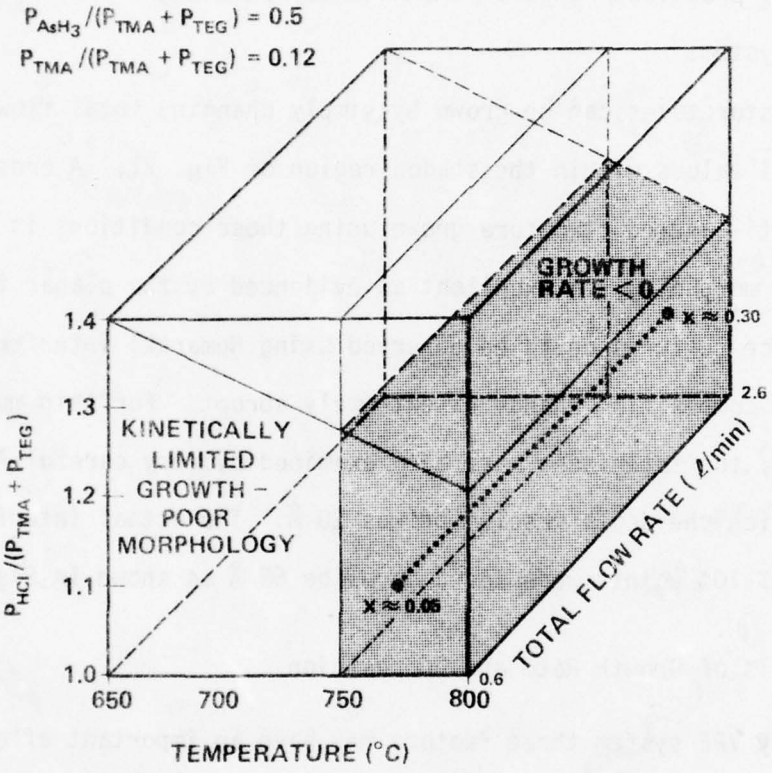

Figure 21. Schematic diagram showing the range of growth parameters yield high quality $Al_xGa_{1-x}As$ layers in the hot wall OMVPE system.

to inefficient transport of Al and Ga on the low end and the occurrence of etching at large values. Etching occurs at lower HCl/III ratios as the growth temperature increases. The total flow rate has only a minor effect on the morphology and occurence of etching but may be varied only over the range from 0.6 to 2.6 ℓ/min. in the present system. Thus the shaded area shown in Fig. 21 gives the practical range of the three key parameters for $Al_xGa_{1-x}As$ in the present system.

Heterosturctures can be grown by simply changing total flow rate for T and HCl/III values within the shaded region of Fig. 21. A cross section of a typical multi-layered structure grown using these conditions is shown in Fig. 22. The morphology is excellent as evidenced by the planar interfaces. No surface features could be observed using Nomarski interference microscopy. The composition change is extremely abrupt. For thin multilayerd structures the interfaces have been examined by very careful Auger profiling for which the depth resolution was 20 Å. The actual interface widths at the 90%-10% points were found to be be 65 Å as shown in Fig. 23.

f. Analysis of Growth Rate and Composition

For any VPE system three factors may have an important effect on the growth process: thermodynamics, mass transport (diffusion and/or convection) and surface kinetics. These processes are serially coupled and thus any one may dominate the growth rate under a given set of growth conditions If the growth process is contolled by surface kinetics the growth rate is typically dependent on substrate orientation, independent of flow rate and proportional to exp $(-\Delta E^*/RT)$ where ΔE^* is the activation energy for the kinetically limited step occuring on the surface.

For typical VPE processes, where the entire gas volume flowing

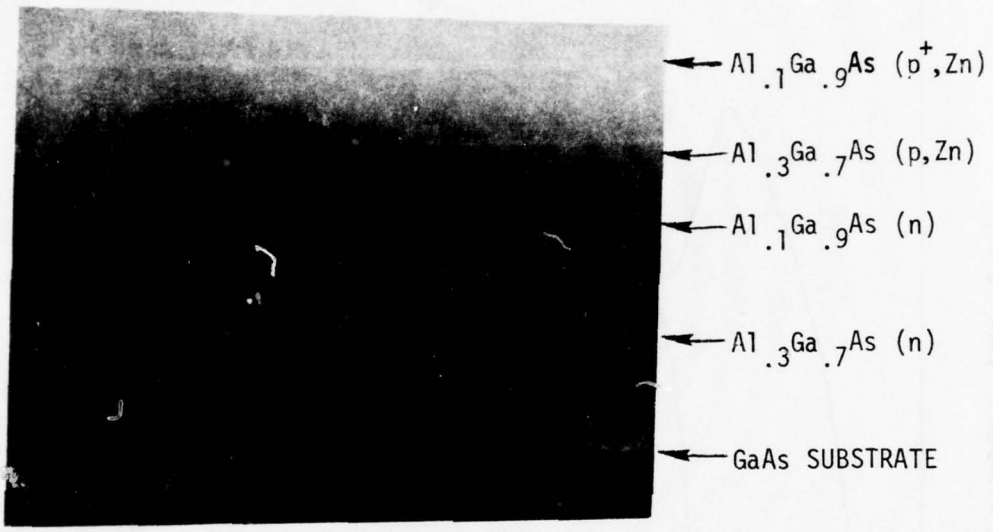

Figure 22. Cross section of multilayer structure.

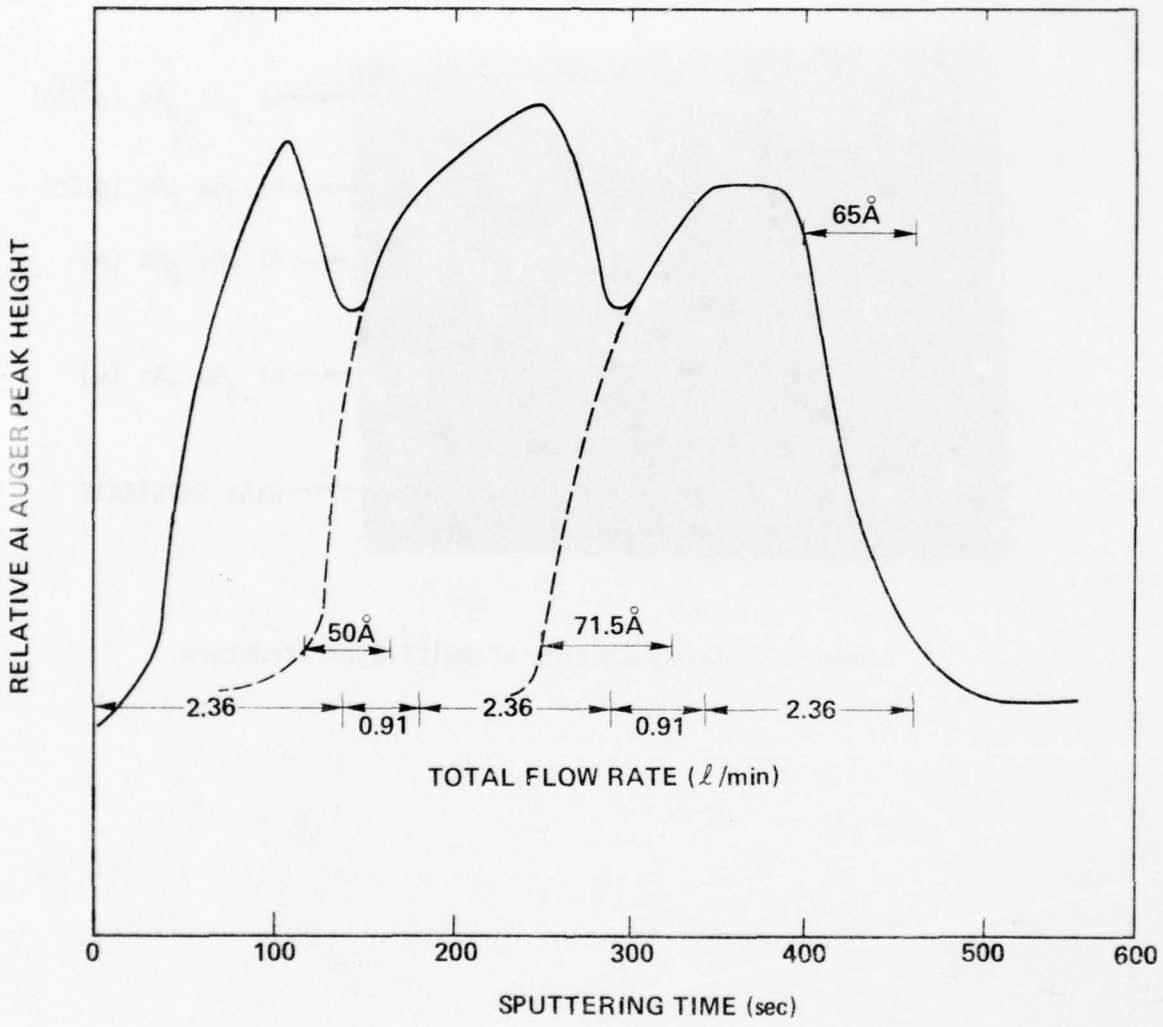

Figure 23. High resolution Auger profile of alternating ultra-thin layers of $Al_{.35}Ga_{.65}As$ and $Al_{.06}Ga_{.94}As$.

through the reactor is not able to equilibrate with the substrate, a combination of mass transport and thermodynamics controls the growth rate. The simplest treatment of this situation is that of Sedgwick[25] where the reactor is characterized by an efficiency, β, which represents the fraction of the gas phase able to equilibrate with the surface. The factor β is nearly independent of temperature and varies approximately at $F_T^{-1/2}$ when the flow velocity is increased by increasing the H_2 diluent rate. Thus in this mass transport limited growth regime, variations in growth rate due to temperature, HCl/III ratio etc. are largely determined by the thermodynamic reaction efficiency at equilibrium.

A thermodynamic model has been constructed for the calculation of the equilibrium reaction efficiency, ε, in the hybrid system. The calculation includes the species GaCl, AlCl, $AlCl_3$, HCl, As_2, As_4, H_2 and the solid $Al_xGa_{1-x}As$ which is taken to be an ideal solution.[26] In this section the analysis of the growth process will include reference to the calculated results obtained from this model.

One of the key parameters determining the rate limiting step is substrate temperature. The dependence on orientation and the sign of the temperature dependence shown in Fig. 14 indicate that at low substrate temperatures (< 750°C) the rate is controlled by surface kinetics. The activation energy is apparently dependent on substrate orientation. At higher temperatures the rate appears to be limited by mass transport. The slope gives the enthalpy of reaction of approximately 73 kcal/mole.

At temperatures above 740°C the effect of HCl/III ratio is in qualitative agreement with the mass tranpsort model, i.e., at high values of HCl/III ratio etching occurs. However, the calculations predict that

much higher values of HCl should be required to cause the rapid reduction in growth rate observed. This phenomenon may be due to the presence of higher HCl/III ratios at the growing interface due to either decomposition of some alkyls on the reactor walls or incorrect vapor pressure data for TEG and/or TMA. The latter is possible since, for example the vapor pressure of TEG was determined in 1941[27] and is likely to be dependent on the purity of the alkyl, which has increased substantially in recent years. A third possibility is that the surface reaction rate is suppressed by HCl as has been observed for the chloride growth of GaAs.[24] This is interpreted to be due to competition between As, GaCl and HCl for the same adsorption sites on the surface.

As described above the effect of HCl/III ratio on composition is not as expected. The model calculation bears out the conclusion that increasing the HCl/III ratio should lead to a reduction in x. That this is not so could be due to either of two effects. 1) Kinetic considerations could very well determine composition even when growth rate is determined by mass transport. For example, adsorption rates of Al and Ga could determine the Al to Ga ratio in the solid. 2) Another factor at relatively low values of HCl/III is that some alkyls not picking up one or more Cl's in the vapor stream would decompose on the walls resulting in an HCl/III ratio at the growing interface much more constant than in the input gas stream.

As described above for growth temperatures above 750°C the effect of V/III ratio and total flow rate are generally as predicted from the mass transport model. The effect of H_2 diluent rate on composition is accurately predicted by the model.

g. P-Type Doping

In the early stages of this program the use of Zn as the acceptor to produce p-type layers in the laser structure was thought to be undesirable, because it might result in rapid degradation of the laser during operation. Thus Ge and Mn were investigated. However neither Ge, introduced as GeH_4 into the reactor, nor Mg, transported as the chloride from a boat in the high temperature mixing zone of the reactor, was found to be suitable. Both produced highly compensated n-type materials. A summary of these results is given in Table II. Details of experiments and calculations of expected distributions coefficients are given in the 3rd Quarterly Report (15 February - 15 May 1978).

The current status of long lived lasers grown by LPE is that either Ge[28] or Zn[29-31] may be used. We have developed the capability to dope p-type using Zn introduced into the reactor by bubbling H_2 through DEZ liquid. The net hole concentration is plotted versus input DEZ partial pressure in Fig. 24. The distribution coefficient is about equal for the hot and cold wall reactors. The data plotted in Fig. 24 indicate that the Zn distribution coefficient, x_{Zn}/p°_{DEZ}, is approximately 2.5, independent of growth technique and mole fraction AlAs in the solid.

For multilayer runs the need exists for an easy method of determining p-type doping level. As discussed in the Experimental section, near edge PL halfwidth is a reasonable indicator of doping level for n-type material even though the halfwidths for VPE material appear to be dependent on parameters other than doping level. In Fig. 25 the PL halfwidth measured at room temperature is plotted versus the free hole concentration obtained from van der Pauw measurements. The correlation seems reasonably good except

TABLE II

Summary of Data for Mg and Ge Doped VPE $Al_xGa_{1-x}As$

Run No.	Morphology	Dopant	x	p°_{MG} or $p^\circ_{GeH_4}$	Conductivity Type	$\Delta W(PL)$	$\Delta p/p^\circ$	$I_{1.2}/I_{edge}$
322	Excellent	Mg	0.33	7.4×10^{-6}	n	71	———	0.08
323	Square Pyramids	Mg	0.37	2.3×10^{-4}	n	57	0.25	0.024
324	Poor-- Square Pyramids	Mg	$\sim$ 0.08	2.3×10^{-4}	n	—	———	———
329	Excellent	GeH_4	0.07	4.4×10^{-5}	n	—	———	———

($n = 3.7 \times 10^{17}$; $\mu = 7.14$)

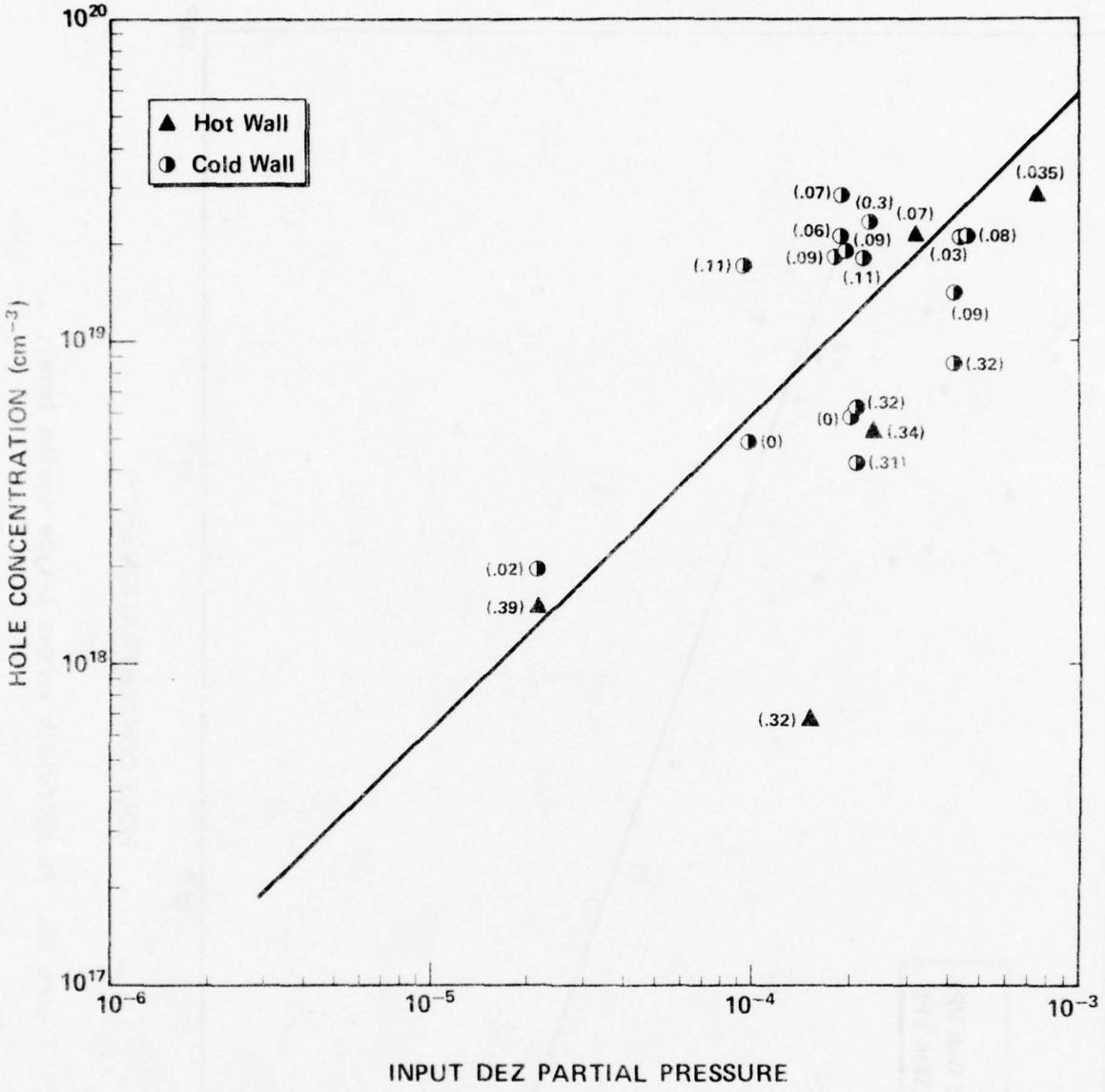

Figure 24. Hole concentration vs DEZ partial pressure.

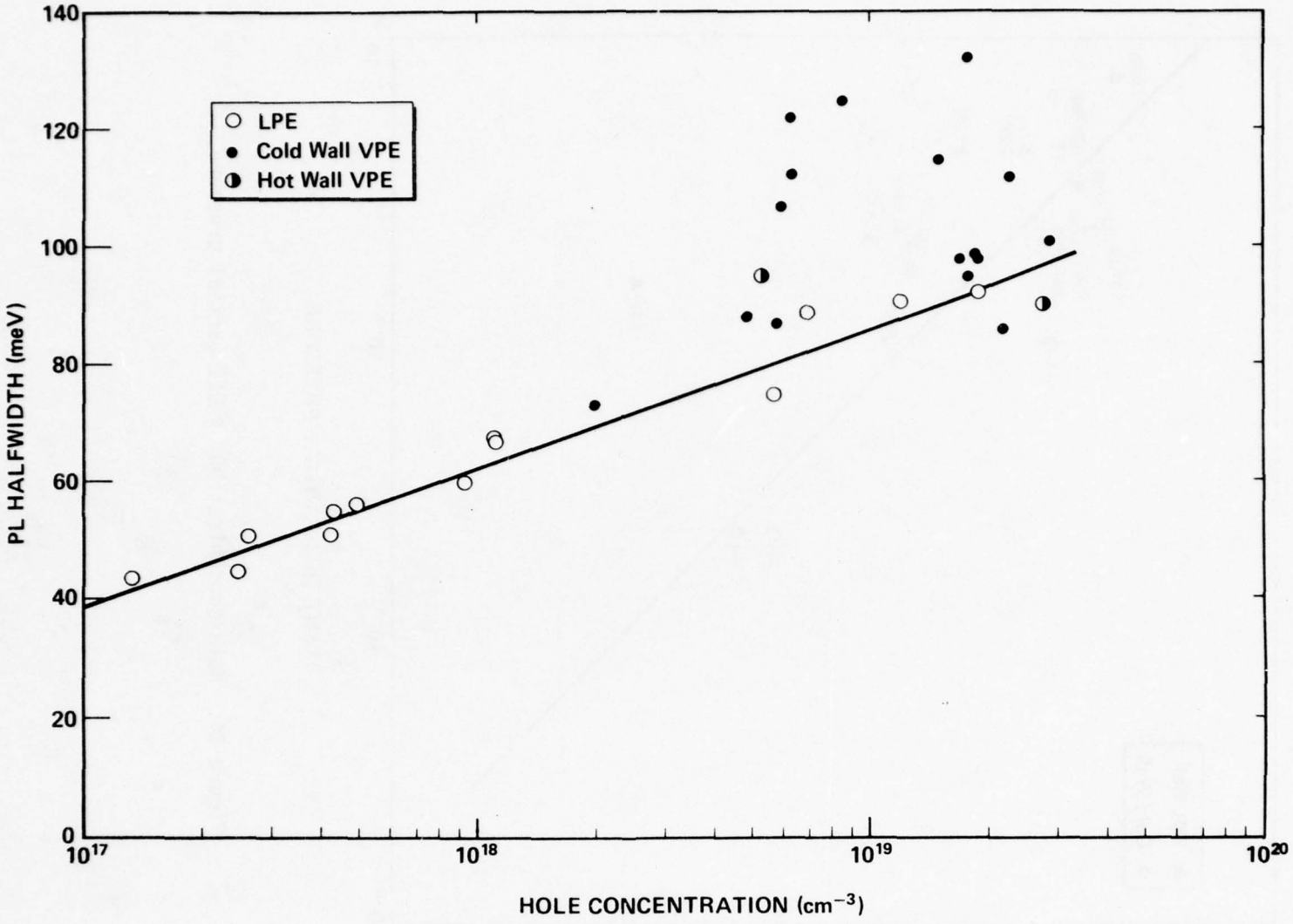

Figure 25. PL halfwidth versus p-type doping level.

for a few data points which again lie somewhat above the curve established from the LPE data. This means that currently PL halfwidth gives a value for the maximum expected carrier concentration. The actual value of p could be up to an order of magnitude smaller.

One other feature of Zn doping in the hot wall system presents somewhat of a problem. A large fraction ($\sim$ 2/3) of the DEZ thermally decomposes depositing Zn inside the graphite inlet tube. Apparently what is needed is a very sharp temperature gradient, probably at the body of the reactor, to allow the DEZ to reach the reactor without decomposing. The DEZ should subsequently decompose in a region of the reactor having a temperature high enough to allow the Zn to remain in the vapor phase as elemental Zn or $ZnCl_2$. In spite of this the Zn doping obtained is currently reproducible enough to allow growth of p-type $Al_xGa_{1-x}As$ for laser structures.

It should also be noted that the partial pressures in Fig. 24 for the hot wall system were corrected for the loss of Zn by decomposition. The Zn deposit has been analyzed using emission spectroscopy. All heavy metals are found to be below the detectability limits of $\sim$ 0.1 ppm. Thus, the organometallic DEZ source seems to be of relatively high purity.

h. Photoluminescence Characterization.

i. Room Temperature PL

A strong relationship between the edge PL intensity and the magnitude of the IR peak at $\sim$ 1.2 eV is evident from the data of Figs. 11, 13, 17, and 20. In Fig. 26 the relative intensity of the edge emission is plotted versus the 1.2 eV peak intensity for the multiple layer runs where T, HCl/III, V/III and total flow rate were varied. For each series the value of n changed by less than 2x as determined from the PL half-widths. The data

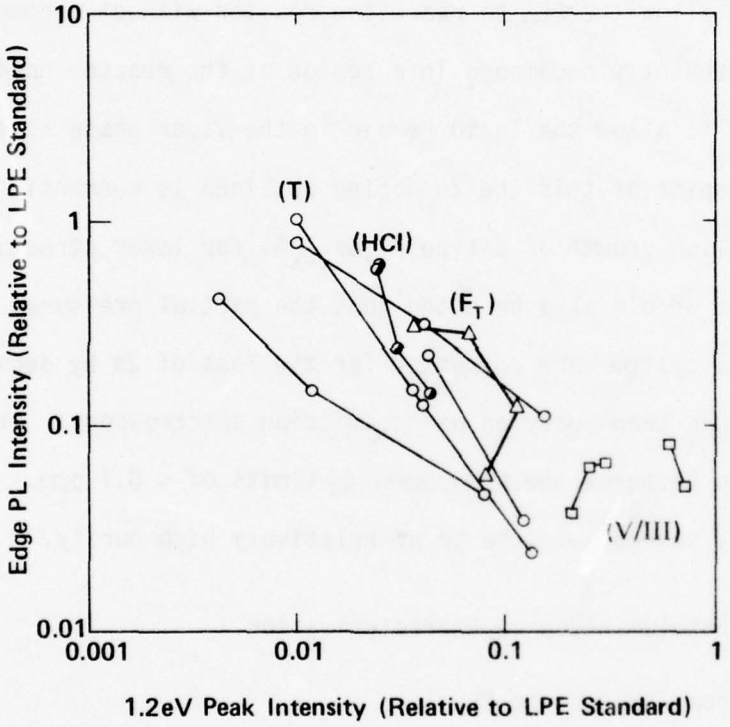

Figure 26. Edge PL intensity versus 1.2 eV peak intensity.

show a general trend with $I_e \propto 1/I_{1.2}$. The data where T was varied show this trend strongly except for the 800°C data points. However, at 800°C the Al distribution coefficient is large and the values of x for these layers range from 0.34 to 0.39, close to the Γ - X crossover where band structure effects might be expected to lead to a reduction in PL intensity. Thus the 800°C points were not included in the plot. The data for the runs where HCl/III, V/III and total flow rate were varied show a similar general relationship, $I_e \propto I_{1.2}^{-n}$ but n appears to be somewhat larger than unity for these data.

Two factors would be expected to have a large influence on PL efficiency. The ratio of minority carrier lifetimes $(1/\tau_e/(\sum_i 1/\tau_i)$ reflects the competition between the band edge recombination path and other paths, and thus PL efficiency should be inversely proportional to the density of non-radiative recombination centers. The PL efficiency should also be proportional to the majority carrier concentration at low excitation levels where the PL intensity is a linear function of excitation intensity. Thus, in Fig. 27 the PL efficiency for hot wall OM VPE $Al_xGa_{1-x}As$ with $x < 0.35$ is compared with that of LPE material plotted versus free carrier concentration determined using van der Pauw or PL half-width measurements.

The PL intensity for LPE samples increases linearly with carrier concentration until at levels of $> 2 \times 10^{18}$ cm^{-3} the donor, Te in this case, begins to be incorporated in non-radiative, neutral complexes. The VPE data are scattered over a considerable range of PL intensity with the highest values being ~ 30% of the similarly doped LPE specimens. Clearly the ratio $1/\tau_e/\sum_i 1/\tau_i$ varies considerably with growth conditions. The infrared PL peak occuring at ~ 1.2 eV appears to be associated with the non-radiative center

The IR peak position is plotted versus edge emission energy in Fig. 28. The peak does shift somewhat with composition but only $\sim$ 1/2 as much as the band gap.

In Fig. 29 spectra measured at 296°K and 96°K for a typical sample are shown. One feature of the spectra evident in this figure but not discussed previously is the apparent shoulder on the short wavelength side of the IR emission peak at both 296°K and 96°K. This occurs near the GaAs absorption edge and is due to the fact that backside reflection increases the PL intensity in the spectral region beyond the GaAs band edge where the substrate is transparent.

The intensity of the IR peak was determined between $\sim$ 96°K and room temperature. It decreases exponentially with an activation energy of $\sim$ 220 meV, as shown in Fig. 30.

The half-width of the 1.2 eV peak is large, $\sim$ 300 Å. Its position and shape are similar to the emission observed in C doped melt grown GaAs and attributed to C - V_{Ga} donor-acceptor pairs,[34] similar to Te_{As} - V_{Ga}, Se_{As} - V_{Ga}, Sn_{Ga} - V_{Ga} and Ge_{Ga} - V_{Ga} donor-acceptor pairs also observed. The energies of the emission bands from these centers are nearly all the same, 1.18 - 1.22 eV. The C - V_{Ga} peak is distinct in one respect, that the temperature dependence of its emission energy is negative, similar to the band gap while all others including $(IV)_{Ga}$ - V_{Ga} centers have the opposite temperature dependence. This may be explained by a recent theoretical thermodynamic analysis by Ivanutin et al.[33] which shows that C_i - V_{Ga} should be the dominant complex in GaAs with 10^{19} C, typical of the level detected in layers grown using TMG and AsH_3.[33] With oxygen present the $(C_{As} - O_i^+)^0$ complex should predominate.

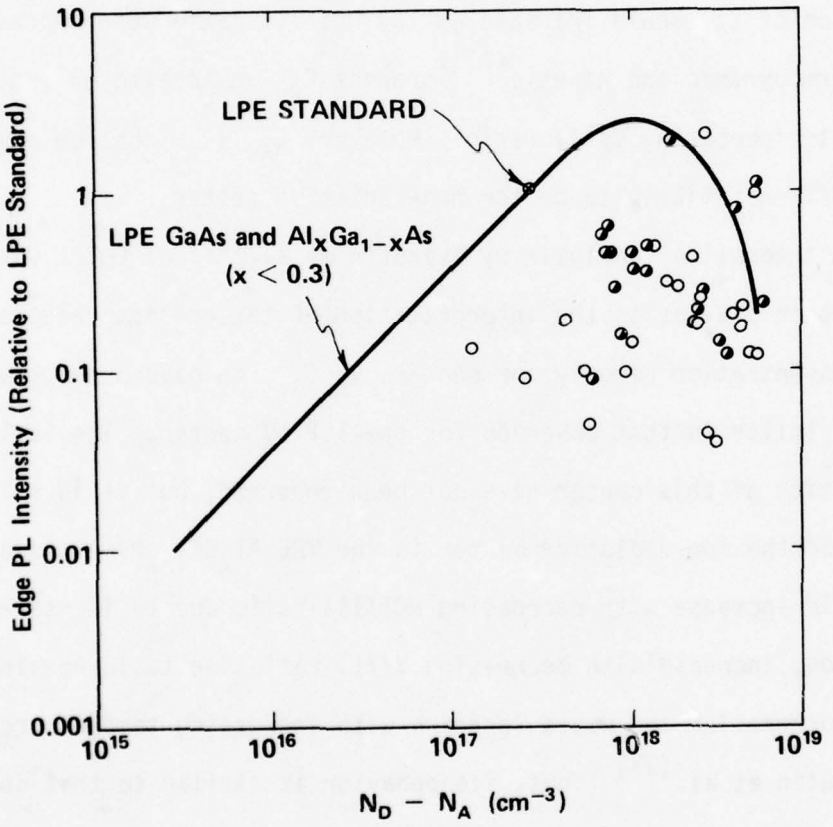

Figure 27. Edge PL intensity vs N_D - N_A for hot wall OMVPE $Al_xGa_{1-x}As$.

since $I_{edge} \propto 1/I_{1.2}$. Determination of the identity of this center may be an important contribution to the improvement of PL efficiency in VPE $Al_xGa_{1-x}As$.

The data presented here indicates the concentration of the non-radiative center and the center giving rise to the 1.2 eV emission to increase with increasing growth temperature, decreasing V/III ratio and decreasing HCl/III ratio. C_{As} might be expected to remain a factor in OMVPE $Al_xGa_{1-x}As$ even in the hybrid system. Previous results indicate that the concentration of C_{As} would increase as the HCl/III ratio were decreased. On both thermodynamic and kinetic[32] grounds C_{As} would also be expected to decrease with increasing V/III ratio. However, C_{As} is a shallow acceptor in GaAs and is not likely to be the non-radiative center.

A theoretical analysis by Ivanutin et al.,[33] of OMVPE GaAs provides a further clue as to the interpretation of the present results. They find the concentration of only one center, $V_{As}C_{As}$, to have a temperature dependence similar to that observed for the 1.2 eV center. The luminescence characteristics of this center have not been reported, but it is a likely candidate for the non-radiative center in the VPE $Al_xGa_{1-x}As$. Its concentration would increase with decreasing HCl/III ratio due to increased C incorporation, increase with decreasing V/III ratio due to increasing V_{As} and C_{As} incorporation and would increase with increasing temperature according to Ivanutin et al.[33] Thus, its behavior is similar to that observed for the $\sim$ 1.2 eV center.

Additional information which might be useful in an attempt to identify the 1.2 eV center are the dependence of peak position and half-width on temperature and alloy composition.

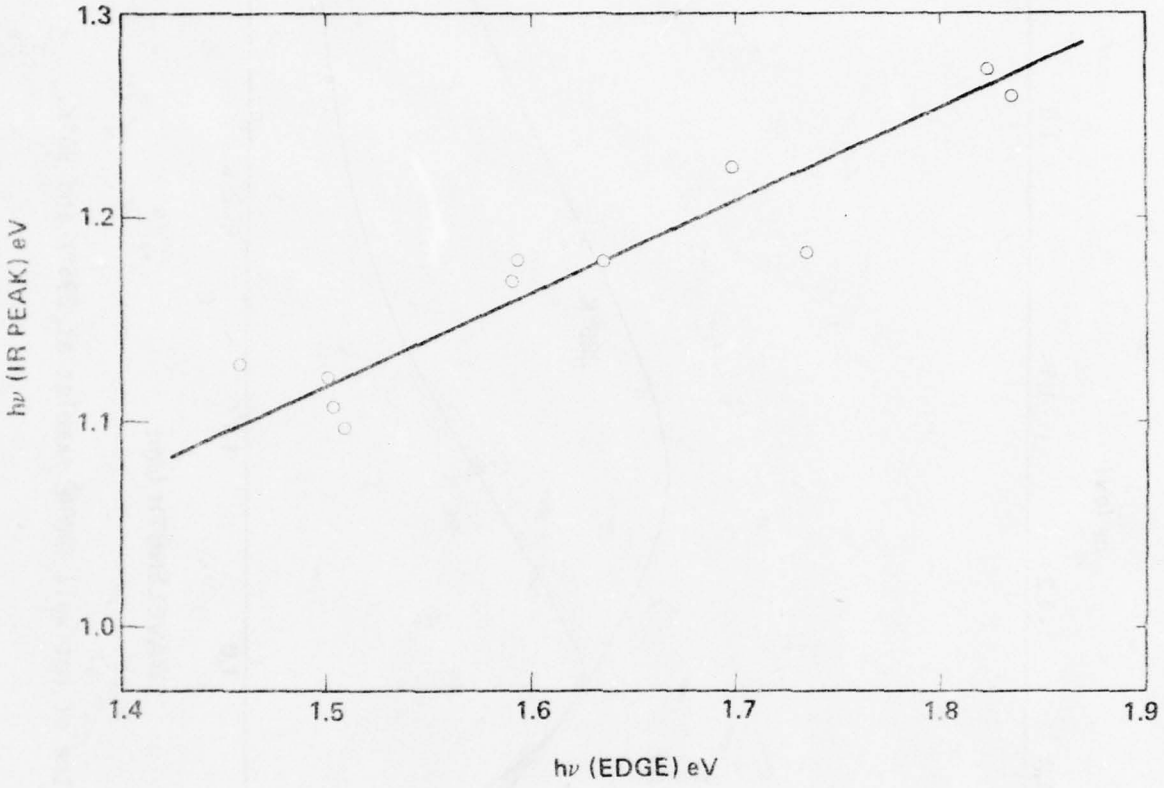

Figure 28. Energy of IR peak versus energy band gap.

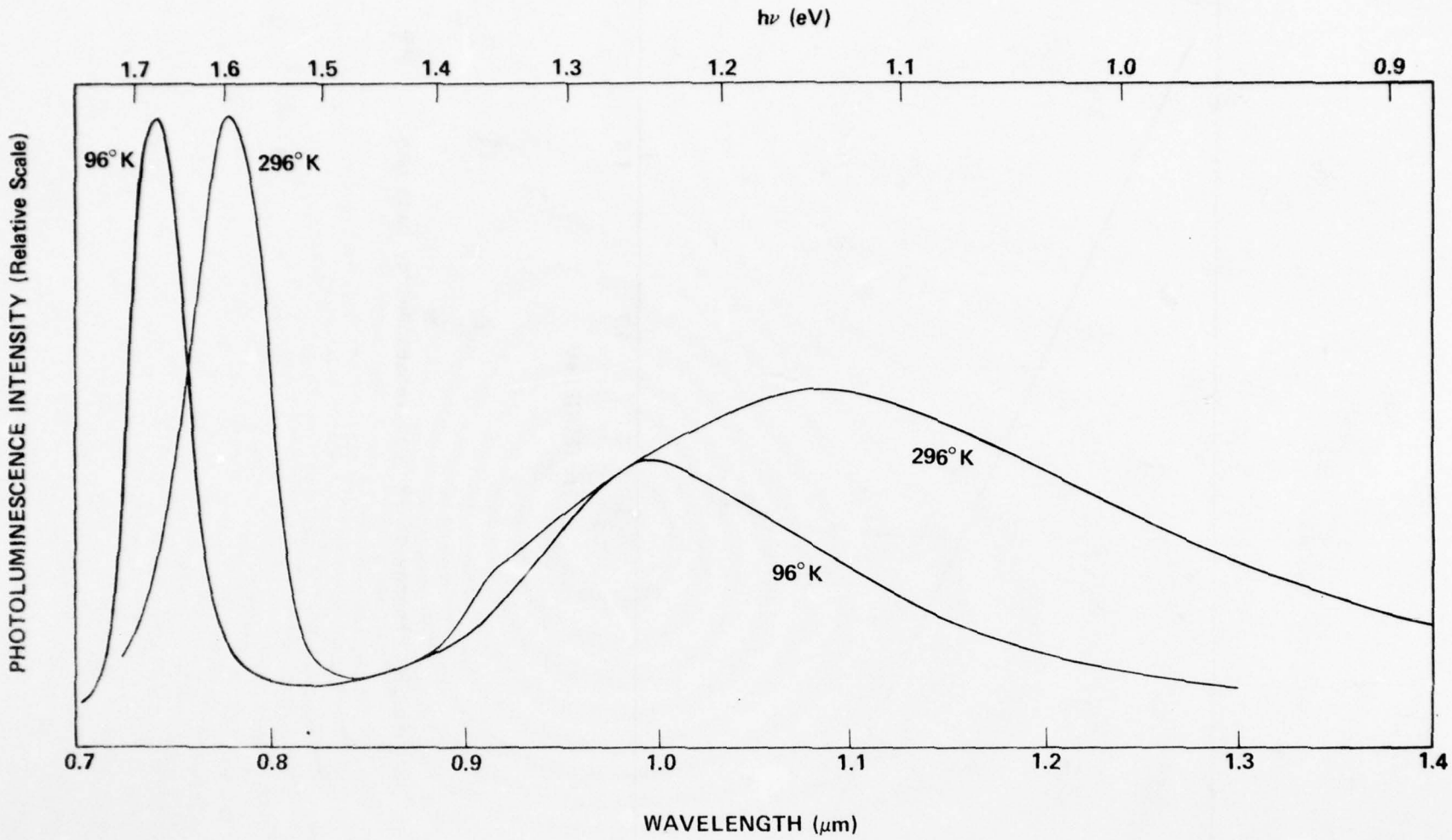

Figure 29. PL spectra of hot wall OMVPE samples at 296°K and 96°K.

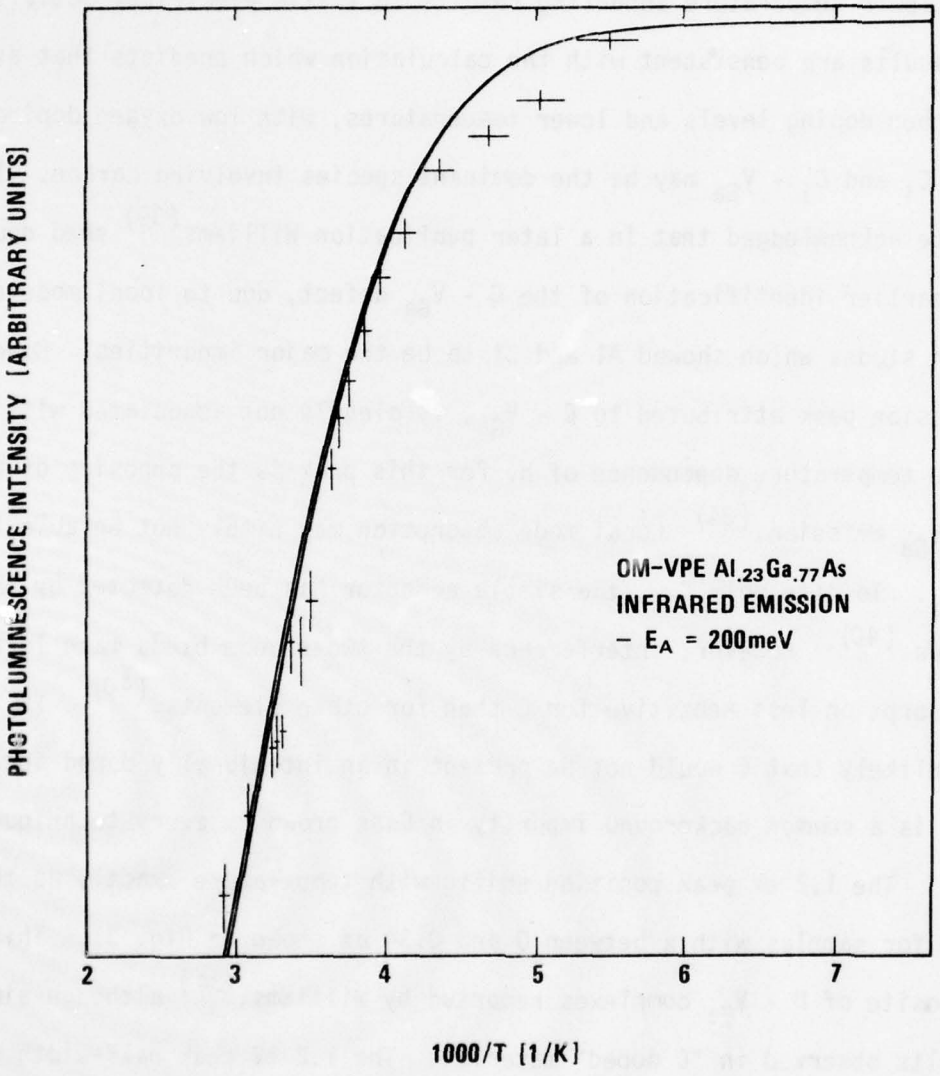

Figure 30. IR peak intensity versus reciprocal temperature.

To put the discussion of C doping into perspective it should be noted that for LPE or conventional VPE GaAs, C appears to be a simple acceptor as seen 4.2° PL.[36] Ion implantation studies have shown that after annealing at 900°C the C is 50% active as a shallow acceptor.[37] However lower temperature annealing results in little electrical activity.[38] These results are consistent with the calculation which predicts that at high carbon doping levels and lower temperatures, with low oxygen doping levels, C_i and $C_i - V_{Ga}$ may be the dominant species involving carbon. It should be acknowledged that in a later publication Williams[39] shed doubt on his earlier identification of the $C - V_{Ga}$ defect, due to local mode absorption studes which showed Al and Si to be the major impurities. However, the emission peak attributed to $C - V_{Ga}$, is clearly not associated with Si since the temperature dependence of hν for this peak is the opposite of the $Si_{As} - V_{Ga}$ emission.[34] Local mode absorption may simply not be able to detect C_i. To date only C_{As}, the simple acceptor has been detected by this technique.[40] However, interference by the two-phonon bands make local mode absorption less sensitive for C than for other elements.[40] It seems unlikely that C would not be present in an intenionally doped ingot when it is a common background impurity in GaAs grown by every technique.[36,40]

The 1.2 eV peak position shifts with temperature exactly as the bandgap for samples with x between 0 and 0.34 as shown in Fig. 31. This is the opposite of $D - V_{Ga}$ complexes reported by Williams,[34] although similar to results observed in "C doped" material. The 1.2 eV peak half-width seems to be proportional to $\sqrt{T}$, as shown in Fig. 32, similar qualitatively to the $D - V_{Ga}$ complexes studied by Williams and predicted from the configurational-coordinate model.[34] The absolute half-widths are considerably larger than

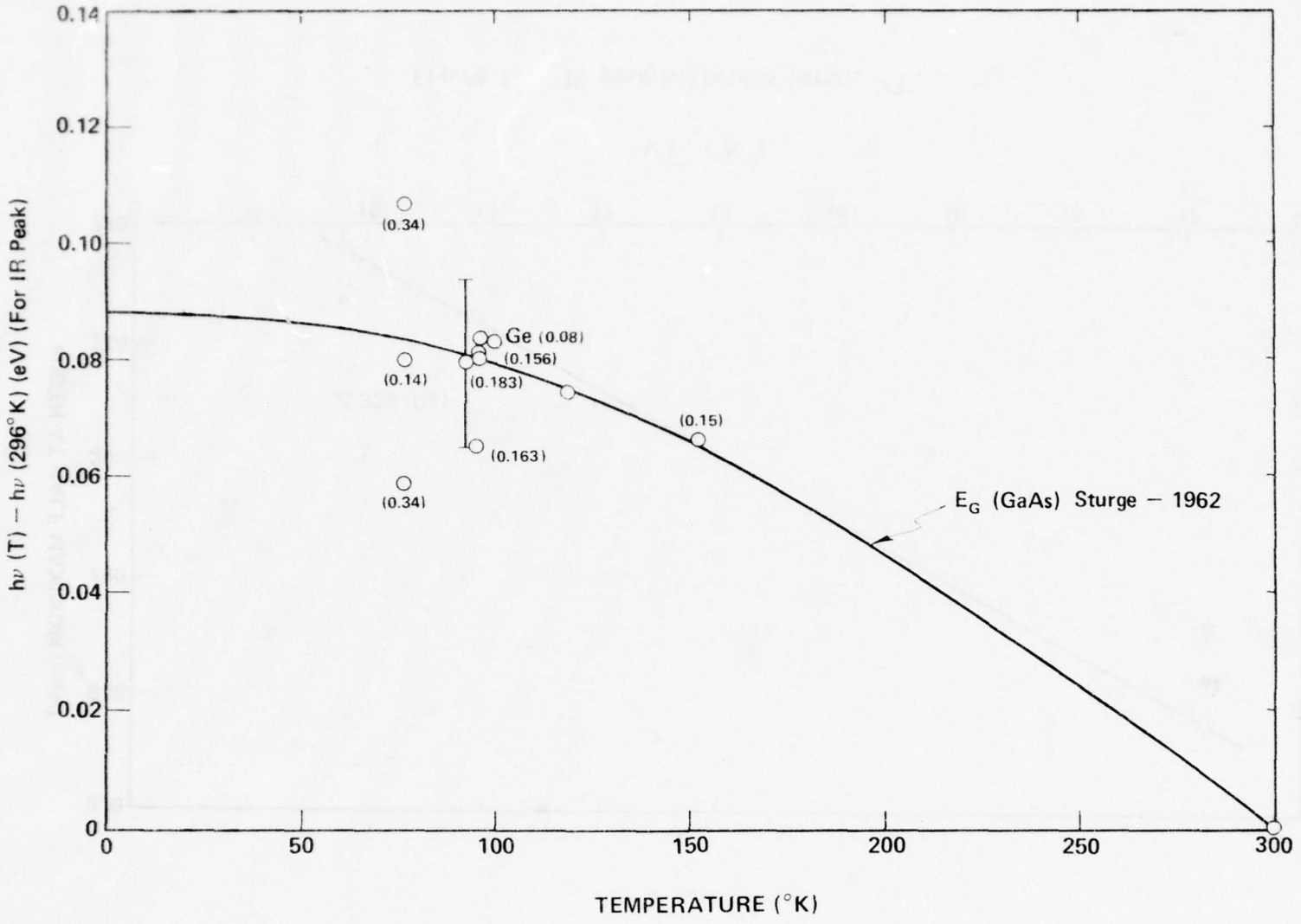

Figure 31. IR peak energy versus temperature.

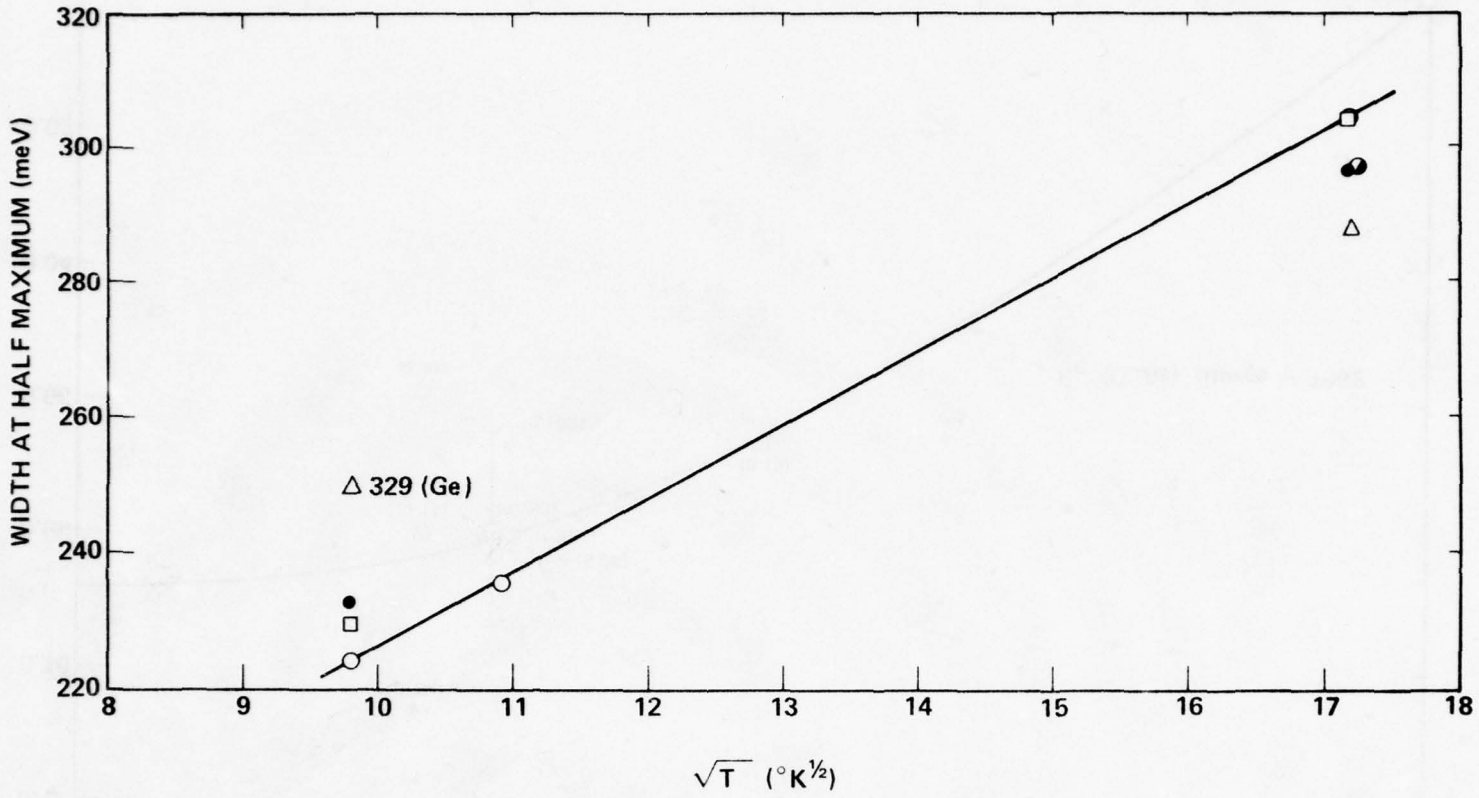

Figure 32. IR peak halfwidth versus $\sqrt{T}$.

all except the $Sn_{Ga}V_{Ga}$ center.

For Si and Ge doped GaAs samples the half-widths reported[35] for peaks believed due to $V_{As}Ge_{As}$ and $V_{As}Si_{As}$ are considerably smaller, 72 meV and 97 meV respectively at 80°K. The trend would indicate the $V_{As}C_{As}$ peak to be considerably broader, possibly as broad as the 230 meV measured for the VPE $Al_xGa_{1-x}As$ samples. The emission energies of 1.416 and 1.378 for Ge and Si respectively are similarly higher than measured on the VPE samples considered here but the trend to lower energy with lower atomic number indicates C could be considerably lower in energy. One might expect the properties of V_{As} $(IV)_{As}$ to scale roughly as the electronegativity or, more conveniently, 1/r. In Fig. 33 the half-widths and peak positions for $V_{As}Si_{As}$ and $V_{As}Ge_{As}$ are plotted with the values for the 1.2 eV center of concern here on a 1/r scale. The relatively larger difference in 1/r between C and Si than between Si and Ge makes the identification of the 1.2 eV center as $V_{As}C_{As}$ appear consistent. The other significant feature of the emission attributed to $V_{As}Ge_{As}$ and $V_{As}Si_{As}$ is that it increases in energy as T is reduced, similar to the center considered here. A summary of characteristics of the 1.2 eV emission band is made in Table III. Many characteristics lead to the tentative conclusion that the $V_{As}C_{As}$ center may give rise to the $\sim$ 1.2 eV emission and be the dominant NRC in this material.

Zn doping virtually eliminates the non-edge emission from the room temperature PL spectra of VPE $Al_xGa_{1-x}As$ samples. At 77°K using the InAs detector, the IR emission can be detected. In Fig. 34 the peak positions obtained at 77°K are plotted versus the band edge emission energy for undoped and Zn doped specimens. The positions of the peaks at $\sim$ 1.2 eV in the Zn doped samples are very similar to those in non-zinc doped specimens. However,

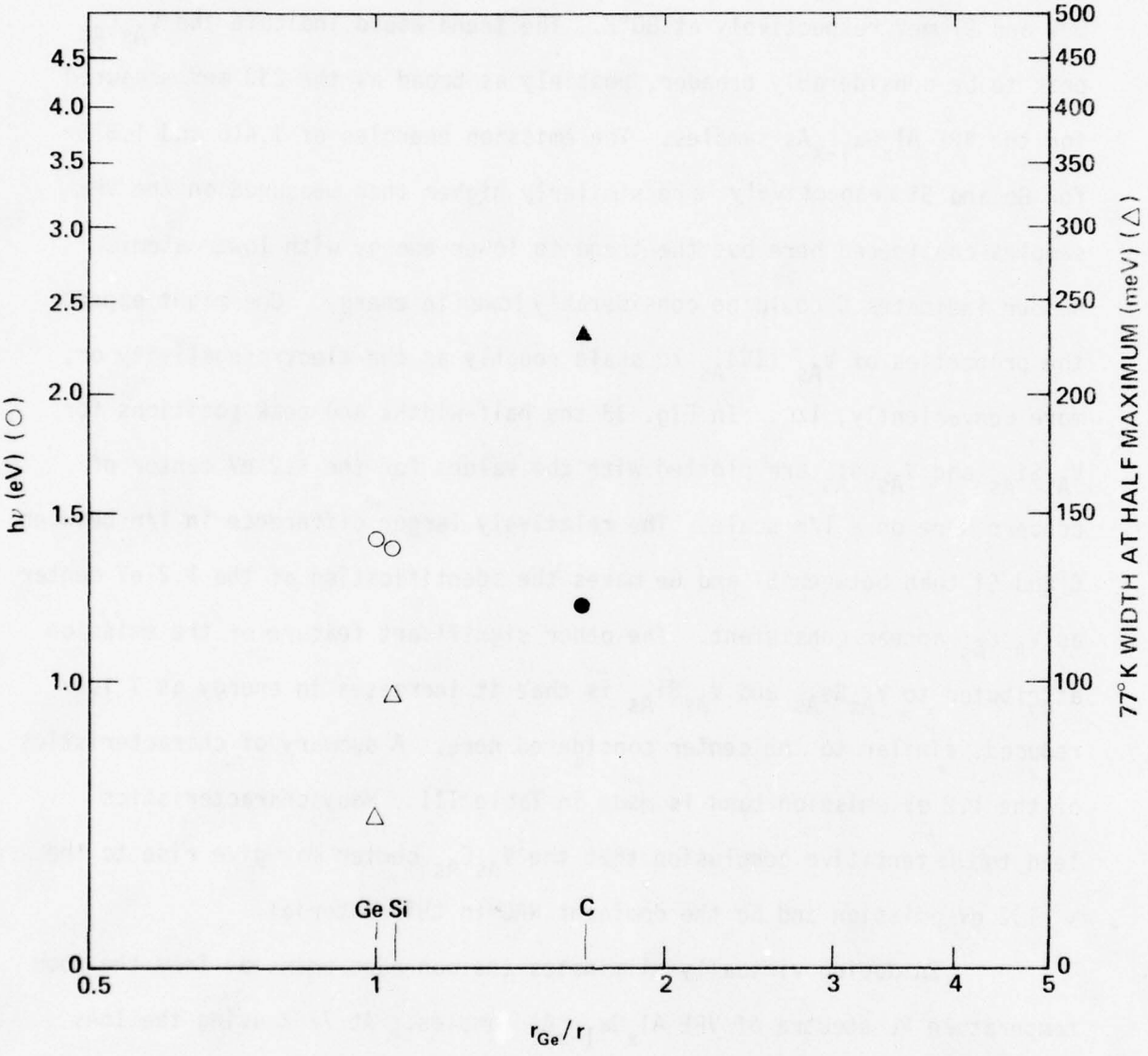

Figure 33. Emission peak energy and halfwidth versus r_{GE}/r for $V_{AS}Ge_{AS}$, $V_{AS}Si_{AS}$ and the 1.2 eV center.

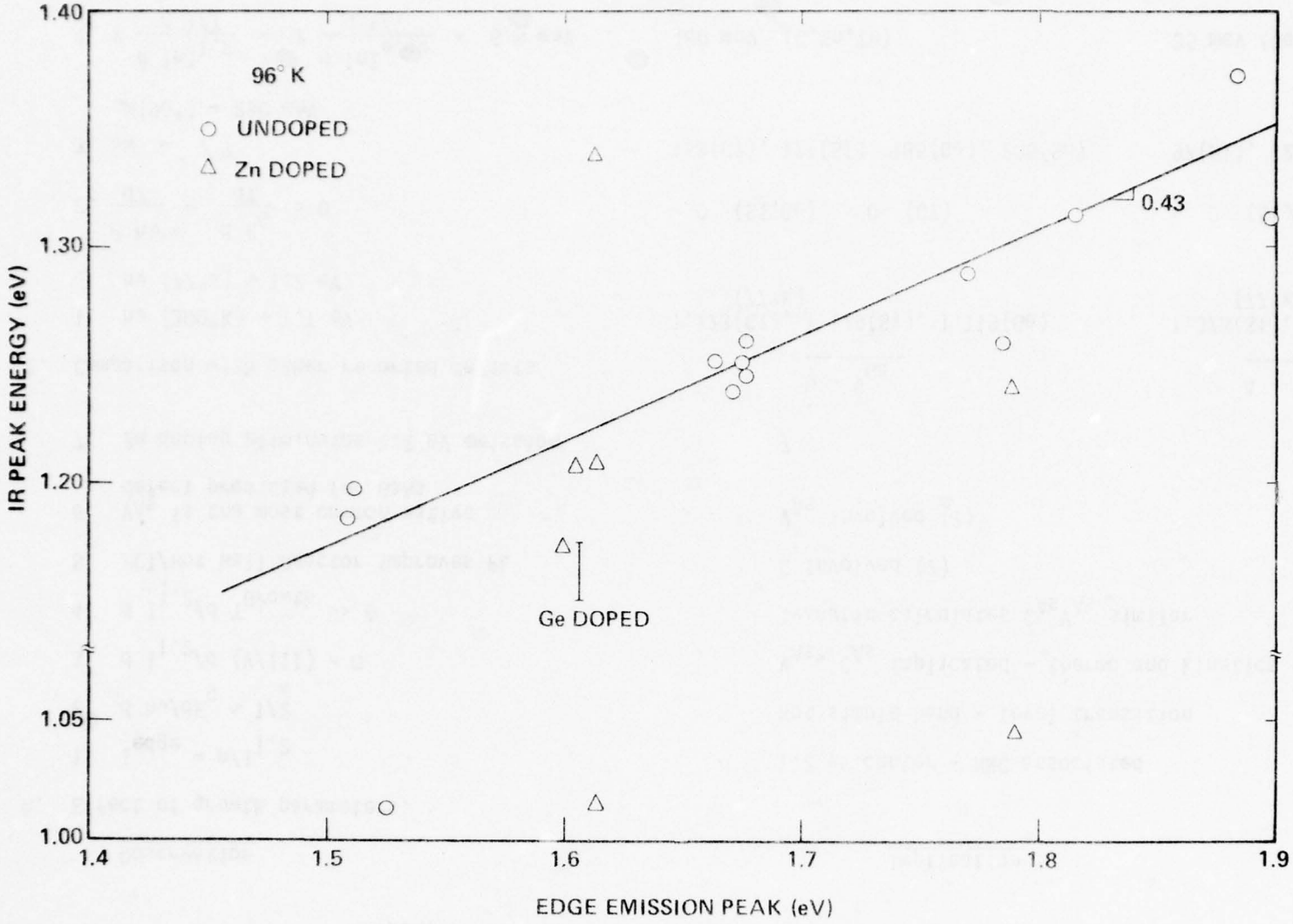

Figure 34. IR peak energy versus edge emission peak for undoped, Zn doped and Ge doped samples.

TABLE III

Properties of 1.2 eV Luminescence

Observation	Implication
A. Effect of growth parameters.	
1. $I_{edge} \propto n/I_{1.2}$	1.2 eV center - NRC associated
2. $d\,h\nu/dE_g \sim 1/2$	Not simple band - level transition
3. $d\,I_{1.2}/d\,(V/III) < 0$	V_{As}, C_{As} implicated - thermo and kinetics
4. $d\,I_{1.2}/d\,T_{Growth} >> 0$	Ivanutin calculates $C_{As}V_{As}$ similar
5. HCl/Hot Wall Reactor improves PL	C involved (?)
6. V_{As} is the most common native defect predicted for GaAs	V_{As} involved (?)
7. Zn doping eliminates 1.2 eV emission	?

B. Comparison with other reported defects	D - V_{Ga}	A - V_{As}
1. $h\nu$ (300°K) ~ 1.1 eV $h\nu$ (77°K) ~ 1.2 eV	1.173(C?), 1.179(Si), 1.119(Ge) (77°K)	1.378(Si), 1.416(Ge) (77°K)
2. $\frac{d\,h\nu}{dT} = \frac{d\,E_G}{dT} > 0$	< 0 (Si,Ge), > 0 (C?)	> 0 (Si,Ge)
3. $\Delta W \propto \sqrt{T}$ $\Delta W(96°) = 230$ meV	158(C?), 171(Si), 185(Ge), 205(Sn)	97(Si), 72(Ge)
4. $K\frac{d\,\ln I_{1.2}}{d\,1/T} = K\frac{d\,\ln I_{edge}}{d\,1/T} = 6.8$ meV	180 meV (C,Sn,Te)	35 meV (Ge)

another lower energy peak is found in some specimens and shown in Fig. 34. This emission band has been seen only in sample 265 of the undoped material. This sample was grown at 650°C. The position of this low energy peak appears to be nearly independent of composition. A higher energy peak at $\sim$ 1.34 eV was observed in one Zn doped specimen. This sample actually had three non-edge emission peaks. No emission for deep levels was observed in the Mg doped specimens.

i. Growth of Laser Structures

Using total flow rate to vary x and with Zn doping it is possible to grow double-heterostructure (DH) laser structures in the hot wall system. A three-layer and four-layer DH laser structure have each been grown with growth conditions shown in Table IV and properties shown in Table V. They are basically $Al_{.3}Ga_{.7}As(p)/Al_{.06}Ga_{.94}As(n)/Al_{.3}Ga_{.7}As(n)$ structures with $\sim$ 0.27 μm active layer thicknesses. An SEM cross section showing the EBIC signal produced at the p-n junction (Fig. 35) shows that it is within the active layer of the device. As might be expected it has diffused a small distance from the $Al_{.3}Ga_{.7}As(p)/Al_{.06}Ga_{.94}As(n)$ interface.

The contraints on growth conditions imposed by the need for good morphology have resulted in layers with I_{PL}/n of only about 10% of LPE values.

This material has been processed into stripe geometry lasers using proton bombardment to define the 8 μm wide stripe. For the VPE material the lasing threshold is approximately 200 mA, approximately a factor of 2 higher than for LPE material, as shown in Table VI. The VPE materials, however, have thicker active layers and lower values of Δx at the boundary layers. Both of these factors lead to higher threshold currents.[41]

TABLE IV

			Molar Flow Ratios						
	Layer	T	Al/III	V/III	HCl/III	Zn/III	F_t (l/min.)	Growth Time (min.)	x
367	3	765	0.122	0.46	0.91	0	2.0	30	0.27
	2	765	0.122	0.46	0.91	0	0.7	2	0.064
	1	765	0.122	0.46	0.91	0.46	2.0	30	0.26
368	4	765	0.122	0.46	0.91	0	2.0	26	0.3
	3	765	0.122	0.46	0.91	0	0.7	2	0.074
	2	765	0.122	0.46	0.91	0.46	2.0	28	0.29
	1	765	0.122	0.46	0.91	0.46	0.8	10	0.06

TABLE V

Characteristics of 3- and 4-Layer Structures for Lasers

Run No.	Layer	t	x	n(p) (from ΔW)	I/I_o	I_{IR}/I_{edge}	I_{PL}/n (Rel to LPE)
367	Top	1.5 μm	0.26	(5×10^{18})	17.4-24.4	0	0.1-0.15
	Active	0.27	0.065	1.5×10^{18}	2.2-6.1	0	0.04-0.12
	Bottom	2.0	0.26	7.5×10^{17}	2.4-2.7	0.3-0.4	0.1
368	Top	1.0	0.06	(4×10^{18})	16	0	0.12
	2nd	2.0	0.29	(3×10^{18})	1.78-3.1	0	0.02-0.31
	Active	0.28	0.07	1.2×10^{18}	15	0	0.38
	Bottom	2.0	0.30	8.0×10^{17}	1.0-1.35	0.64	0.05

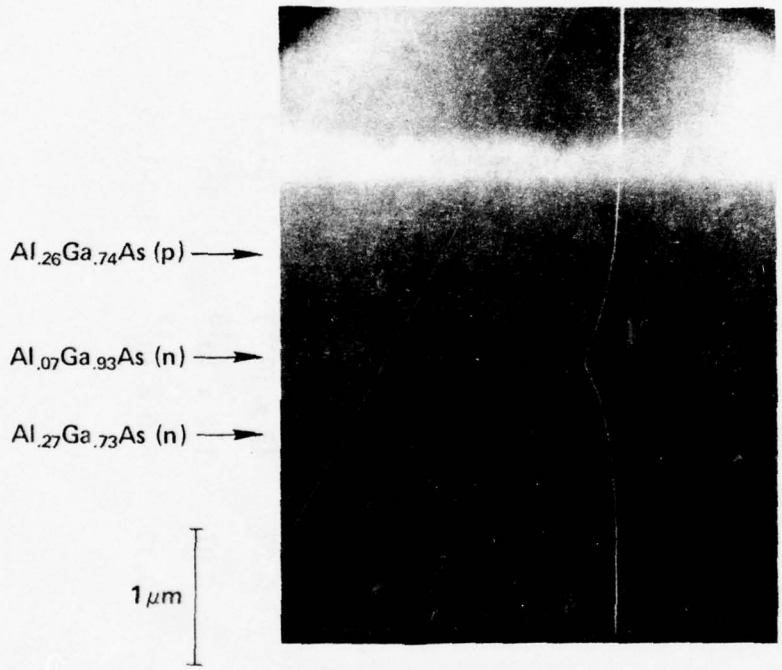

Figure 35. EBIC photograph of the cross section of a laser structure grown by the hot wall OMVPE technique.

TABLE VI

Summary of Laser Data

Sample	J_{th}^{*} (kA/cm^2)	I_{th} (mA)	n (one face)	t(μm)	Δx
367	6.97	212	12.2	0.27	0.20
368	6.35	193	12.3	0.28	0.22
LPE(typical)	∿ 3.3	80 - 100	∿ 15%	0.1 - 0.2	0.29

*Lasers are stripe 8 μm wide and 380 μm long, area = 3 x 10^{-5}cm^2. Stripes misoriented 2° from <110> direction.

B. COLD WALL REACTOR

1. Effect of Baffles

As discussed in the introduction, early results using the conventional cold wall OMVPE apparatus produced perfectly acceptable GaAs, with $N_D - N_A \sim 10^{17}$ cm^{-3} and I_{PL}/n equivalent to LPE material. The $Al_xGa_{1-x}As$ however, had no detectable photoluminescence and had a net electron concentration in undoped material of $\sim 10^{15}$ cm^{-3}. Further sustained effort to reduce oxygen contamination to less than 0.1 ppm yielded a small, but measurable PL signal. As discussed in the Experimental section, baffles were added to the reactor to catalyze the reaction between TMA and O_2 or H_2O to "getter" them from the system.

To understand why the TMA and O_2 (or H_2O) do not react homogeneously in the vapor phase to form small Al_2O_3 particles, it is necessary to perform a simple calculation of the activation barrier impeding this reaction. The equilibrium free energy change for the reaction is approximately -378 kcal/mole[42] of Al_2O_3 at 296°K. However, for the formation of a minute particle the surface energy must be included in the calculation of the total free energy of the system. For very small particles the surface energy is so large that the free energy of the system increases as the particle grows, hence the particle is unstable. Larger particles are stable, and the critical step in the calculation is the determination of the free energy of the critical nucleus where $dG/dr = 0$. This has been determined for the classical case where the macroscopic surface free energy is defined and isotropic:[45,47]

$$\Delta G^* = \frac{16\pi\sigma^3}{3\Delta G_v^2} \qquad (2)$$

where ΔG_v is the thermodynamic free energy of the reaction per unit volume of solid and σ is the surface free energy. Since the density of Al_2O_3 is 3.5 gm/cm^3, ΔG_v = 13 $kcal/cm^3$ but the value of σ at Al_2O_3 at room temperature is not available from the literature. At 1850°C σ = 905 erg/cm^2[48] but the surface energy increases rapidly as temperature is decreased. The best estimate may be to use the general observation that $\sigma \cong \frac{\Delta H^{at}}{2}$ per surface atom. ΔH^{at} of Al_2O_3 at 296°K is 734 kcal/mole[43,49] (ΔH_f°, Al_2O_3 + 2 $\Delta H_{v,Al}$ + $\frac{3}{2}$ $\Delta H_{at,O_2}$). Thus $\sigma \cong 2.09 \times 10^{-6}$ $kcal/cm^2$. Using these parameters ΔG^* can be calculated to be 9.05×10^{-19} kcal for the critical sized nucleus of radius 32 Å. The density of nuclei of different sizes can be shown to form a Boltzmann distribution, thus for $n(i) << n^\circ(1)$ (the number of molecules of O_2 in the vapor phase before any nuclei are formed):

$$n(i^*) = n^\circ(1) \exp(-\Delta G^*/kT) \quad . \qquad (3)$$

Since $\exp(-\Delta G^*/kT)$ equals 5.8×10^{-41} for the Al_2O_3 nuclei this number is essentially zero. Thus homogeneous nucleation would not occur with the value of σ estimated for Al_2O_3 particles.

The free energy barrier for heterogeneous nucleation, for example on a graphite baffle, is much lower:[45]

$$\Delta G^* = \frac{(2 - \cos\theta)(1 - \cos\theta)^2}{4} \quad \frac{16\pi \sigma^3}{3\Delta G_v^2} \qquad (4)$$

assuming the nuclei are in the shape of hemispherical caps.

We do not know θ, the contact angle between the nuclei surface and the substrate, but for a range of reasonable values, θ = 10, 20, 30 and 45°, the term in brackets by which ΔG^* is reduced as compared to the homogeneous

case is 5.90×10^{-5}, 9.60×10^{-4}, 4.76×10^{-3} and 2.77×10^{-2} respectively. Since the number of nuclei is exponentially dependent on ΔG^* the number of nuclei increases dramatically even for the largest angle. For $\Theta = 45°$, $\exp(-\Delta G^*/kT) = 7.66 \times 10^{-2}$. For $p^\circ_{O_2} = 10^{-6}$ this would give 1.84×10^{11} nuclei/cm^3 and would allow nucleation to proceed nearly to completion, thus allowing essentially all O_2 to be removed from the vapor phase by reaction with Al_2O_3.

It should be emphasized that this simple calculation is only a feasibility argument designed to show only that the presence of baffles might allow "gettering" of O_2 by TMA which would not occur by homogeneous nucleation. For a really meaningful calculation the value of σ would have to be known, rather than estimated, since the density of nuclei formed by homogeneous nucleation is proportional to the exponential of a term proportional to σ^3. Thus a factor of 2 in σ makes an enormous difference in the calculated density of nuclei.

The improvement in the quality of the $Al_xGa_{1-x}As$ grown with the baffles present is striking, as shown by the results included in Table VII. In several cases with no change in growth conditions the presence of baffles increases the PL intensity from 0 (undetectable) to respectable values relative to LPE material. The use of 6 baffles seems preferable to 3. The PL intensity is plotted versus $N_D - N_A$ in Fig. 36 and compared with results obtained for LPE materials. A number of samples have PL efficiencies of $\geq$ 50% of LPE material. These are the best results yet obtained for VPE $Al_xGa_{1-x}As$.

Several changes other than the number of baffles were also made in the sequence of runs shown in Table VII and Fig. 36. The V/III ratio and growth temperature were found to produce significant changes in doping and PL efficiency and will be discussed further. In addition for all runs after LS-83 a SiC coated susceptor was used. This might be expected to

TABLE VII

Characteristics of $Al_xGa_{1-x}As$ Layers Grown
Grown With and Without the Presence of Cold Baffles

Run No.	x	I_{PL} (rel to LPE)	$n(cm^{-3})$	I_{PL} (rel to LPE)	Number of Baffles
LS-52	0.03	0.02	4.9×10^{18}(p)	0.001	0
LS-53	0.05	0.007	5.8×10^{18}(p)	3×10^{-4}	0
LS-34	0.002	0.004	5.7×10^{15}	0.21	0
LS-51	0.05	0	———	0	0
LS-54	0.06	0.12	7.9×10^{17}	0.05	3
LS-55	~ 0.06	0	———	0	0
LS-56	0.01	0.65	1.6×10^{17}	1.2	3
LS-63	0.23	0.41	8.8×10^{17}	0.14	3
LS-68	0.06	0.56	9.4×10^{17}	0.18	3
LS-69	0.08	0.60	9.1×10^{17}	0.14	3
LS-70	0.07	0.60	9.2×10^{17}	0.20	3
LS-79	0.06	0	5.9×10^{15}	0	0
LS-83	0.03	0.47	1.0×10^{18}	0.14	5
LS-84	0.02	0.17	1.5×10^{17}	0.34	6*
LS-85	0.03	0.13	8.7×10^{16}	0.45	6*
LS-86	0.03	0.18	2.8×10^{17}	0.19	3*
LS-87	0.05	0.15	9.9×10^{16}	0.45	6*
LS-88	0.38	0.01	4.7×10^{16}	0.06	6*
LS-89	0.02	0.009	2.7×10^{15}	0.71**	6*
LS-94	0.07	0.15	9.2×10^{16}	0.49	6*

*SiC coated pedestal

**I_{PL}/n obtained at low excitation intensity

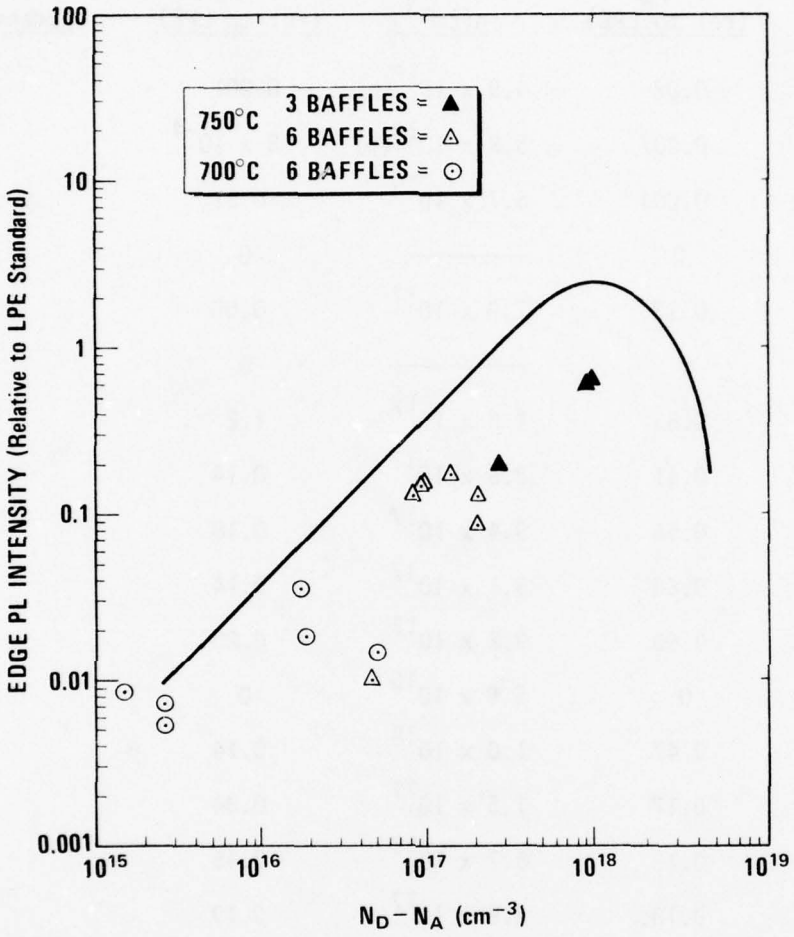

Figure 36. PL intensity versus N_D - N_A for cold wall OMVPE samples.

reduce outgassing from the graphite. This would be a problem not solved by the baffles since the source of oxygen contamination would be down stream from the baffles. Thus the use of a SiC coated pedestal would be expected to further enhance material quality. The results presented in Table VII do indicate that the SiC coating does result in increased PL efficiency.

The addition of baffles in the cold wall system apparently strongly increases PL efficiency presumably by decreasing oxygen contamination of the $Al_xGa_{1-x}As$ layer. This makes the organometallic system much more attractive for commercial applications. Having a commerical growth process extremely sensitive to oxygen contamination, even down to << 0.1 ppm would not seem practical. The gettering provided by the baffles makes the system more "forgiving", similar to LPE where Al_2O_3 precipitates on the top of the melt act to reduce oxygen contamination at the growth interface. The presence of baffles should produce other desirable results such as providing more uniform mixing and suppressing the enormous convection currents caused by the rapid heating of the gases at the pedestal. The suppression of these convection currents by the baffles should allow more rapid changes in composition . We have only investigated the abruptness of changes in composition for laser structures where the relatively thick layers limit the depth resolution of the Auger profiling technique to $\sim$ 500 Å. Thus we have only determined that in the laser structures the change in composition from 0.05 to 0.30 occurs in < 500 Å.

The addition of baffles has one other effect, possibly related to the reduction of the convection. The growth rate is decreased as shown in Fig. 37. The effect is nearly the same for three or six baffles and the reduction is more pronounced for the small separation between the lower baffle and the pedestal. The reduction in growth rate is not related to

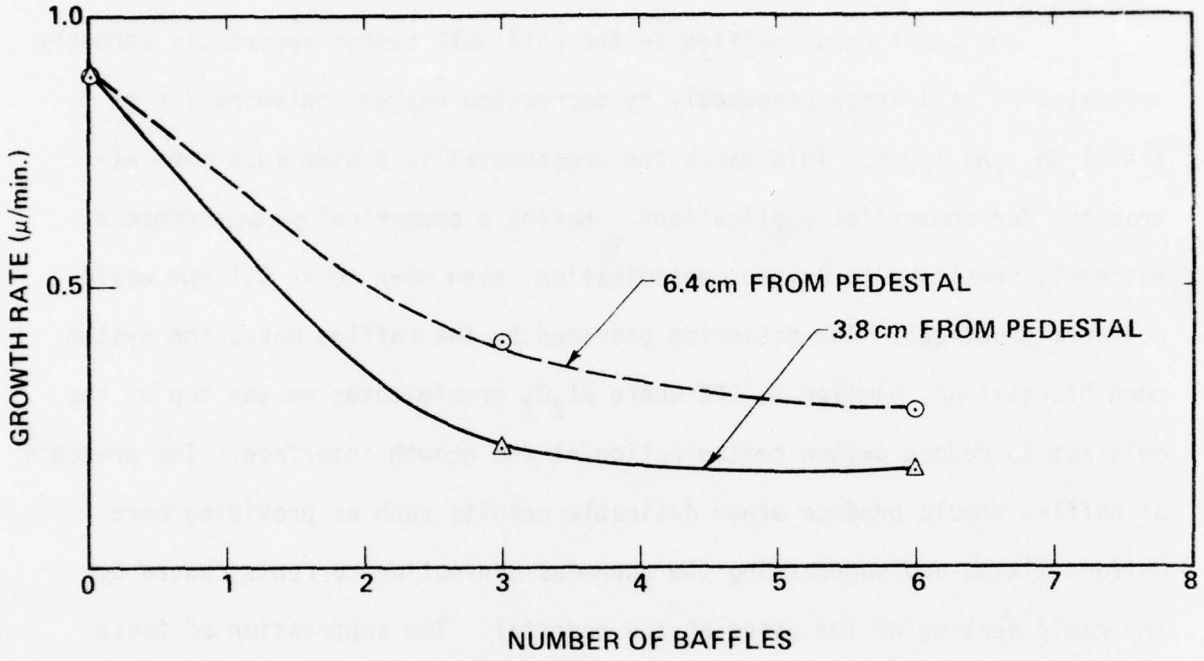

Figure 37. Growth rate versus number of baffles in the gas stream.

predeposition on the baffles since little is observed. Since we know that the growth rate is limited by diffusion through a boundary layer at the substrate,[11] the effect could be explained by elimination of the large convection currents. This would be expected to markedly increase the boundary layer thickness thus decreasing the growth rate.

2. Effect of V/III Ratio and T

In Table VIII data are tabulated for a series of runs where V/III ratio and substrate temperature were varied. The carrier concentration is plotted versus V/III ratio in Fig. 38. The data are widely scattered but a trend to p-type doping at higher values of V/III ratio is observed. This is exactly the opposite effect reported for GaAs growth in similar systems,[50,51] and attributed to the effect of stoichiometry of the solid on the site distribution of amphoteric group IV impurities. It was postulated that the effect we observe might be due to the presence of an acceptor being carried in the AsH_3, thus in Fig. 39 carrier concentration is plotted versus the AsH_3 flow rate. This plot shows clearly that the p-type doping occurs only at high AsH_3 flow rates, and is apparently independent of V/III ratio.

Another important parameter, as seen in Figs. 38 and 39 is growth temperature. The carrier concentration drops by a factor of $\sim 10^2$ when the growth temperature is decreased from 750°C to 700°C. From the limited data the reduction in growth temperature also appears to increase the PL efficiency normalized by n, as shown in Fig. 40. For samples with low values of n ($< 5 \times 10^{15}$ cm^{-3}) the number of electrons produced by the typical PL excitation, Δn, exceeds n. Thus the ratio of the PL intensity to that of the LPE standard is dependent on excitation intensity and I_{PL}/n is no longer a good indicator of minority carrier lifetime. For such samples the excitation

TABLE VIII

Summary of the Efeects of V/III Ratio and Temperature

No.	x	T	$f_{AsH_3} \times 10^4$ (m/min)	$f_{TMG} \times 10^5$ (m/min)	$f_{TMA} \times 10^6$ (m/min)	V/III	$n(cm^{-3})$	I_{PL}/n
98	0.01	700	9.8	6.8	2.8	14.0	3.1×10^{15}(p)	0.41*
99	0.03	"	"	3.4	"	27.0	7.9×10^{14}(p)	0.18**
84	0.02	750	4.9	7.2	1.9	7.0	1.5×10^{17}	0.34
85	0.03	"	"	"	"	7.0	8.7×10^{16}	0.45
86	0.03	"	"	"	"	7.0	2.8×10^{17}	0.19
87	0.05	"	"	"	7.8	7.0	9.9×10^{16}	0.45
88	0.38	"	"	2.6	13.0	12.0	4.7×10^{16}	0.06
91	0.06	"	"	5.8	2.8	8.0	2.0×10^{17}	0.12
100	0.04	"	"	3.4	"	14.0	3.1×10^{14}	——
90	0.05	760	"	6.8	"	7.0	2.1×10^{17}	0.17
89	0.02	700	"	"	"	7.0	2.7×10^{15}	0.71*
127	0.06	"	"	"	"	7.0	1.6×10^{15}	1.8*
128	0.06	"	"	"	"	7.0	5.3×10^{14}	0.40**
104	0.05	"	"	"	5.6	6.6	2.7×10^{15}	0.53*
105	0.03	"	"	3.4	2.8	14.0	2.6×10^{13}	0.04**
94	0.07	750	2.4	"	"	7.0	9.2×10^{16}	0.49
95	0.05	700	"	"	"	7.0	1.8×10^{16}	0.60
96	0.06	"	0.89	"	"	2.4	2.0×10^{16}	0.27
97	——	"	"	6.8	"	1.2	Polycrystalline	Polycrystalline
106	0.04	"	"	3.4	"	2.4	5.0×10^{16}	0.08

*SiC coated pedestal

**I_{PL}/n obtained at low excitation intensity

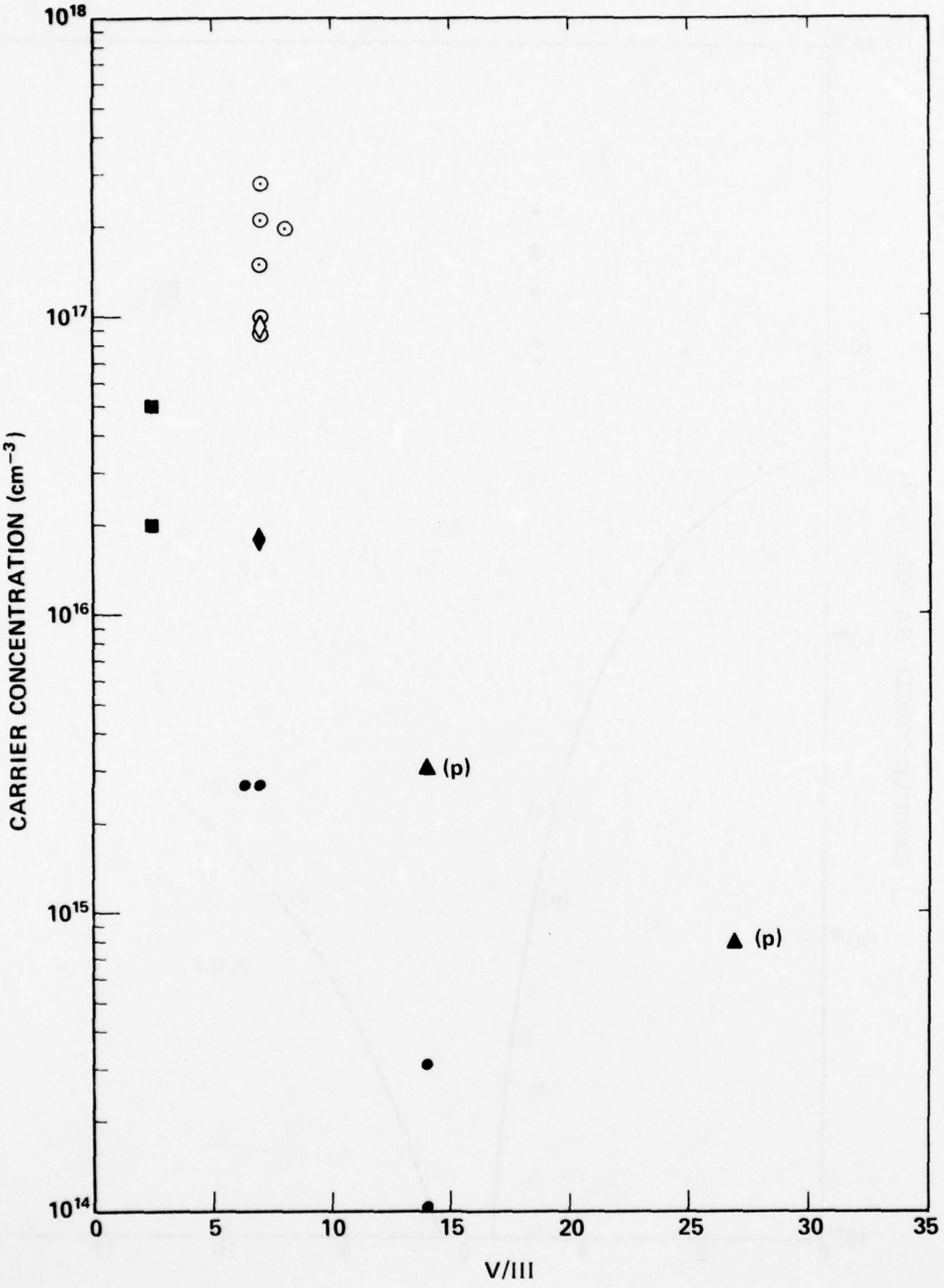

Figure 38. Carrier concentration versus V/III reactor.

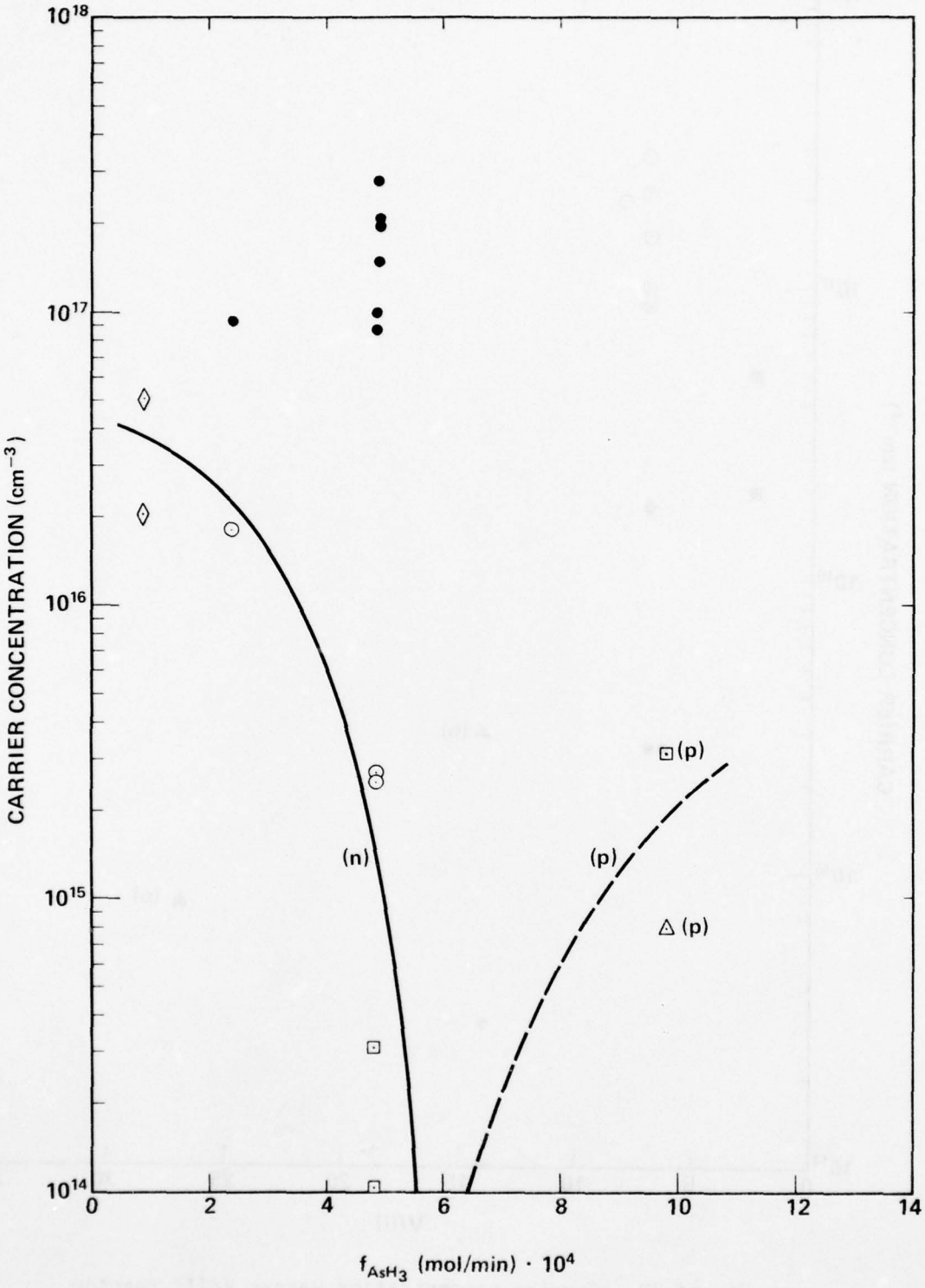

Figure 39. Carrier concentration versus AsH_3 flow rate.

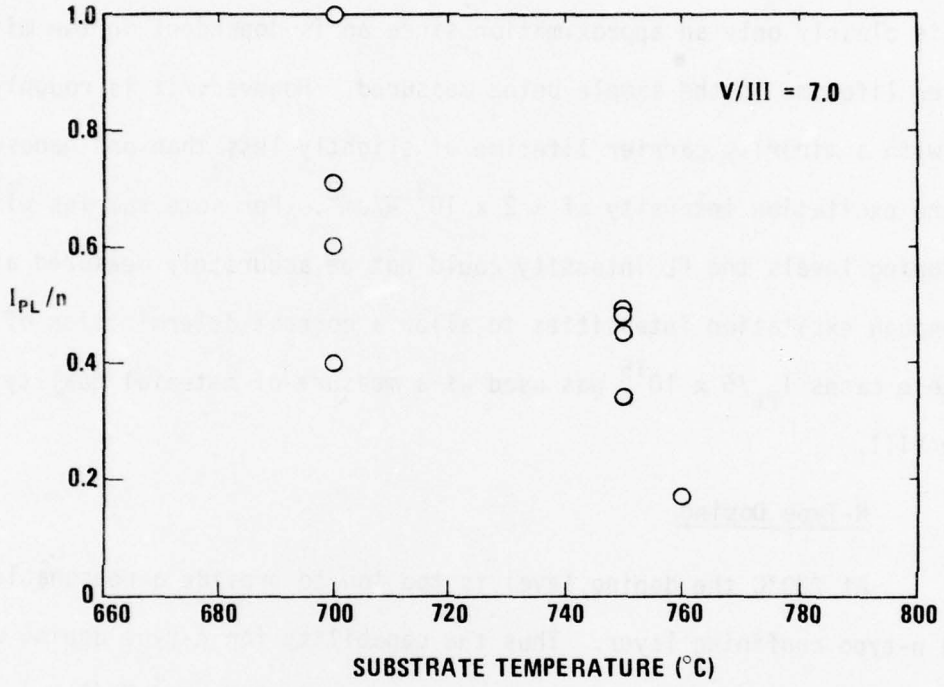

Figure 40. PL intensity versus growth temperature for cold wall OMVPE $Al_xGa_{1-x}As$.

intensity has been reduced until the ratio becomes excitation independent. The values of I_{PL}/n obtained in this way are found to be approximately equivalent to taking $I_{PL}/5 \times 10^{15}$ for many samples. This is equivalent to saying that $\Delta n \approx 5 \times 10^{15}$ cm^{-3} under standard PL excitation intensities. This is clearly only an approximation since Δn is dependent on the minority carrier lifetime in the sample being measured. However, it is roughly consistent with a minority carrier lifetime of slightly less than one nanosecond and the excitation intensity of $\sim 2 \times 10^{3}$ W/cm^{2}. For some samples with very low doping levels the PL intensity could not be accurately measured at low enough excitation intensities to allow a correct determination of I_{PL}/n. In these cases $I_{PL}/5 \times 10^{15}$ was used as a measure of material quality in Table VIII.

3. N-Type Doping

At 700°C the doping level is too low to provide a reasonable undoped n-type confining layer. Thus the capability for n-type doping was developed. Several dopants were investigated: H_2S, SiH_4 and $Te(C_2H_5)_2$. H_2S diluted to 50 ppm in H_2 was investigated first. At 700°C in $Al_{.2}Ga_{.7}As$, the material for which n-type doping would be most important, essentially no increase in the carrier concentration was measured and the PL emission was totally eliminated as shown in Table IX. Thus, the effort was immediately shifted to SiH_4. This would seem to be a logical choice since nominally undoped material is thought to be doped to $> 10^{17}$ cm^{-3} with Si present in the organometallic sources. As shown in Table IX and Figure 41, some small amount of n-type doping is observed but the mobility is drastically reduced, which may be a sign of increased self compensation. Thus the use of DETe was explored. At 700° the DETe is somewhat more effective as an n-type dopant as shown in

TABLE IX

Summary of n-Type Doping Runs

Sample No.	T	x	Dopant	p_D°	n	μ	(rel to std)	I_{IR}/I_e	$h\nu_{IR}$	1/2 ΔW^* (eV)
111	700	~ 0.3	H_2S	1.8×10^{-6}	5.1×10^{15}	1204	0			
112	"	~ 0.3	"	3.0×10^{-6}	———	———	0			
123	"	0.30	SiH_4	2.9×10^{-6}	2.6×10^{15}	195	0.50**	12	1.35	0.13
124	"	0.29	"	4.7×10^{-6}	2.8×10^{15}	142	0.65**	24	1.34	0.12
125	"	0.27	"	1.4×10^{-5}	1.5×10^{16}	170	0.14	39	1.33	0.13
129	"	0.05	DETe	4.6×10^{-6}	7.1×10^{17}	2016	0.03	0.05	1.18	0.09
130	"	~ 0.30	"	4.5×10^{-6}	4.3×10^{15}	132	0	0		
131	"	0.30	"	1.2×10^{-5}	1.1×10^{17}	313	0	0.6 of std	1.31	0.13
136	750	0.30	"	4.6×10^{-5}	1.3×10^{18}	1234	0.58	0.10	1.31	0.13

*Estimated from 1/2 of peak

**Low excitation intensity

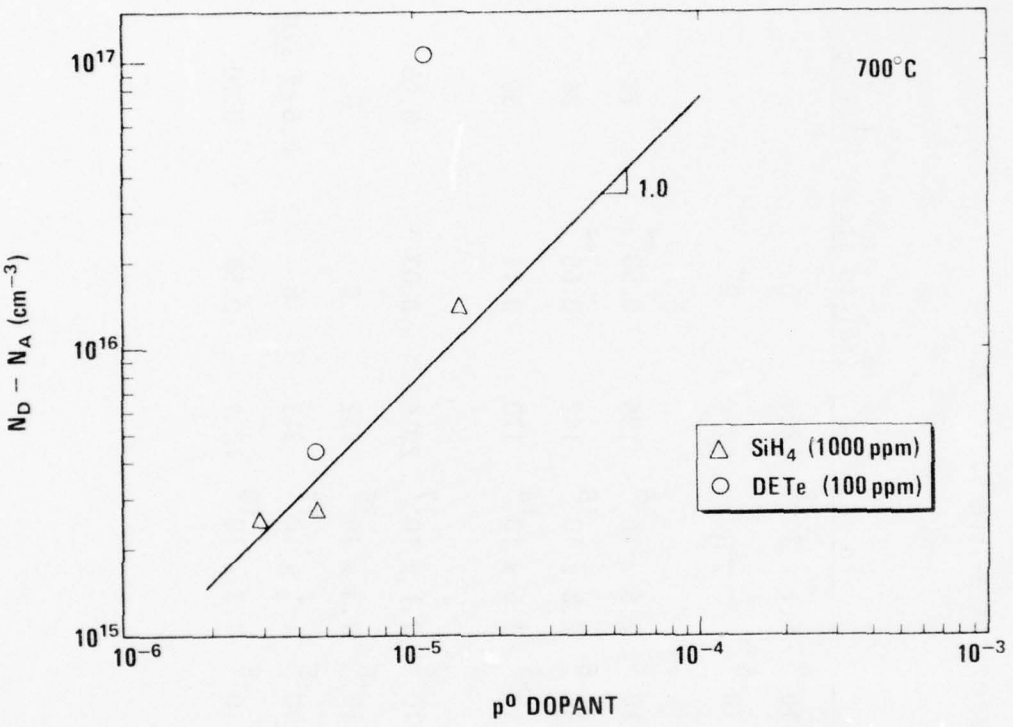

Figure 41. N-Type doping level versus dopant partial pressure.

AD-A078 264 HEWLETT-PACKARD CO PALO ALTO CALIF SOLID STATE LAB F/G 20/12
VPE GROWTH OF (AL, GA)AS.(U)
OCT 79 G B STRINGFELLOW
UNCLASSIFIED RADC-TR-79-207 F19628-77-C-0199 NL

2 OF 2
AD A078264

END
DATE FILMED
1-80
DDC

Table IX and Fig. 41, although it also reduced the edge PL intensity and gives rise to a large IR emission peak.

Increasing the growth temperature to 750°C increases the doping efficiency. The IR peak produced by S, Si and Te doping occurs at $\sim$ 1.3 eV and is similar in both position and halfwidth to the IR peaks observed in hot wall samples which have $n > 10^{17}$ cm^{-3} when unintentionally doped. This will be discussed in more detail in the section on DLTS results.

4. Laser Performance

Two 4-layer runs grown in the cold wall reactor were submitted for processing into laser devices. The runs, LS 74 and LS 78, were grown in the system with three baffles, T = 750°C and V/III = 7.0 at a time before the SiC coated pedestal was added to the system. LS 74 had a GaAs active layer and LS 78 an $Al_{.05}Ga_{.95}As$ active layer. Neither active layer was intentionally doped. Two EBIC cross sections of LS 78 are shown in Fig. 42. Fig. 42(a) was obtained on a lightly etched device, so that the coincidence of p-n junction with the edge of the active layer could be observed. No detectable movement of the p-n junciton has occurred. The shape of the EBIC signal is however rather unusual. Since the effect is not seen for the unetched cross section (Fig. 42(b)), it must be related to the etching process. The characteristics of the two structures are given in Table X along with the laser characteristics. The average threshold current density for the $Al_{.05}Ga_{.95}As$ active layer devices is approximately two times higher than those obtained in LPE material. Lasers in the higher efficiency material have not yet been fabricated for evaluation.

(a)

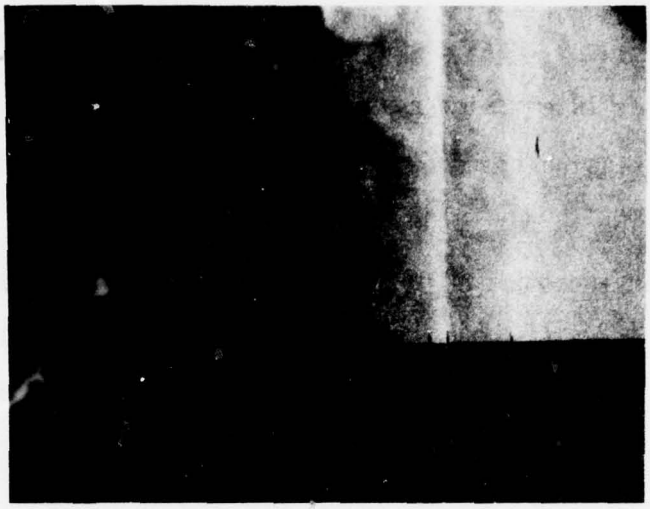

1 μm

(b)

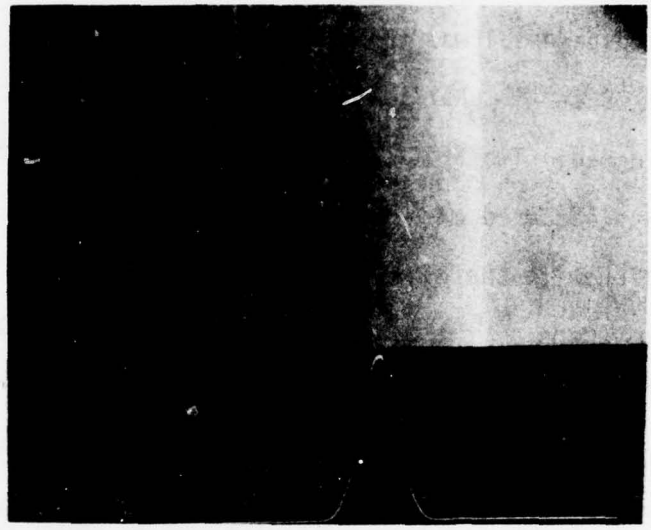

Figure 42. EBIC photographs of cross sections for cold wall OMVPE laser structures.

TABLE X

Summary of Laser Performance of Material From the Cold Wall Reactor

No.	t(μm)	x	Dopant	I_{th}^{*}	η^{*}
LS-74				252 mA	8%
(1)	2.35	0.28	None		
(2)	0.20	0	None		
(3)	0.62	0.29	Zn		
(4)	0.30	0	Zn		
LS-78					
(1)	1.60	0.24	None	177	9%
(2)	0.15	0.05	None		
(3)	0.60	0.32	Zn		
(4)	0.40	0	Zn		

*Comparable lasers grown using LPE have $I_{th} \approx$ 100 mA and η = 15%.

These devices are apparently less likely to have "kinks" in the ϕ-I characteristics than comparable devices fabricated in LPE material. For run number LS 74 eight out of the ten devices tested had linear ϕ-I characteristics up to 8 mW. The devices also had identical ϕ-I curves for each face, a situation seldom observed in LPE devices. These two positive features of the VPE lasers may be related to better uniformity of thickness and/or composition.

For comparison with other results reported for OMVPE lasers it is necessary to compare values of the threshold current density of VPE with LPE devices, since the details of the devices used in different laboratories are different. For example Dupuis and Dapkus[52,53] have fabricated only broad stripe lasers which have low threshold current densities as compared with the narrow stripe geometry lasers made in HP Labs. Other factors affecting threshold current density are active layer thickness and Δx, the composition change between active and confining layers. In Fig. 43 the threshold current densities of our VPE devices are plotted versus the threshold current densities of our LPE 8 μm stripe geoemtery lasers with nearly the same values of active layer thickness and Δx. The results of Dapkus and Dupuis[52] are also plotted for their broad stripe lasers with active layer thickness of 0.083 - 0.157 μm, $\Delta x \sim 0.50$ and $Al_xGa_{1-x}As$ active layers with x = 0.08 - 0.12. Since no results for LPE lasers were published, their results are compared with OMVPE lasers with GaAs active layers.[53] These devices have threshold current densities very close to those reported for LPE devices since for LPE J_{th} is independent of the value of x in the active layer for these low values of X. The GaAs active layer devices used for comparison were selected from the values listed in ref. (53) to have comparable values of active layer thickness and x. From the data plotted in Fig. 43 it is apparent that the

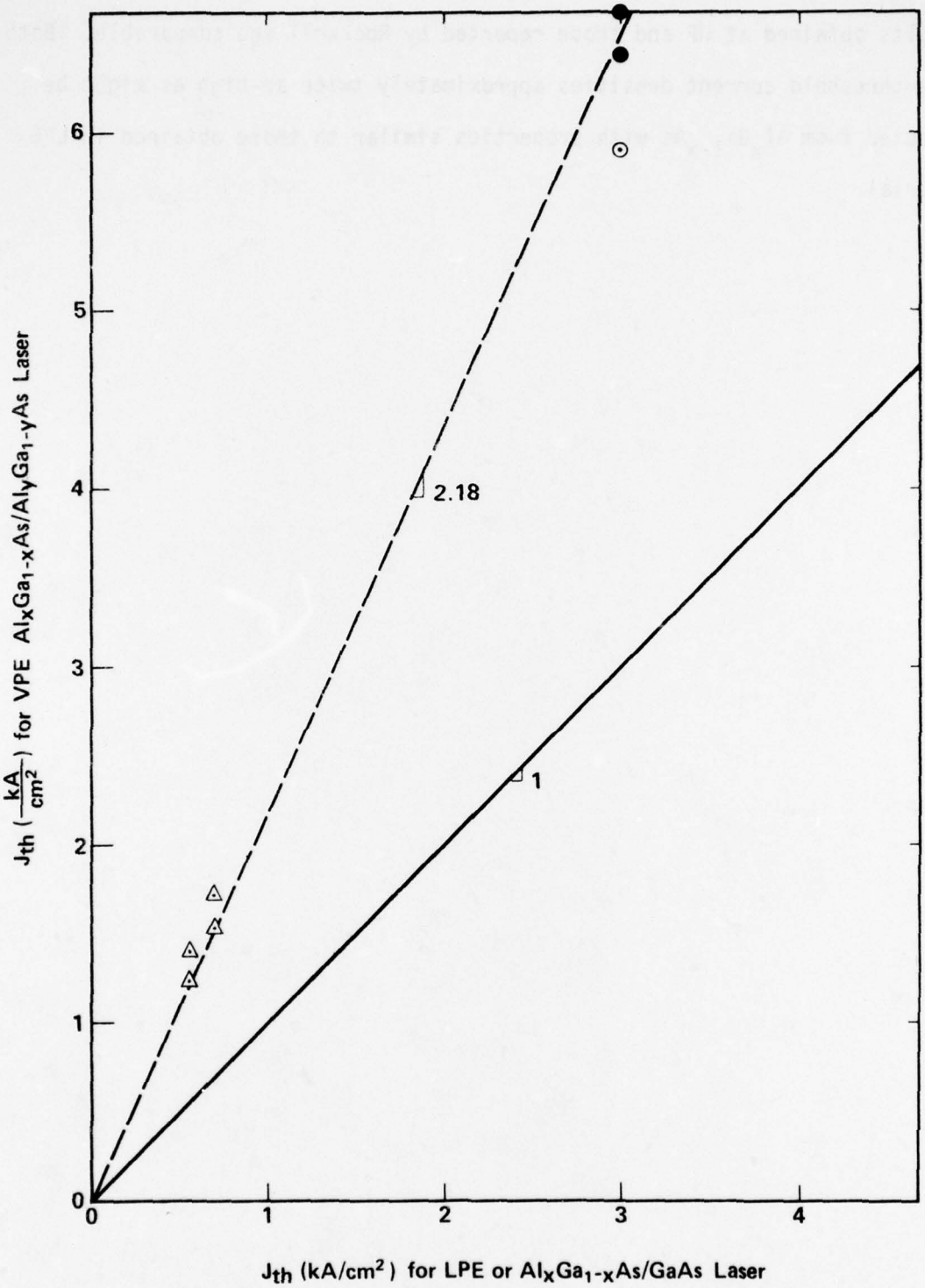

Figure 43. Threshold current density of OMVPE lasers with $Al_xGa_{1-x}As$ active layers versus results for LPE lasers. Data points are for hot wall (●) and cold wall (⊙) systems at HP Labs and cold wall results of Dupuis and Dapkus[52] (△).

results obtained at HP and those reported by Rockwell are comparable. Both have threshold current densities approximately twice as high as might be expected from $Al_xGa_{1-x}As$ with properties similar to those obtained in LPE material.

C. CHARACTERIZATION OF HOT- AND COLD-WALL OMVPE

1. Electron Mobility

The experimental values of room temperature electron mobility in samples of $Al_xGa_{1-x}As$ with $0 < x < .35$ grown by both LPE and VPE techniques are plotted versus free electron concentration in Fig. 44. For GaAs, mobility data are included for samples grown using three techniques: LPE, chloride + hydride VPE,[54] and cold wall organometallic VPE using either TMG or TEG. The mobility in GaAs appears to be independent of growth technique. The solid curve is simply a reasonable fit to the experimental data. It is similar to the calculations by Rode and Knight[55] with $N_A = 5 \times 10^{15}$ cm^{-3} thus the samples are apparently somewhat compensated at low values of n. At high values of n the calculation fits neither the data presented in reference (55) nor the present results. The mobilities in $Al_xGa_{1-x}As$ at all values of n are clearly lower than in GaAs, and the reduction in mobility seems to increase with increasing x.

The electron mobility measured at 77°K is plotted versus n in Fig. 45. Here the scale is changed at $n = 10^{17}$ cm^{-3} to allow the higher mobilities obtained in GaAs at lower values of n to be plotted. The strong increase in mobility obtained by cooling the GaAs from 300°K to 77°K is not observed in the $Al_xGa_{1-x}As$ layers. In fact, from a comparison of Figs. 44 and 45 the $Al_xGa_{1-x}As$ mobility appears to be nearly temperature independent.

A detailed study of the temperature dependence of mobility in the range from 56°K to > 300°K was made for several samples. Only specimens with $n < 10^{17}$ cm^{-3} were chosen for this study. The effect of x on mobility is strongest for these specimens due to the smaller ionized impurity scattering. An additional very important reason for restricting ourselves to samples with $n < 10^{17}$ cm^{-3} is that in this range the scattering mechanisms

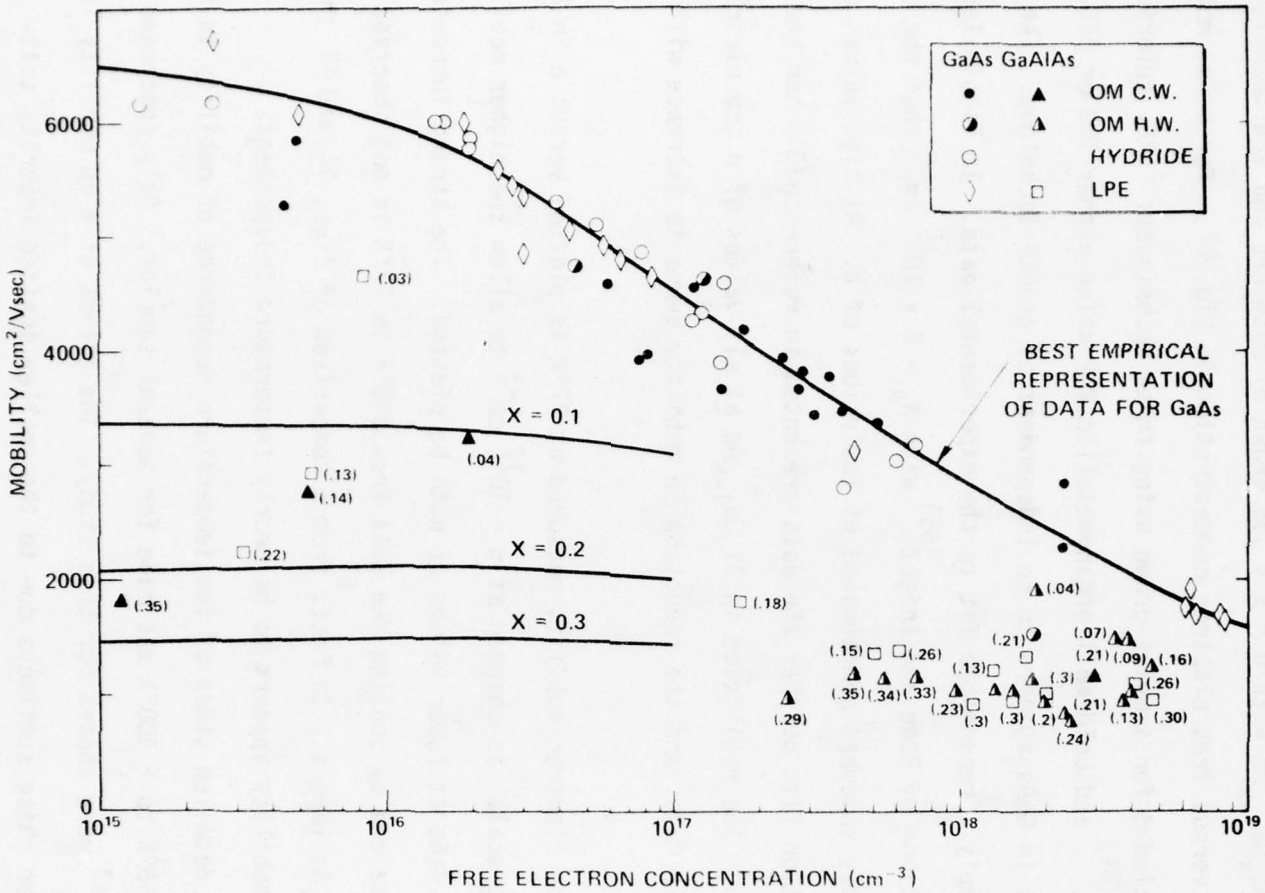

Figure 44. Mobility (300°K) versus $N_D - N_A$.

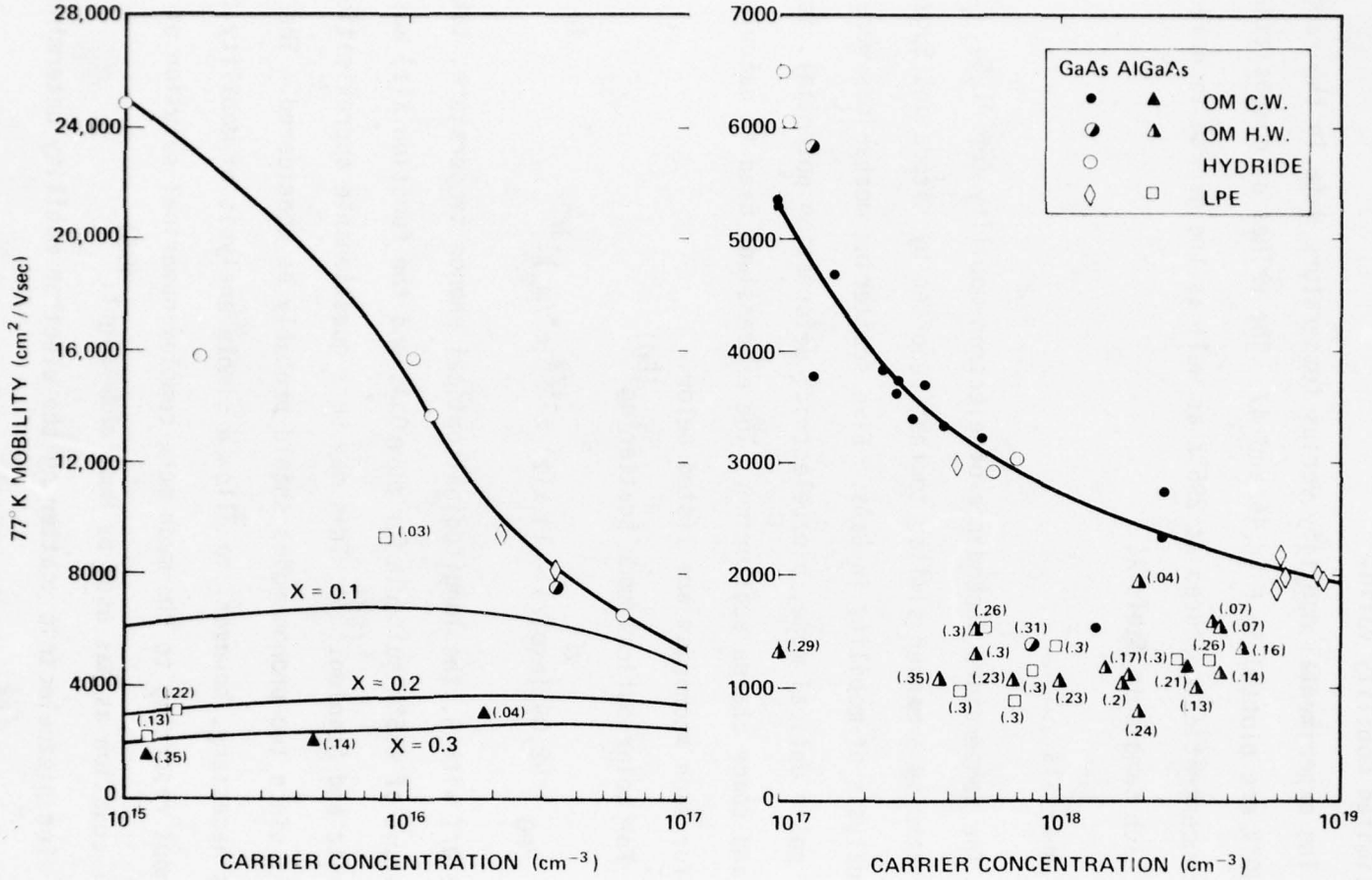

Figure 45. Mobility (77°K) versus $N_D - N_A$.

can be investigated by fitting a calculated $\mu(T)$ function to the experimental data. Only in this range of n is the Brooks-Herring[56] calculation of ionized impurity limited mobility valid.[57,58]

The experimental mobility versus temperature data in the range from 56°K to 400°K are plotted in Figs. 46 and 47. The values of composition and electron concentration measured at 296°K as well as the growth technique are given for each sample in Table XI.

a. Analysis

The temperature dependence of electron mobility for $Al_xGa_{1-x}As$ was calculated in a manner similar to that reported by Katoda and Sugano[59] for the analysis of mobility in GaAs. Five scattering mechanisms were considered: polar optical mode, piezoelectric, deformation potential, ionized impurity and space charge scattering. The expressions used to calculate the mobility for each mechanism are listed below.

For polar optical mode scattering[60]

$$\mu_{PO} = 92.09\ (\exp(z) - 1)\ x(z)\ z^{-1/2}(m^*/m_o)^{-3/2} \quad , \qquad (5)$$

where $z = \theta/T$ with θ, the longitudinal optical phonon temperature, taken to be a constant of 416°K suitable for pure GaAs and the function $x(z)$ was obtained from Petritz and Scanlon.[60] This may be a questionable approximation for $Al_xGa_{1-x}As$ since two phonon modes should probably be considered. The approximation is necessary, however, to allow a simple analysis of mobility to be made without resorting to the much more complex numerical solution of the Boltzmann equation as was used by Rode and Knight.[55]

For piezoelectric scattering the electron mobility determined by Van Daal[61] and Hutson[62] may be written

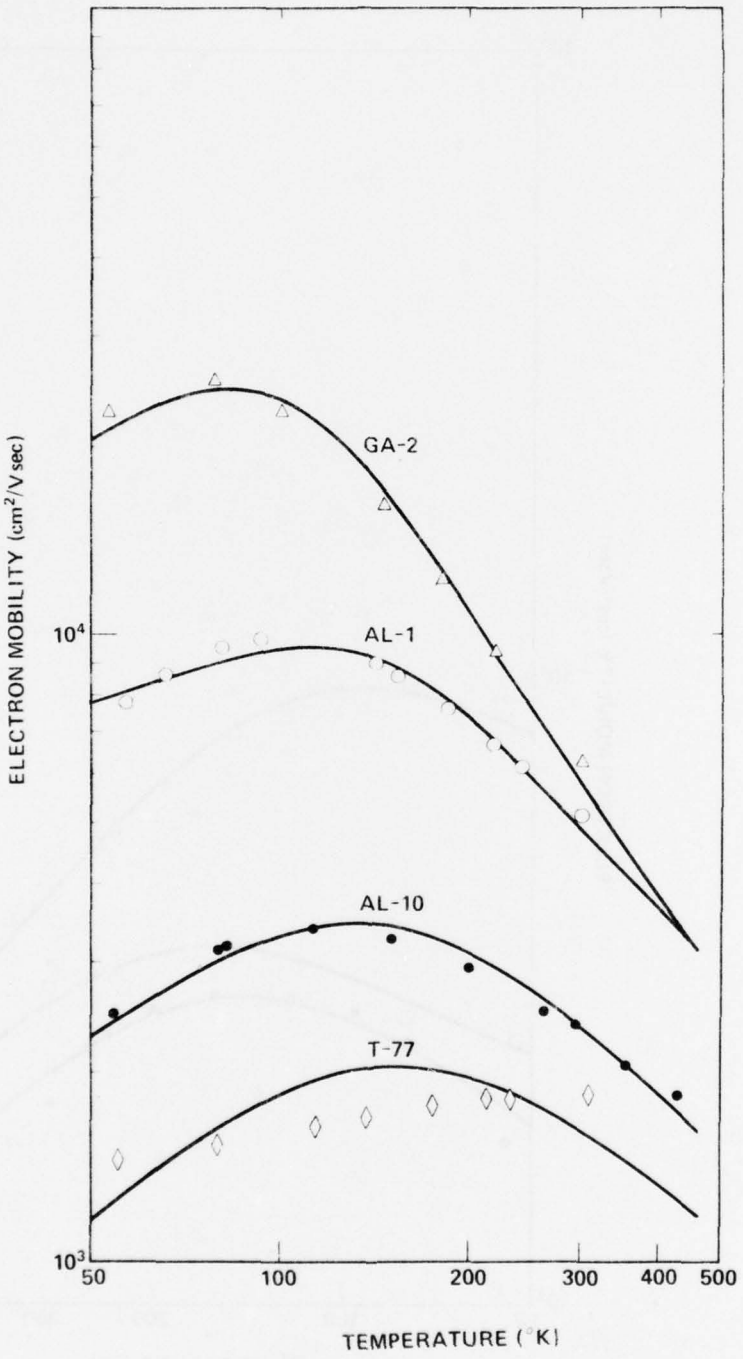

Figure 46. Mobility versus T for $Al_xGa_{1-x}As$.

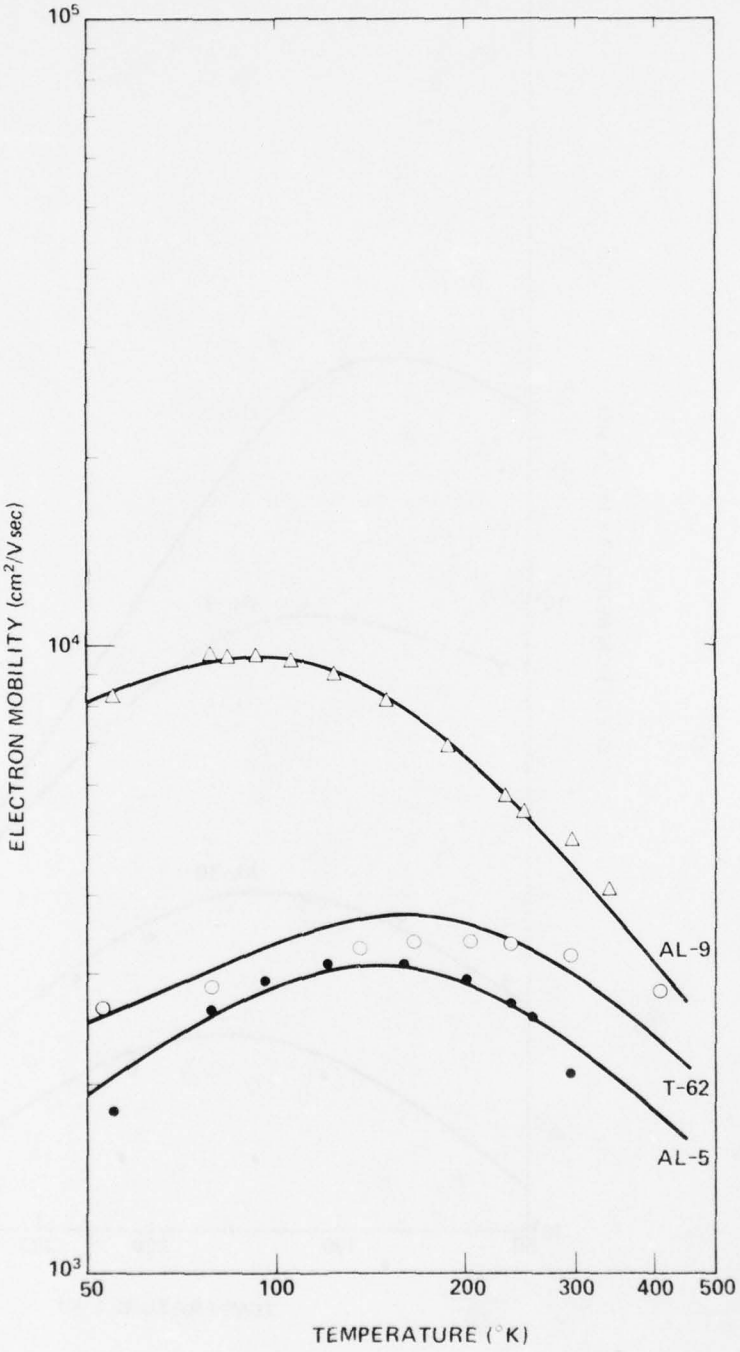

Figure 47. Mobility versus T for $Al_xGa_{1-x}As$.

TABLE XI

Summary of Parameters For $Al_xGa_{1-x}As$ Samples

Sample Number	Growth Technique	x	$10^{-15} \times n(cm^{-3})$	$10^{-16} \times N_A(cm^{-3})$	$10^{-5} \times N_S Q(cm^{-1})$
GA-2	VPE-chloride	0	1.30	0.234	0.120
AL-1	LPE	0	27.4	1.24	0.314
AL-9	LPE	0.03	7.13	0.873	0.444
T-62	OMVPE (Cold Wall)	0.04	19.8	6.51	0.616
AL-5	LPE	0.13	3.50	4.22	1.08
AL-10	LPE	0.22	3.10	2.81	1.07
T-77	OMVPE (Cold Wall)	0.35	1.15	5.45	2.10

$$\mu_{PE} = 9.40 \times 10^{4}\ T^{-1/2}\ (m^*/m_o)^{-3/2} \quad . \qquad (6)$$

The mobility for deformation potential scattering was derived by Bardeen and Schockley[63]

$$\mu_{DP} = 6.39 \times 10^{5}\ T^{-3/2}\ (m^*/m_o)^{-5/2} \quad . \qquad (7)$$

An expression for the ionized impurity limited mobility was obtained by Brooks and Herring[56]

$$\mu_{II} = 2.118 \times 10^{18}\ T^{3/2}\ (m^*/m_o)^{-1/2}/N_t[\ln\ (1 + C) - C/(1 + C)] \qquad (8)$$

where $N_t = N_D + N_A$ and $C = 1.395 \times 10^{15}\ (m^*/m_o)\ T^2/n$ when the donors and acceptors are fully ionized as in the present case. This expression is valid only for $n < 10^{17}\ cm^{-3}$.[51,58]

The mobility limited by space charge scattering was first obtained by Conwell and Vassell[64,65]

$$\mu_{SC} = 2.4 \times 10^{9}/N_s Q\ (T\ m^*/m_o)^{1/2} \quad , \qquad (9)$$

where $N_s Q$ represents the density-cross section product for the scattering centers.

The total mobility is calculated using the simplifying assumption

$$1/\mu = \sum_i 1/\mu_i \qquad (10)$$

summed over all of the individual mobilities for each scattering mechanism.

The curves plotted for each set of experimental data in Figs 46 and 47 were calculated as described above with the values of N_A and $N_s Q$ adjusted to give the least squares fit to the data. The values of effective mass were determined from the expression[15]

$$m^* = 0.067 + 0.083\ x \quad . \tag{11}$$

The experimental data plotted in Figs. 46 and 47 show a marked decrease with increasing x in the high temperature portion of the curve. The slope decreases from $-\frac{3}{2}$ to $-\frac{1}{2}$. These facts are indicative of the increase in space charge scattering with increasing x. The low temperature branch decreases even more rapidly indicating that ionized impurity scattering also increases with increasing x even though n is relatively constant. These general observations are borne out by the values of $N_s Q$ and N_A listed in Table XI.

A similar analysis of LPE $Al_xGa_{1-x}As$ mobility led Kaneko et al.[66] to conclude that $N_s Q$ increases linearly with solid composition, x. As shown in Fig. 48 the present data for both VPE and LPE samples over a much wider range of x agree with their empirical relation

$$N_s Q = 5 \times 10^3 + 6.3 \times 10^5 x \quad . \tag{12}$$

For GaAs Katoda and Sugano[59] found that an increase in space charge scattering is always associated with a proportional increase in the compensation ratio, $(N_D + N_A)(N_D - N_A)$. The space charge centers apparently become more prevalent as compensation ratio increases in GaAs as might be expected. The present data for $n < 10^{16}$ cm^{-3} seem to confirm this relationship for $Al_xGa_{1-x}As$. However, for $n > 10^{16}$ cm^{-3} the large values of compensation ratio for $x > 0.1$ give calculated values of mobility much lower than the experimental data of Figs. 44 and 45. Therefore, the compensation ratio must be a function of <u>both</u> x and n. A simple alternate interpretation for the present data and those of Katoda and Sugano[59] is that, in fact, N_A rather than the compensation ratio increases linearly with x and $N_s Q$. As shown in Fig. 49 this interpretation of the data yields a good correlation for the present data and those of Katoda and Sugano.[59]

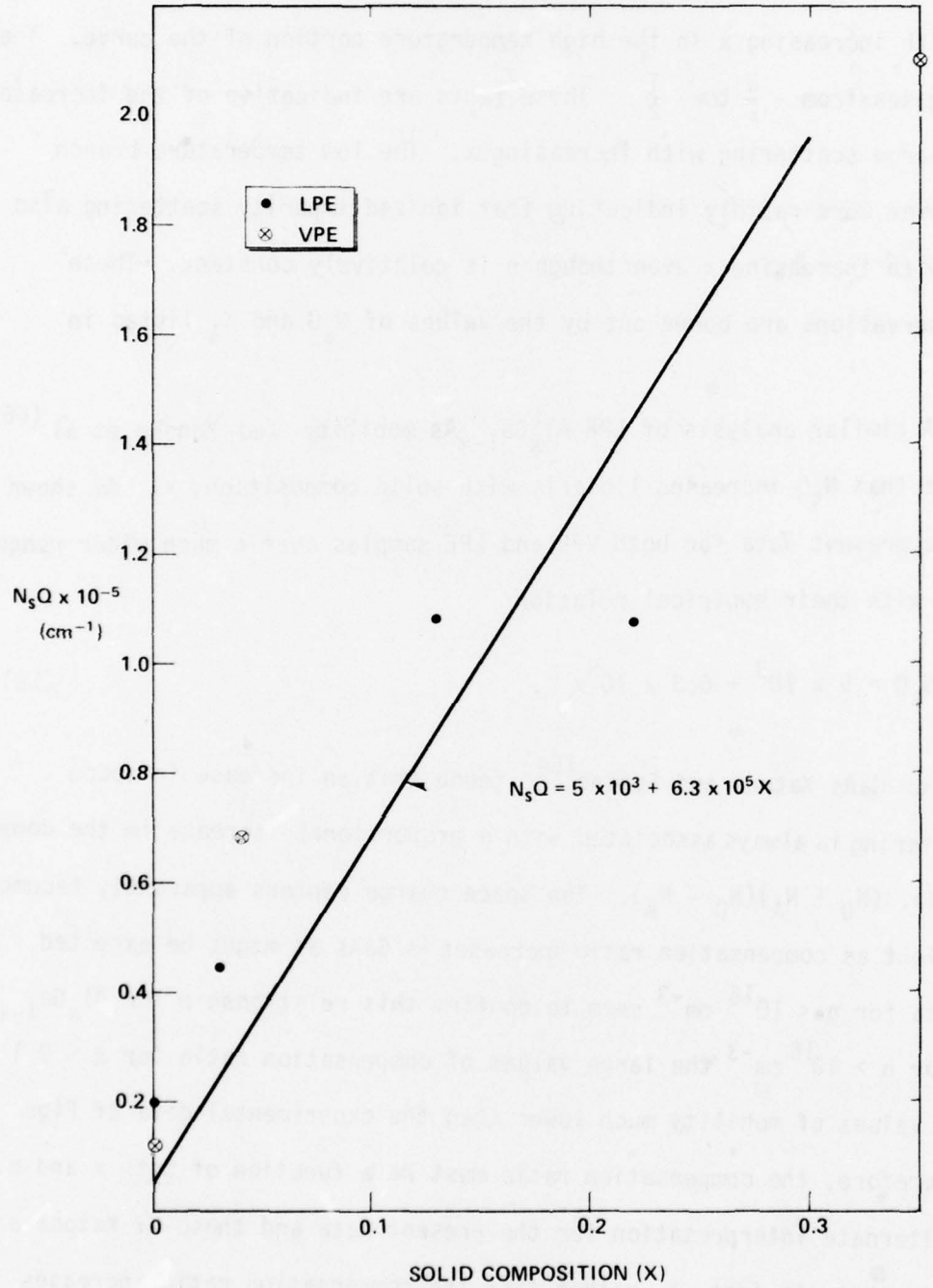

Figure 48. N_sQ (space charge scattering) versus X.

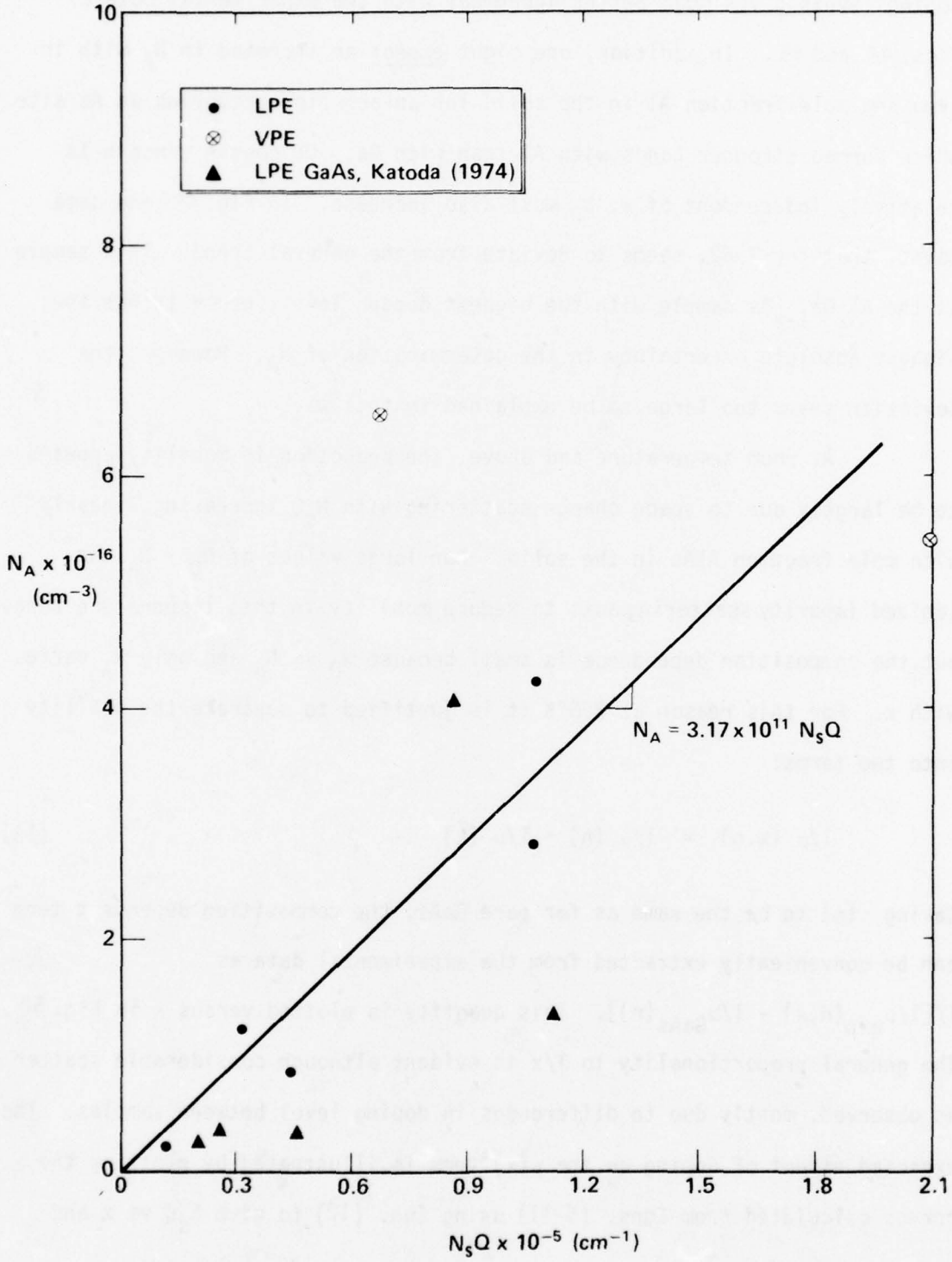

Figure 49. N_A vs $N_S Q$.

The linear increase in N_A with x, when extrapolated to higher doping levels gives much better agreement with the experimental data of Figs. 44 and 45. In addition, one might expect an increase in N_A with increasing mole fraction Al in the solid for an acceptor occupying an As site which formed stronger bonds with Al than with Ga. Of course since n is relatively independent of x, N_D must also increase. In Fig. 49 one data point, that for T-62, seems to deviate from the general trend. This sample is the $Al_xGa_{1-x}As$ sample with the highest doping level, hence it has the highest absolute uncertainty in the determination of N_A. However, the deviation seems too large to be explained in this way.

At room temperature and above, the reduction in mobility appears to be largely due to space charge scattering with N_sQ increasing linearly with mole fraction AlAs in the solid. For large values of $N_D - N_A$ the ionized impurity scattering acts to reduce mobility in this temperature range but the composition dependence is small because $N_D >> N_A$ and only N_A varies with x. For this reason at 296°K it is justified to separate the mobility into two terms:

$$1/\mu\ (x,n) = 1/\mu\ (n) + 1/\mu\ (x) \quad . \tag{13}$$

Taking (n) to be the same as for pure GaAs, the composition dependent term can be conveniently extracted from the experimental data as $1/[1/\mu_{exp}(n,x) - 1/\mu_{GaAs}(n)]$. This quantity is plotted versus x in Fig. 50. The general proportionality to 1/x is evident although considerable scatter is observed, mostly due to differences in doping level between samples. The expected effect of doping on the $\mu(x)$ term is illustrated by plotting the curves calculated from Eqns. (5-11) using Eqn. (12) to give N_sQ vs x and

and letting $N_A = 1.59 \times 10^{15} + 2.00 \times 10^{17}\ x$. The curves are plotted for two cases: 1) ignoring the increase in ionized impurity scattering, 2) including the increase in ionzied impurity scattering with x for $n = 10^{17}\ cm^{-3}$, the highest value of n for which the Brooks-Herring equation is accurate. The data for samples with higher values of n lies somewhat below this curve as would be expected.

Alloy scattering should be considered as an alternative to space charge scattering as an explanation for the reduction of $Al_xGa_{1-x}As$ mobility in the regime where ionized impurity effects are not dominant. The magnitude of mobility limited by alloy scattering has been calculated by Brooks:[67-69]

$$\mu_a = \frac{(2\pi)^{1/2} e\hbar^4 N_a}{3(kT)^{1/2} m_e^{5/2} (E_1 - E_2)^2 \times (1 - x)} \qquad (14)$$

where m_e is the effective mass, taken to be $m_o\ (0.067 + 0.083\ x)$,[15] and $E_1 - E_2$ is the energy separation between the conduction band edges of the unalloyed components, (3.018 - 1.424), using the direct band gaps. N_a is the density of lattice sites, a constant equal to $4.46 \times 10^{22}\ cm^{-3}$ since lattice parameter is independent of x. This expression was used to calculate $\mu(x)$ which is also included in Fig. 50. The mobility limited by alloy scattering appears to be about twice as large as that obtained by fitting N_sQ to the experimental data with $n < 10^{17}\ cm^3$. The two have the same dependence on composition and temperature. The factor which makes space charge scattering seem more plausible is the behavior of pure GaAs. Alloy scattering is obviously not a factor, yet the same complex reduction of mobility occurs involving an increase in both ionized impurity scattering which dominates at low temperatures, and the scattering having a $T^{-1/2}$ dependence which

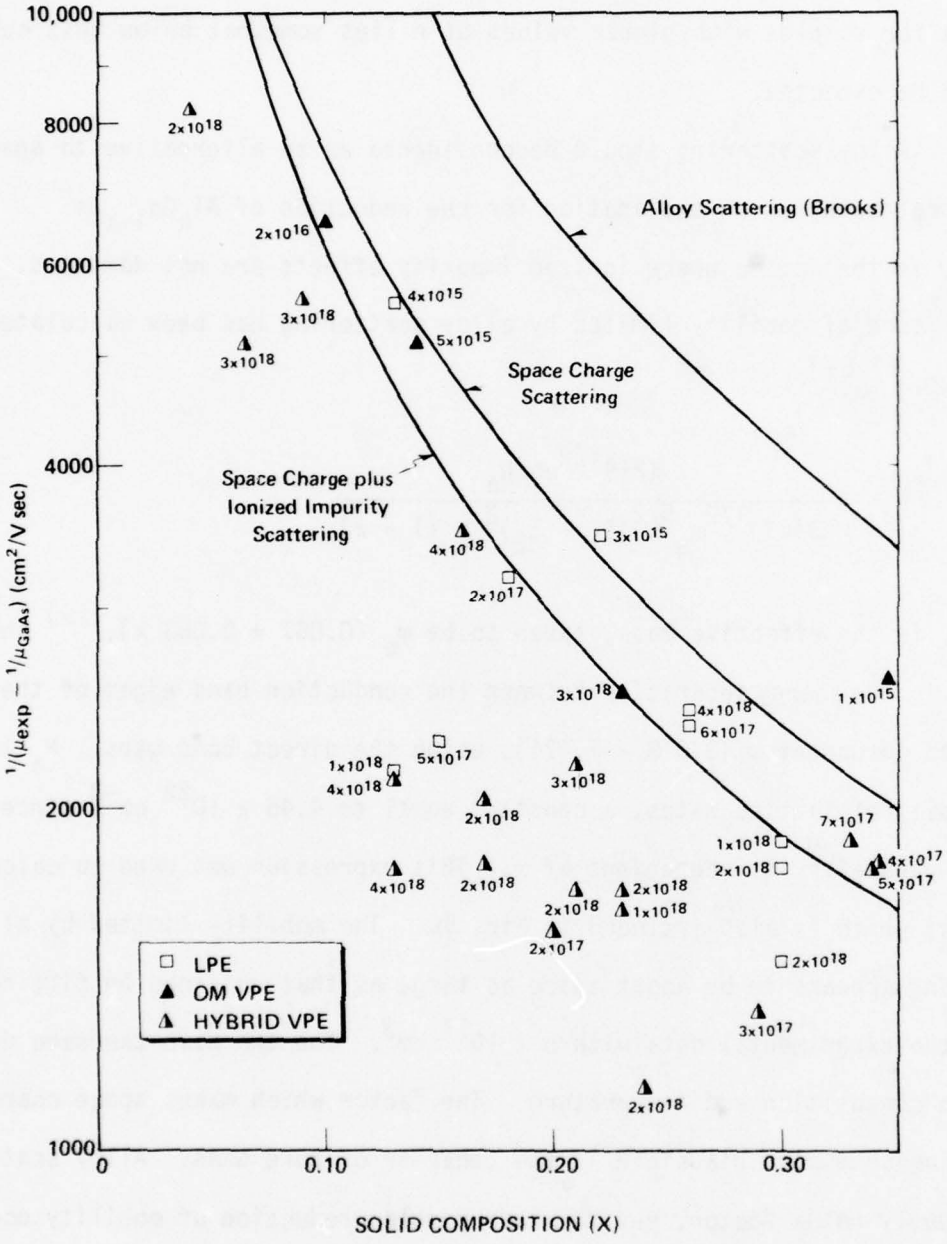

Figure 50. Mobility reduction due to alloying versus X.

dominates at high temperature.[59]

One other effect which must be considered for sample T-77, for which x = 0.35, is the effect of loss of electrons from the Γ to the lower mobility X and L minima. To insure that this effect does not affect the interpretation of these results, a calculation was carried out using the values of E_G and m^* versus x for the Γ, X, and L minima of Casey and Panish,[15] and values of $\mu_L = \mu_X = 140\ cm^2/Vsec$. At 305°K, the highest temperature data point, the calculated effect of the X and L minima is to decrease the electron mobility by only 6%. In addition the value of n determined using the single one band equations shows no significant decrease at the higher temperatures, indicating that the one band analysis is sufficient.

This analysis indicates the reduction in mobility with increasing x to be due to two factors: 1) an increase in ionized impurity scattering due to a linear increase in N_A with x and 2) a linear increase in the space charge scattering factor N_sQ with x. The behavior of specimens grown by both cold wall organometallic VPE and LPE exhibited similar behavior. Thus, the high degree of compensation previously observed in organometallic VPE $Al_xGa_{1-x}As$ is confirmed by this more detailed investigation and is surprisingly found to be similar to LPE material with low doping level.

2. SIMS and Auger Analysis

Clearly one of the important problems in the VPE growth of $Al_xGa_{1-x}As$ is the introduction of unwanted carbon, oxygen or both. These dopants are apparently associated with the lower lifetime and luminescence efficiency. Two techniques which show promise for the detection of low levels of C and O in thin $Al_xGa_{1-x}As$ epitaxial layers are secondary ion mas spectroscopy (SIMS)[67]

and Auger electron spectroscopy (AES). With both techniques profiles of impurity concentration can be obtained deep in the layer away from ubiquitous surface contaminants. Thus, both hot and cold wall (without baffles) VPE $Al_xGa_{1-x}As$ specimens have been analyzed for comparison with LPE $Al_xGa_{1-x}As$ and GaAs grown by various techniques. The results are subject to considerable uncertainty due to contamination within the instrument, but appear to show several trends. 1) VPE $Al_xGa_{1-x}As$ grown before baffles were introduced into the cold wall reactor is generally much more contaminated with O and C than either LPE $Al_xGa_{1-x}As$ or GaAs (either LPE or VPE). 2) For the cold wall system (without baffles) a clear correlation between decreasing O contamination and increasing PL efficiency is observed as oxygen contamination of the system was decreased by making the system more leak tight. 3) Oxygen contamination in the latest hot and cold wall samples are comparable although C seems to be lower in the hot wall system.

3. Deep Level Transient Spectroscopy

DLTS is an important tool for the characterization of deep traps which may be non-radiative recombination centers (NRCs) in semiconductors.[18,19] The system illustrated in Fig. 9 was used to measure the concentration, energy level and emission cross sections of traps contained in OMVPE $Al_xGa_{1-x}As$ grown in the cold wall system.

DLTS is essentially a measurement of the capacitance transient of a Schottky barrier or p-n junction when a reverse bias is applied forming a depletion region. The free carriers and electrons trapped at shallow levels are removed from the depletion region very rapidly. The capacitance transient measured is due to the carriers trapped and emitted from deep levels with a longer time constant. This occurs at a rate proportional to

exp ($-\Delta E/KT$). The so called DLTS signal is the difference in capacitances measured at times t_i and t_{i+1} during the transient. In Fig. 51 the DLTS signal for electron traps in a typical specimen of OMVPE $Al_xGa_{1-x}As$ is plotted versus T for four values of the decay time constant τ ($\tau = t_{i+1}-t_i/\ln (t_{i+1}/t_i)$).

The magnitude of the signal is related to the trap concentration, the position of the minimum as a function of τ is related to the trap depth and the absolute value of peak position can be used to determine the emission cross section, knowing the trap depth. In Fig. 52 the emission rate, $1/\tau$ normalized by dividing by $T^{2(68)}$ is plotted versus the reciprocal of the temperature of the minimum for the 8 traps observed in a specimen notable only for its low doping level and good quality p-n junction which allowed the observation of levels present at very low concentrations. The traps range in energy between 0.38 eV and 1.11 eV and the emission cross sections (σ) range from $\sim 10^{-12}$ cm^2 to 10^{-10} cm^2. The levels denoted E_2 and E_3 at 0.41 and 0.49 eV respectively are dominant in most OMVPE specimens investigated. In Table XIII the concentrations of each trap are tabulated for specimens grown with either 3 or 6 baffles. In Fig. 53 the sum of E_2 and E_3 trap concentrations is plotted versus free electron concentration to illustrate the detection limit of the technique ($N_T/n < 10^{-4}$) and the large change in both n and deep level concentration caused by going from 3 to 6 baffles (with the addition of a SiC coated pedestal). This change was also observed to cause a considerable increase in the PL efficiency as discussed in Section B.1. In Fig. 54 the PL intensity, normalized by dividing n, is plotted versus the sum of E_2 and E_3 level concentrations. The PL efficiency clearly increases for decreasing E_2 and E_3 concentrations, but the relationship is not linear as expected if E_2 and E_3 were the only non-radiative recombination centers.

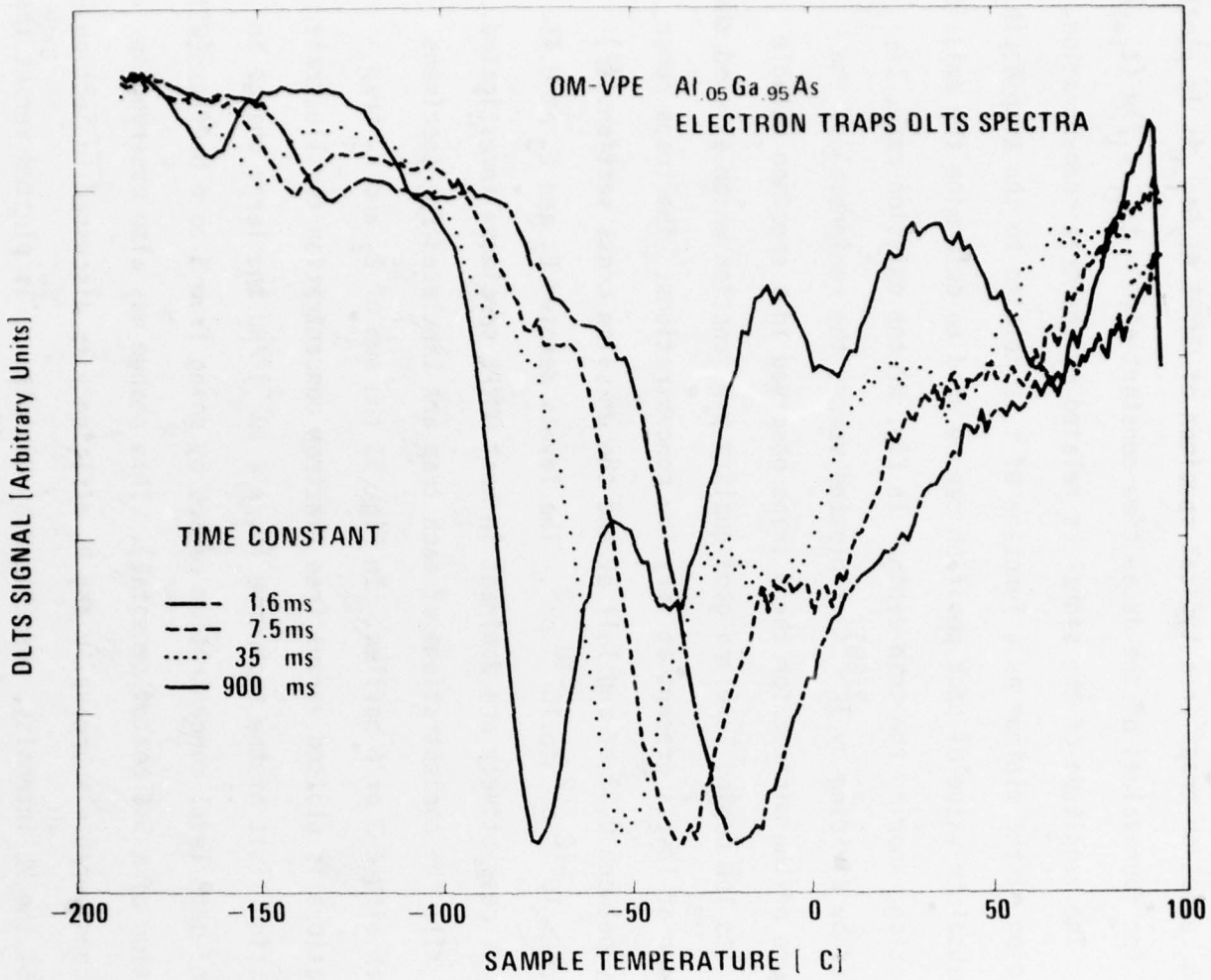

Figure 51. DLTS spectra at various values of decay time constant for sample LS-122 grown in the cold wall OMVPE system.

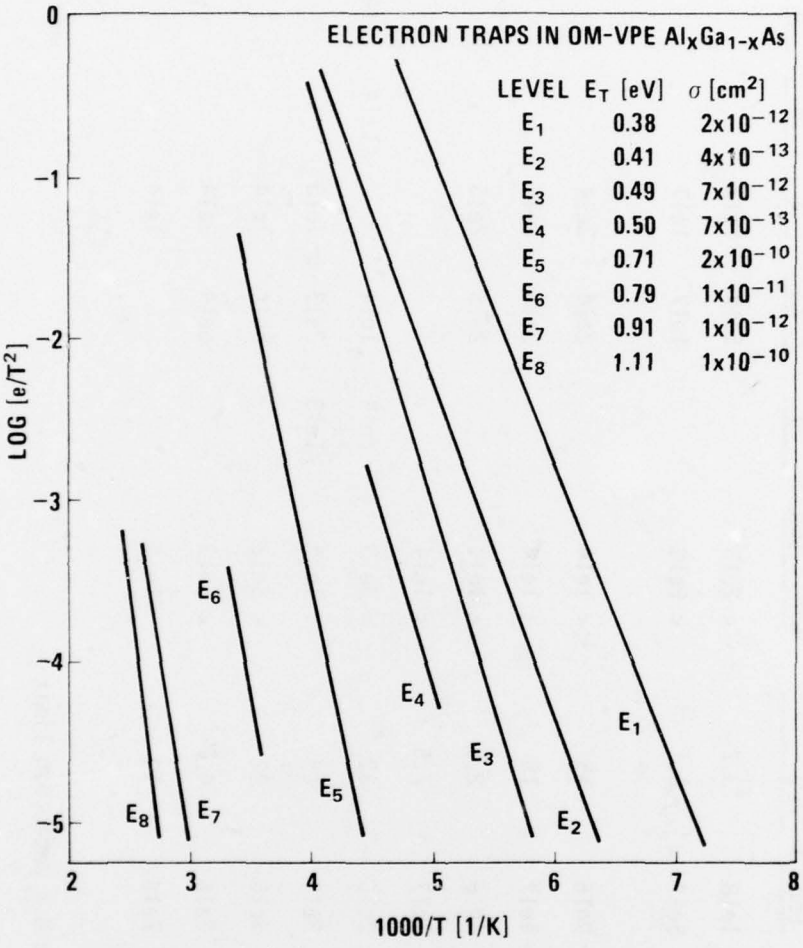

Figure 52. Emission rate ($1/\tau$ normalized by $1/T^2$) versus reciprocal temperature for OMVPE specimens.

TABLE XII

Summary of Deep Level Transient Spectroscopy Results

Sample No.	x	Number of Baffles	n (cm^{-3})	$I_{PL}/n \cdot 10^{18}$	Detection Limit (cm^{-3})	Deep Level Concentration (N), cm^{-3}						
						E_1	E_2	E_3	E_4	E_5	E_6	E_7	E_8
LS 62	0.28	3	1e18	3.2	< 2e15		5e17	5e17					
LS 63	0.25	3	8e17	5.1	< 2e15		1e17	1e17					
LS 85	0.03	6*	9e16	15	< 1e14		2e14	2e14				2e14	
Ls 87	0.05	6*	1e17	15	< 1e14		2e14	2e14				1e14	
LS 88	0.38	6*	4e16	2.5	< 1e14		2e15	2e15			2e15	1e15	
LS 94	0.07	6*	1e17	7.5	< 1e14							3e14	
LS 95	0.05	6*	2e16	33	< 5e13	2e14	1e14		1e14	1e14	1e14	5e14	5e14
LS 123	0.05	6*	3e15	19	< 1e13	1e13	2e13	1e13					
LS 124	0.06	6*	3e15	22	< 5e12		8e14	1e14					
LS 125	0.07	6*	2e16	4.7	< 5e13		6e14	2e14					
LS 134	0.06	6*	7e16	10	< 1e14			1e14					

NOTE: Where no entry is made N < Detection limit

*SiC coated pedestal

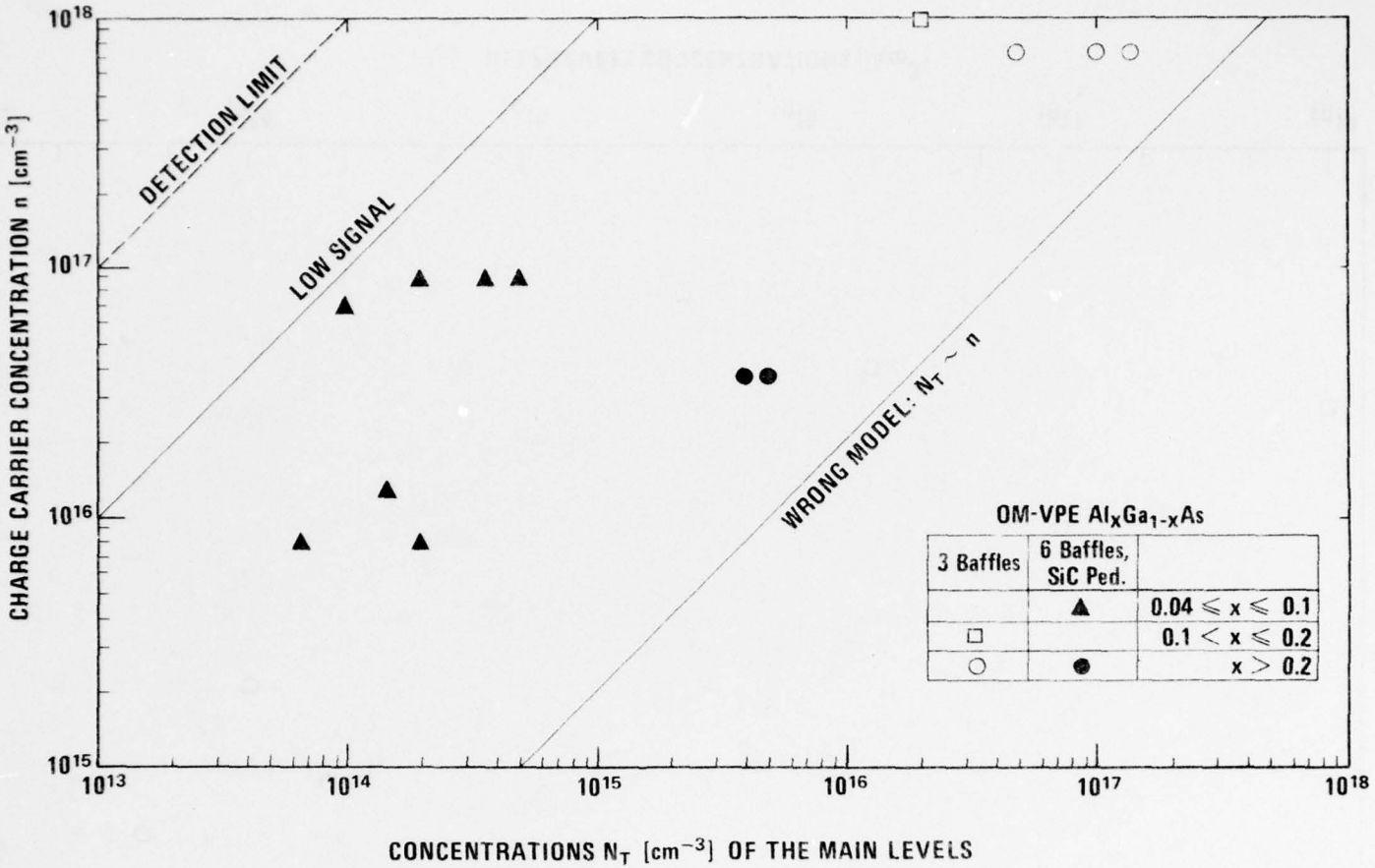

Figure 53. Free electron concentration (296°K) versus sum of E_2 and E_3 concentrations for samples grown in the cold wall VPE system containing 3 baffles and 6 baffles plus SiC coated pedestal.

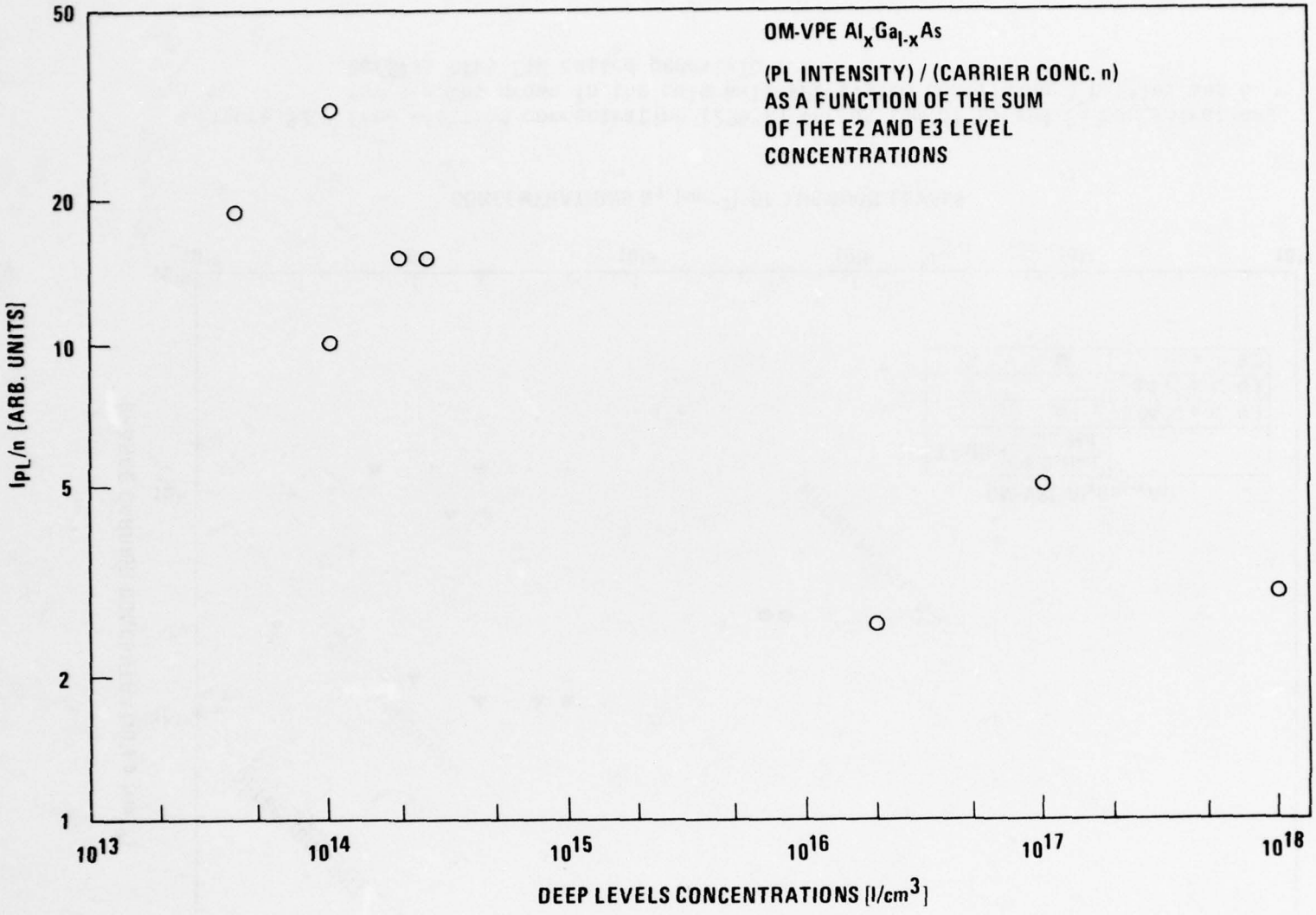

Figure 54. I_{PL}/n versus the sum of E_2 and E_3 trap concentrations.

The activation energies for E_2 and E_3 are only weakly dependent on alloy composition. As shown in Fig. 55, dE_T/dE_G is only ~ 0.08.

The improvement of PL efficiency obtained by introducting baffles into the cold wall OMVPE reactor is believed to be related to a reduction in oxygen contamination of the $Al_xGa_{1-x}As$. The concentration of deep levels labeled E_2 and E_3 seems to be related to the PL efficiency, thus it is interesting to consider whether they may be related to oxygen. No information is available about deep levels in $Al_xGa_{1-x}As$ due to oxygen. However, DLTS and capacitance transient measurements have been used to study oxygen in GaAs. Hughes[69] observed levels at 0.82 eV and 0.47 eV in capacitance relaxation experiments in GaAs. Lang and Logan[70] later surveyed levels observed in GaAs and concluded the level near ~ 0.89 observed by themselves and by Hughes in bulk grown VPE material was due to oxygen, although the cross section reported by Lang and Logan of 10^{-16} - 10^{-17} cm^2 much smaller than the 1.4×10^{-12} cm^2 reported by Hughes. Intentional doping with Ga_2O_3 failed to increase the concentration of the 0.89 eV level above 10^{13} cm^{-3}.[70] We observe small concentrations of traps at 0.79 and 0.91 eV in many samples, although they do not appear predominant in any specimens. The trap at 0.47 eV may be the same as our 0.49 eV deep E_3 although there is not data to connect it with oxygen. Overall, there is insufficient evidence to tell whether or not any of the levels observed are directly related to oxygen.

D. SUMMARY AND CONCLUSIONS

The OMVPE growth of $Al_xGa_{1-x}As$ ($x < 0.35$) has been studied during the course of this project. This is probably one of the most difficult III/V alloys to grow by VPE because of the strong Al-C and Al-O bonding which apparently gives rise to contamination problems not encountered in conventional VPE.

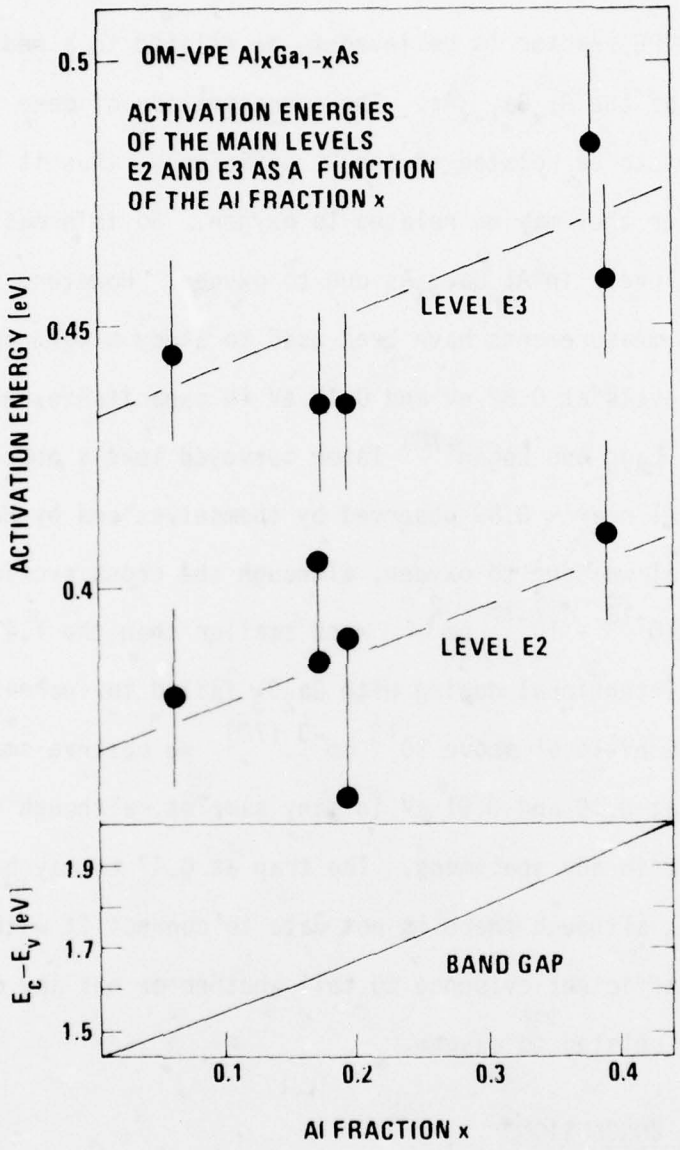

Figure 55. Activation energies for E_2 and E_3 versus alloy composition. E_a vs x is included for comparison.

The original thrust of the project was to concentrate on the Al-C problem by adding HCl in a hot wall system to replace the organic radicals by Cl on the Al and Ga while still in the gas phase. Later results indicate a major factor in the improvement in quality (PL efficiency) achieved was due to the hot baffles present in the gas stream which catalyzed the $Al(CH_3)_3$ + O_2 (or H_2O) reaction to form Al_2O_3 on the baffles.

Using this technique the maximum values of I_{PL}/n were about 30% of typical LPE results. Double heterostructure lasers were fabricated with values of J_{th} about twice as large as obtained on similar structures grown by LPE. The range of parameters which could be used was restricted to a relatively narrow range by morphology, composition and growth rate constraints.

A much simpler system operationally, is the cold wall system without HCl present. Later in the project it was found that by adding cold baffles to this system, excellent PL efficiencies could be obtained with excellent morphology and control of composition over a wide range of growth conditions. With this sytem values of I_{PL}/n comparable to values obtained in LPE material was obtained. Double heterostructure lasers have been fabricated with values of J_{th} of $\sim$ 2 times those obtained in equivalent LPE material. This system is the one selected for further development.

This report describes the optimization of both systems with respect to growth parameters, p-type (Zn) and n-type (Te) doping studies. The results of detailed studies on the characterization of the OMVPE $Al_xGa_{1-x}As$ at this date is approaching the quality of LPE material but considerably more work must be done to bring it to LPE quality in all respects.

The results obtained during this project and reported here indicate that OMVPE $Al_xGa_{1-x}As$ research should be pursued and that because of the inherent advantages of VPE over LPE this system may be the most useful system

for large scale production of GaAs and $Al_xGa_{1-x}As$ for optoelectronics and microwave device applications in the future.

REFERENCES

1. H. Kressel, J. Electron. Mater. 3, 747 (1974).

2. D. L. Rode, Phys. Stat. Solidi A32, 425 (1975).

3. M. B. Small, J. M. Blum and R. M. Potemski, Appl. Phys. Lett. 30, 42 (1977).

4. F. R. Nash, W. R. Wagner and R. L. Brown, Paper No. V-3, Device Research Conference, Salt Lake City, June 1976.

5. F. R. Nash, R. W. Dixon, P. A. Barres and N. E. Schumaker, Appl. Phys. Lett. 27, 234 (1975).

6. A. Y. Cho, R. W. Dixon, H. C. Casey, Jr. and R. L. Hartman, Appl. Phys. Lett. 28, 501 (1976).

7. M. Ettenberg, A. G. Sigai, A. Dreeben and S. L. Gilbert, J. Electrochem. Soc. 118, 1355 (1971).

8. A. G. Sigai, M. S. Abrahams and J. Blanc, J. Electrochem. Soc. 119, 952 (1972).

9. W. M. Yim, J. Appl. Phys. 42, 2854 (1971).

10. J. J. Tietjen, R. Clough, R. Enstrom, M. Ettenberg, H. P. Marsuka and A. G. Sigai, Report for NASA Contract No. NAS12-538 (April 1970).

11. G. B. Stringfellow and H. T. Hall, Jr., J. Crystal Growth 43, 47 (1978).

12. H. M. Mansevit, J. Electrochem. Soc. 118, 647 (1971).

13. A. E. Blakeslee and B. K. Bischoff, Electron. Soc. Extended Abstracts, Spring Meeting, Cleveland, Ohio (1971).

14. JANAF, International Thermochemical Critical Tables (Thermal Laboratories, Dow Chemical Co., Midland, Michigan, 1965).

15. H. C. Casey, Jr. and M. B. Panish, Heterostructure Lasers Part A, Fundamental Properties (Academic Press, New York, 1978).

16. A. Schumann, Jr. and R. P. Phillips, Solid-State Electron. 10, 943 (1967).

17. M. Ilegems and G. L. Pearson, Phys. Rev. B1, 1576 (1970).

18. D. V. Lang and L. C. Kimerling, Inst. Phys. Conf. Ser. 23, 581 (1975).

19. D. V. Lang and R. A. Logan, J. Electron. Mat. 4, 1053 (1975).

20. G. B. Stringfellow and H. T. Hall, Jr., J. Electrochem. Soc. 123, 916 (1977).

21. C. E. E. Stewart, J. Crystal Growth 8, 259 (1971).

22. H. M. Manasevit and W. I. Simpson, J. Electrochem. Soc. 112, 1725 (1969).

23. T. Y. Wu, J. Crystal Growth 21, 85 (1974).

24. D. W. Shaw, J. Crystal Growth 31, 130 (1975).

25. T. O. Sedgwick, J. Electrochem. Soc. 111, 1381 (1964).

26. G. B. Stringfellow, J. Crystal Growth 27, 21 (1974).

27. A. W. Laubeugayer and W. F. Gilliam, J. Am. Chem. Soc. 63, 477 (1941).

28. W. B. Joyce, R. W. Dixon, and R. L. Hartman, Appl. Phys. Lett. 28, 684 (1976).

29. M. Ueno and H. Vonezu, Presented at the 1978 Laser Device Specialists Conference, San Francisco, November 1978.

30. G. H. B. Thompson, D. F. Lovelace and S. E. H. Turley, Presented at the 1978 Laser Device Specialists Conference, San Francisco, November 1978.

31. M. Nakamura (Private communication).

32. D. J. Schlyer and M. A. Ring, J. Electrochem. Soc. 124, 569 (1977).

33. L. A. Ivanutin, N. N. D'yachkova and A. Yu. Malinin, Inorg. Mat. 11, 348 (1975).

34. E. W. Willimas, Phys. Rev. 168, 922 (1968).

35. E. W. Williams and C. T. Elliott, Brit. J. Appl. Phys. 2, 1657 (1959).

36. D. J. Ashen, P. J. Dean, D. T. J. Hurle, J. B. Mullin, A. M. White and P. D. Greene, J. Phys. Chem. Solids 36, 1041 (1975).

37. B. D. Shin, Appl. Phys. Lett. 24, 438 (1976).

38. J. D. Sansbury and J. F. Gibbons, Radiat. Eff. 6, 269 (1970); J. S. Harris, in International Conference on Ion Implantation in Semiconductors, ed. by I. Ruge and J. Graul (Springer - Verlag, Berlin, 1971), p. 157.

39. E. W. Williams and H. B. Bebb, in Semiconductors and Semimetals, V. 8, ed. R. K. Willardson and A. C. Beer, Academic Press, New York (1972).

40. R. C. Newman and F. Thompson, Solid State Communications 10, 505 (1972).

41. H. Kressel and J. K. Butler, Semiconductor Lasers and Heterojunction LEDs, (Academic Press, New York, 1977).

42. $\Delta G^{\circ}_{f,298}$ = -378 kcal/mole for Al_2O_3 (43)

$\Delta H^{\circ}_{f,298}$ = -20.8 kcal/mole for $Al(Ch_3)_3$ (44)

Thus ΔG for the reaction is $\sim$ 340 kcal/mole. As an estimate of the "worst G_{Se}," i.e., the case most likely to produce homogenous nucleation, we use ΔG = -378 kcal/mole.

43. JANAF, International Thermochemical Critical Tables (Thermal Laboratories, Dow Corning Co., Midland, Michigan, 1965).

44. M. B. Smith, J. Organometallic Chem. 76, 171 (1974).

45. D. R. Uhlmann and B. Chalmers in "Nucleation Phenomena" (Am. Chem. Soc., Washington, D.C., 1966) p. 1.

46. J. E. McDonald, in "Homogeneous Nucleation Theory", Academic Press, New York, 1974, p. 225t.

47. G. M. Pound in "Energetics in Metallurgical Phenomena V. II", ed. by W. M. Mueller, "Gordon and Breach, New York, 1965) p. 85.

48. W. D. Kingery "Introduction to Ceramics", John Wiley and Sons, New York (1960).

49. D. R. Stull and G. C. Sinke, Thermodynamic Properties of the Elements, (American Chemical Society, Washington D.C., 1956).

50. S. Ito, T. Shinohara and Y. Seki, J. Electrochem. Soc. 120, 1419 (1973).

51. Y. Seki, K. Tanno, K. Iida, and E. Ichiki, J. Electrochem. Soc. 122, 1108 (1975).

52. R. D. Dupuis and P. D. Dapkus, Appl. Phys. Lett. 31, 839 (1977).

53. R. D. Dupuis and P. D. Dapkus, Appl. Phys. Lett. 32, 473 (1978).

54. G. B. Stringfellow and G. Hom, J. Electrochem. Soc. 124, 1806 (1977).

55. D. L. Rode and S. Knight, Phys. Rev. (b) 3, 2534 (1971).

56. H. Brooks in Advances in Electronics and Electron Physics, ed. L. Marton (Academic Press, New York, 1955), p. 156.

57. G. E. Stillman and C. M. Wolfe, Thin Solid Films 31, 69 (1976).

58. E. Gerlach and M. Rautenberg, Phys. Stat. Solidi (b) 86, 479 (1978).

59. T. Katoda and T. Sugano, J. Electrochem. Soc. 121, 1066 (1974).

60. R. L. Petritz and W. W. Scanlon, Phys. Rev. 97, 1620 (1955).

61. H. J. Van Daal, Philips Res. Repts. 3, 44 (1965).

62. A. R. Hutson, J. Appl. Phys. S32, 2287 (1961).

63. J. Bardeen and W. Schockley, Phys. Rev. 80, 72 (1950).

64. E. M. Conwell and M. O. Vassell, Phys. Rev. 166, 797 (1968).

65. L. R. Weisberg, J. Appl. Phys. 33, 1817 (1962).

66. K. Kaneko, M. Ayabe and N. Watanabe, Int. Phs. Conf. Ser. 33a, 216 (1977).

67. The SIMS analyses were performed by W. Katz and C. Evans at the University of Illinois.

68. C. H. Henry, J. Electron. Mat 4, 1037 (1975).

69. F. D. Hughes, Acta. Elect. 15, 43 (1972).

70. D. V. Lang and R. A. Logan, J. Electron. Mat. 4, 1053 (1975).

MISSION
of
Rome Air Development Center

RADC plans and executes research, development, test and selected acquisition programs in support of Command, Control Communications and Intelligence (C^3I) activities. Technical and engineering support within areas of technical competence is provided to ESD Program Offices (POs) and other ESD elements. The principal technical mission areas are communications, electromagnetic guidance and control, surveillance of ground and aerospace objects, intelligence data collection and handling, information system technology, ionospheric propagation, solid state sciences, microwave physics and electronic reliability, maintainability and compatibility.

Printed by
United States Air Force
Hanscom AFB, Mass. 01731